# Analysis of chromosome segregation and its coordination with cell division in alphaproteobacteria

Dissertation

zur Erlangung des Grades eines
Doktor der Naturwissenschaften
(Dr. rer.nat.)
des Fachbereichs Biologie der Philipps-Universität Marburg

Vorgelegt von
**Revathi Pulpetta**
aus Thrissur, Indien

Marburg, im Dezember 2022

Vom Fachbereich Biologie der Philipps-Universität Marburg (HKZ: 1180)
als Dissertation angenommen am 25.1.2023

Erstgutachter: Prof. Dr. Martin Thanbichler
Zweitgutachter: Prof. Dr. Peter Graumann

Tag der mündlichen Prüfung: 3.2.2023

Die Untersuchungen zur vorliegenden Arbeit wurden von September 2017 bis Februar 2022 am Max-Planck-Institut für terrestrische Mikrobiologie und an der Philipps Universität Marburg unter der Leitung von Prof. Dr. Martin Thanbichler durchgeführt.

**Publications**

Jung, A., Raßbach, A., Pulpetta, R.L. *et al.* Two-step chromosome segregation in the stalked budding bacterium *Hyphomonas neptunium*. *Nat Commun* 10,3290(2019).

*To Achu*

## Abstract

Chromosome replication and segregation as well as their coordination are indispensable for the propagation of life. In bacteria, these processes are so far studied in morphologically simple and well-established model organisms. In this study, we shed light on chromosome segregation, cell division and their coordination in alphaproteobacteria. We use two model organisms, the stalked budding bacterium *Hyphomonas neptunium* and the well-studied model organism *Caulobacter crescentus.* Both bacteria possess a unique cell cycle wherein flagellated swarmer cells that are replication incompetent develop into replication-competent stalked cells. In the case of the dumb-bell shaped species *H. neptunium*, new offspring is generated by budding at the distal end of its stalk, making it necessary to translocate a copy of its chromosome through the stalk to the future daughter cell. This happens in a unique two-step process reminiscent of eukaryotic chromosome segregation, wherein the first step, the segregation within the mother cell, occurs in a manner dependent on the ParAB*S* DNA partitioning system, like in its close relative *C. crescentus*. The duplicated origin stays at the stalked pole and then later, in response to an unknown trigger, initiates the second step of segregation through the stalk. In this study, we systematically analyse the dynamics of chromosome replication of *H. neptunium* and its coordination with segregation through the stalk. We find out that the replication of more than half of the chromosome is finished before the second step of segregation is initiated. This study opens up several questions such as the reason behind the pause between the two segregation steps and the potential players and the mechanism involved in the coordination of these steps. *H. neptunium* possesses several ParA homologues. Since the DNA partitioning ATPase ParA and ParA-like proteins are known to be involved in chromosome segregation, we proceed to investigate the novel ParA-like protein HNE_0708 as a potential candidate involved in the coordination of DNA segregation. Interestingly, we find in this study that this homologue belongs to a separate sub-family of ParA-like proteins. Apart from that, this protein contains a TIR domain, which is known to be involved in protein-protein interaction in bacteria. Like ParA, this homologue shows ATPase activity and binds DNA non-specifically. Apart from that, the lack of this protein leads to a characteristic stalk-bulging phenotypic defect and functional defects in chromosome replication and segregation. Thus, HNE_0708 potentially co-ordinates cell morphogenesis with chromosome replication, segregation and potentially, cell division. As a prime example of a system coordinating cell division and chromosome segregation in alphaproteobacteria, we further study the well-established model species *C. crescentus*. The DNA partitioning protein ParB of *C. crescentus* interacts with canonical ParA to bring about chromosome segregation and it interacts with the ParA-like protein MipZ to bring about division site placement, thus coordinating chromosome segregation with cell division. The interaction between ParB and MipZ is crucial for the robust placement of the division site, as this interaction primarily stimulates the dimerisation of MipZ monomers, which effectively block the formation of the cytokinetic FtsZ ring in their vicinity. In this study, we systematically analyse this interaction by biochemical methods. We find out that the C-terminal domain of ParB dimers interacts with the C-terminal region of MipZ in both its monomeric and dimeric form. We also conclude that the C-terminal region of ParB is necessary and sufficient for

its interaction with MipZ *in vitro* through a series of biochemical experiments, in which we tested this interaction by constructing chimeric ParB variants as well as using a C-terminal fragment of ParB to recruit MipZ *in vitro*. Together, these findings shed light on the interaction between the complex machinery bacteria employ to regulate and coordinate chromosome segregation and cell division.

## Zusammenfassung

Chromosomenreplikation und -segregation sowie deren Koordination sind für die Fortpflanzung von Lebewesen unabdingbar. In Bakterien wurde dieser Prozess bisher in morphologisch simplen und bereits etablierten Modellorganismen untersucht. In dieser Arbeit erweitern wir das bekannte Wissen um die Chromosomenreplikation, Zellteilung und deren Koordination in alpha Proteobakterien. Hierfür wurden zwei Modellorganismen zur Untersuchung verwendet, das gestielte, sich über Knospung vermehrende Bakterium *Hyphomonas neptunium* und der bereits gut untersuchte Modellorganismus *Caulobacter crescentus*. Beide Bakterien besitzen einen einzigartigen Zellzyklus, in dem sich begeißelte Schwärmerzellen, welche teilungsunfähig sind, in teilungsfähige gestielte Zellen entwickeln. Im Falle der Hantelförmigen Spezies *H. neptunium*, wird die neue Zelle mittels Knospung am Distal-Ende des Stiels gebildet. Dadurch ist die Translokation einer Kopie des Chromosoms, durch den Stiel in die zukünftige Tochterzelle nötig. Dies geschieht durch einen einzigartigen, zwei teiligen Prozess, der an die eukaryotische Zellteilung erinnert. Der erste Teil dieses Prozesses, die Segregation des Chromosoms in der Mutterzelle, geschieht in Abhängigkeit des ParABS DNA-Segregationssystems, ähnlich wie im nah verwandten Bakterium *C. crescentus*. Der duplizierte Ursprung verbleibt vorerst am gestielten Pol und wird später im zweiten Teil dieses Prozesses, ausgelöst durch einen unbekannten Faktor, durch den Stiel segregiert. In dieser Arbeit haben wir systematisch die Dynamik der Chromosomenreplikation in *H. neptunium*, sowie deren Koordination mit der Segregation des Chromosoms durch den Stiel analysiert. Wir haben herausgefunden, dass bereits mehr als die Hälfte des Chromosoms verdoppelt wurde, bevor der zweite Schritt der Segregation initiiert wird. Diese Studie zeigt mehrere Fragen auf, wie zum Beispiel nach dem Grund hinter der Pause der zweitteiligen Segregation, nach potentiellen beteiligten Faktoren sowie den Mechanismen welcher in die Koordination dieser zwei Schritte involviert ist. *H. neptunium* besitzt mehrere ParA Homologe. Da bekannt ist, dass die DNA segregierende ATPase ParA und ParA-ähnliche Proteine involviert in Chromosomensegregation sind, haben wir das neuartige potentiell in die Koordination der DNA-Segregation involvierte ParA-ähnliche Protein HNE_0708 untersucht. Interessanter Weise haben wir in dieser Arbeit herausgefunden, dass dieses Protein zu einer separaten Untergruppe der ParA-ähnlichen Proteine gehört. Ebenfalls interessant ist das Vorhandensein einer TIR-Domäne, welche dafür bekannt ist in Protein-Protein Interaktionen involviert zu sein. Ähnlich wie ParA zeigt dieses Homolog ATPase-Aktivität und bindet unspezifisch an DNA. Davon abgesehen führt die Abwesenheit dieses

Proteins zu einem charakteristischen Phänotyp, mit ausgestülptem Stiel und einem Defekt in Chromosomensegregation und -replikation. Daher koordiniert HNE_0708 potentiell Zellmorphogenese durch Chromosomenreplikation, -segregation und potentiell auch Zellteilung. Als ausgezeichnetes Beispiel für ein System, welches Zellteilung und Chromosomensegregation in Alpha-Proteobakterien koordiniert, wurde im Weiteren der gut etablierte Modellorganismus *C. crescentus* untersucht. Das DNA-Segregation-Protein ParB von *C. crescentus* interagiert einerseits mit dem kanonischen ParA, um die Chromosomensegregation herbeizuführen und andererseits mit dem ParA-ähnlichen Protein MipZ um die Positionierung der Teilungsebene zu definieren. Dadurch koordiniert ParB sowohl die Chromosomensegregation als auch die Zellteilung. Die Interaktion zwischen ParB und MipZ ist von zentraler Bedeutung für die Platzierung der Teilungsebene der Zelle, da durch die Interaktion primär die Dimerisierung des MipZ-Monomers angeregt wird, welche effektiv die Bildung des zytokinetischen FtsZ-Ringes in dessen Nähe blockiert. In dieser Studie wurde diese Interaktion systematisch mittels biochemischer Methoden analysiert. Wir haben herausgefunden, dass die C-terminale Domäne von ParB-Dimeren mit der C-terminalen Region von MipZ, sowohl in der monomeren als auch in der dimeren Form interagiert. Durch eine Reihe von biochemischen Experimenten konnten wir ebenfalls schlussfolgern, dass die C-terminale Region von ParB notwendig und auch ausreichend für die Interaktion mit MipZ *in vitro* ist. Durch diese Experimenten konnten wir diese Interaktion, durch die Konstruktion von ParB-Chimären sowie der Verwendung eines C-terminalen ParB-Fragments testen, was zur in *vitro* Rekrutierung von MipZ führte. Zusammenfassend erweitern diese neuen Erkenntnisse das Wissen über die Interaktion zwischen der Zellteilung und der komplexen Maschinerie, die Bakterien entwickelt haben um Chromosomensegregation zu regulieren und koordinieren.

**Abbreviations**

x g - multiple of acceleration of gravity
aa - amino acids
APS - ammonium persulfate
ADP - adenosine diphosphate
ASM -
ATCC - American Type Culture Collection
ATP - adenosine triphosphate
ATPγS - slowly hydrolyzable adenosine triphosphate
bp - base pair(s)
BLI - bio-layer interferometry
BSA - bovine serum albumin
CDP - cytidine diphosphate
CFP - cyan fluorescent protein
CTD - C-terminal domain
CTP - cytidine triphosphate
CV - column volume
DAP - diaminopimelic acid
DBD - DNA binding domain
DIC - differential interference contrast
DMSO - dimethyl sulfoxide
DNA - deoxyribonucleic acid
dNTPs - deoxyribonucleoside triphosphate
DTT - dithiothreitol
EDTA - ethylenediaminetetraacetic acid
HDX - hydrogen deuterium exchange
HRP - horseradish peroxidase
HTH - helix-turn-helix
IPTG - isopropyl-β-D-thiogalactopyranoside
kb - kilo base pair(s)
kDa - kilo Dalton
LB - Luria-Bertani
MB - Marine Broth
NCBI - National Center for Biotechnology Information
NTD - N-terminal domain
OD - optical density
PAGE - polyacrylamide gel electrophoresis
PCR - polymerase chain reaction
pI - isoelectric point
PMSF - phenylmethanesulfonyl fluoride
PVDF - polyvinylidene fluoride
PYE - peptone yeast extract
rpm - revolutions per minute
RT - room temperature
SDS - sodium dodecyl sulphate
SEC - size exclusion chromatography
SUMO - small ubiquitin-like modifier
TEM - transmission electron microscopy
TEMED - N, N, N’, N’-tetramethylethylenediamine

TIR - Toll/interleukin-1 (IL-1) receptor
WT - wild type
YFP - yellow fluorescent protein

## Contents

# Chapter 1: Introduction

Every organism has to replicate and faithfully segregate its genetic material. Bacteria are no exception. These processes need to be carried out in a coordinated manner so as to accommodate other cellular activities such as cell division. One of the main challenges bacteria face in this respect is to manage the humongous size of its genetic material. Bacterial genomes comprise replicating units that are essential for survival, called chromosomes. Most bacteria appear to have a single large circular chromosome, but this is not always the case. Many species have multiple chromosomes, such as *Vibrio cholerae* (Truksis et al, 1998) with two chromosomes and *Burkholderia cepacia* (Lessie et al, 1996), which has three chromosomes with respective sizes of 3.6, 3.2, and 1.1 Mb. Some species such as the spirochete *Borrelia burgdorferi* (Iyer et al, 2013) and *Streptomyces coelicolo*r (Kinashi et al, 1992) contain linear DNA. Besides, non-essential genes can also be part of extrachromosomal elements such as plasmids. Unlike eukaryotes, the genetic material in bacteria is not enclosed in a membrane-bounded organelle like the nucleus. The bacterial genetic material has a total contour length that is almost three orders of magnitude longer than the cell itself (Lederberg, 1952). Therefore, it has to be compacted very well to be able to fit into the cytoplasmic space. However, at the same time, this giant molecule must still be accessible to essential processes such as transcription, replication, repair, segregation etc. Unlike in eukaryotes, DNA replication, repair and segregation occur concomitantly in bacteria (Badrinarayanan et al, 2015 ). The proper placement of the replication origin (*ori*) and terminus (*ter*) regions and thus, the overall organisation of chromosomes is essential for the future daughter cells to carry out segregation in a faithful and robust manner.

Bacterial chromosomes were initially thought to be attached to the cell membrane and distributed passively as the cell grows. However, recent studies (Robinow et al,1994), supported by technological advances, have shed light on how chromosomal DNA is arranged within the cell. Based on the results of biochemical, biophysical and cell biological approaches, we now know that bacterial chromosomes are highly organised and bacteria use various dedicated machineries to compact, organise and segregate their copies after replication.

Early light microscopy studies revealed the presence of discrete regions within the cell devoid of ribosomes, called nucleoids (Ishihama, 2009). Subsequent electron microscopy and cryo-EM studies revealed the arrangement of chromosomal DNA in *Escherichia coli* cells. Similar observations were also made in *Bacillus subtilis* by observing fluorescently labelled nucleoid-associated proteins (NAPs) that bind non specifically to DNA (Köhler et al, 1997). These results showed that the chromosome is not randomly packed into the cell but rather may be present as a more discrete structure, the nucleoid. Apart from gaining insights into the spatial arrangement of chromosomal DNA, time-lapse microscopy to visualise the NAPs also revealed the temporal dynamics of nucleoid organisation. Over the next few years, a combination of cell biological, biochemical (Sinden et al, 1981) and computational methods (Postow et al, 2004) shed light on the topological aspects of

chromosome organisation, thus expanding our understanding on chromosome dynamics during processes such as replication and segregation.

## Bacterial chromosome organisation

As early microscopic evidence revealed the existence of the nucleoid, the next question was if there was an order to the organisation of chromosomal DNA within the cell. As we know, most bacterial chromosomes are circular, with a single origin of replication (*ori*) and a terminus (*ter*) region located opposite *ori,* in which the replication process terminates. The rest of the chromosomal DNA stretches between these two regions as two chromosomal arms. In order to understand the spatial organisation of bacterial chromosomes and their different regions within the cell, a fluorescence-based technique called FROS (fluorescent repressor-operator system) in which the region of interest is illuminated by the specific binding of fluorescently labelled repressors, was developed (Figure 1.1). Apart from this, the ParB/*parS* system was also employed to study the positioning of loci within the cell (the ParB protein specifically identifies and binds to its cognate *parS* site), thus making it possible to visualise the region where the *parS* site is incorporated in the chromosome (Robinette et al, 1996).

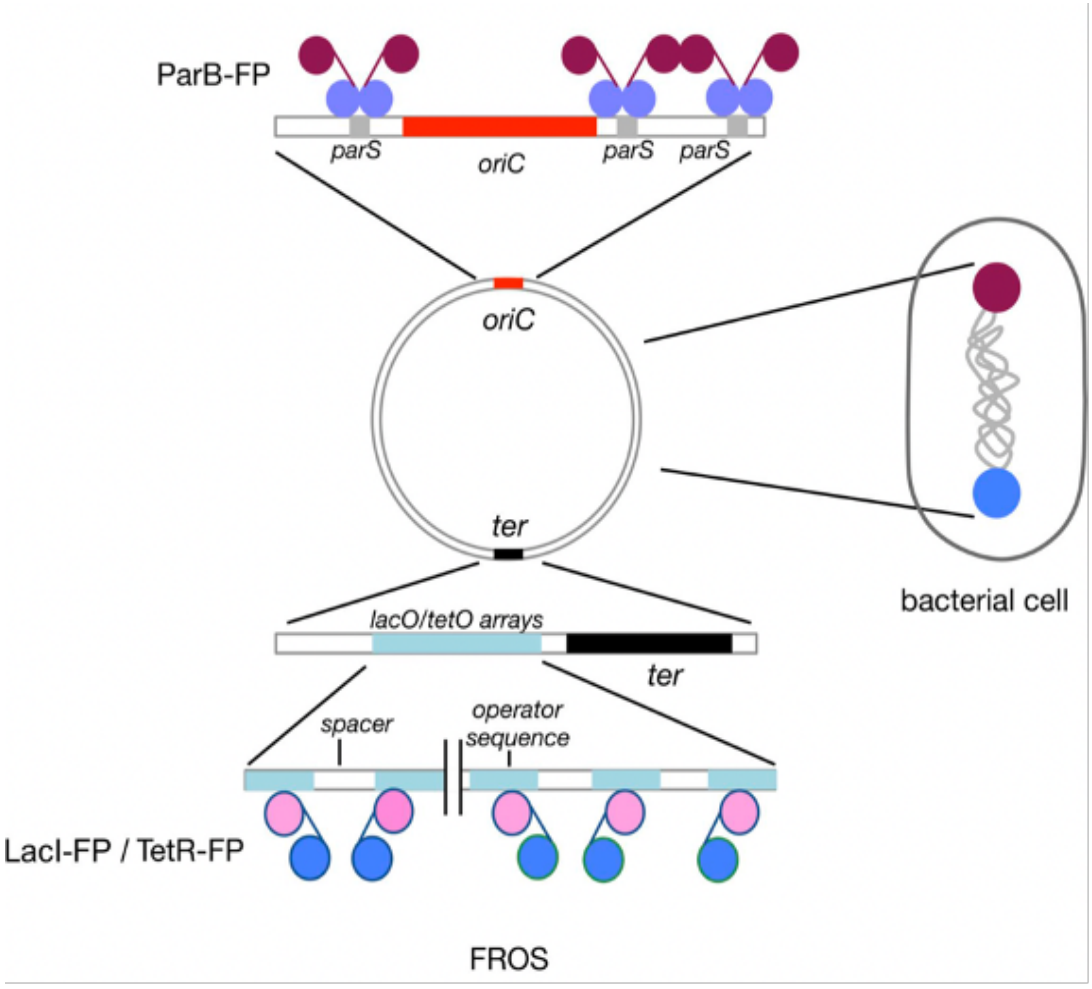


**Figure 1.1: Systems to determine the subcellular location of chromosomal loci**. Chromosomal *parS* sites that are associated with ParB fused with a fluorescent protein can be seen located close to *ori*. However, it

should be noted that an orthogonal plasmidic *parS* site can be inserted anywhere on the chromosome that is then bound by its cognate ParB tagged with fluorescent protein, thus enabling the visualisation of any chromosomal region. Close to the *ter* site, transcriptional operator sequences separated by spacers are inserted, as depicted by blue bands, which are bound by activators or repressors recognizing these operators fused with a fluorescent protein, thus enabling the detection of the insertion site. Adapted from (Robinette et al, 1996).

Using these techniques, two major organisational patterns were observed in bacteria (Figure 1.2). The first one is a longitudinal arrangement (Badrinarayanan et al, 2015) of the chromosome in which the origin of replication is close to one pole of the cell, usually held in place with the help of a pole-organising protein, such as PopZ in the case of *C. crescentus*. The *ter* region is positioned close to the opposite pole. Consequently, the two chromosomal arms stretch between the origin and the terminus, side by side, across the length of the cell. Hence, this pattern of organisation is also called the *ori-ter* organisation. When the chromosome replicates, the *ori* region duplicates first and moves towards the opposite cell pole, followed by the rest of the newly replicated chromosome (Ishihama et al, 2009). This event displaces the terminus towards the mid-cell position in the pre-divisional cell. Thus, a pre-divisional cell will have an *ori-ter-ter-ori* pattern, which restores the longitudinal organisation in the daughter cells after cell division. The second pattern is the left-*ori*-right pattern or transverse pattern of chromosome organisation (Robinow et al, 1994). Here, the chromosome is organised such that the *ori* and *ter* regions are positioned at the mid-cell, with the left and right arms of the chromosome stretching towards either pole of the cell. During replication, the duplicated *ori* region will move towards the quarter positions of the cell, followed by the rest of the duplicated chromosome.

Chromosome organisation has been mostly analysed in rod-shaped bacteria. Many species, such as *C. crescentus* (Wang et al, 2006)*, Myxococcus xanthu*s (Harms et al, 2013) and *V. cholerae* (David et al, 2014) display a longitudinal arrangement. However, in slow-growing *E. coli* cells*,* the chromosome has a transverse arrangement (Wang et al, 2006). It is found that *B. subtilis* switches between these two organisations during a replication-segregation cycle (Wang X et al, 2014).

Several lines of evidence suggest the existence of discrete structured subdomains called chromosomal macrodomains in bacteria (Valens et al, 2004). Studies of the *E. coli* chromosome have revealed that it is divided into four macrodomains, each of which (Ori, Right, Left and Ter) contains approximately 1 Mbp of DNA. The localization of these macrodomains can change during the cell cycle, but is agreeably defined. The degree of linear DNA compaction can be measured *in vivo* using several genomic markers. This was found to vary among these domains. For example, the 800-kb domain around *ter* is on average five times less compact than the rest of the chromosome (Wiggins et al, 2010). The presence of high-density clusters of chromosomal DNA has also been observed by super-resolution microscopy in the case of *C. crescentus*. The presence of these “superdomains” is corroborated using computational methods as well (Messelink et al, 2021).

The organisation of chromosomes is dependent on molecular machinery, such as the ParAB*S* system, which plays a crucial role in maintaining the longitudinal organisation of the chromosomal DNA in many bacteria such as *C. crescentus*. In bacteria like *E. coli* that lack a ParAB*S* system (Ventura et al, 2013), the transverse organisation is aided by the MukB or its more widespread distant homolog SMC (structural maintenance of chromosomes) (Niki et al, 1992).

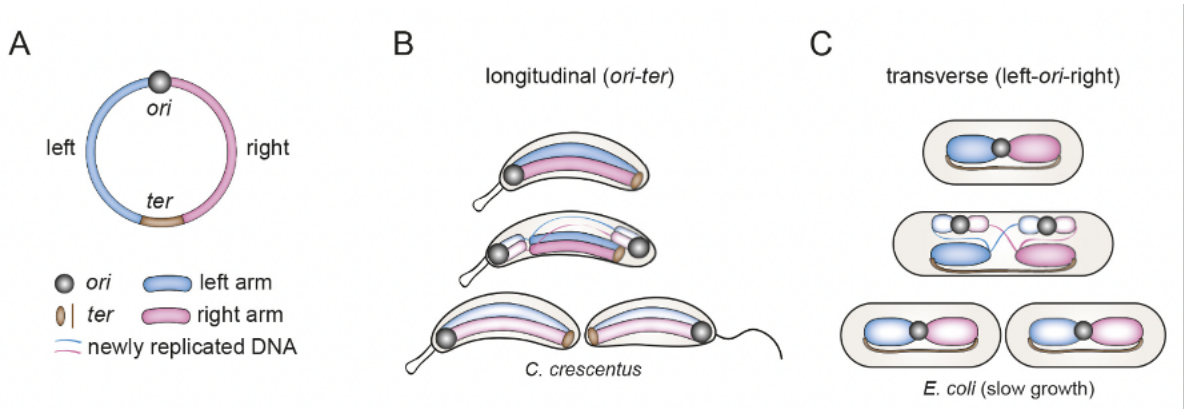


**Figure 1.2: Chromosome organisation in bacteria**. A. *Ori* and *ter* with the left and right arms of the chromosome organised in a circular manner. B. Longitudinal organisation as seen in *C. crescentus*, where *ori* is at one pole and *ter* is at the opposite pole. C. Transverse organisation of chromosome as seen in slow-growing *E.coli*, with *ori* and *ter* at the mid-cell position and the left and right arm occupying either halves of the cell. Adapted from (Wang et al, 2006).

## Molecular machineries that organise the bacterial nucleoid

In contrast to prokaryotes, eukaryotes have a well-defined nucleus that encases the DNA. In this case, the cells face the challenge of neatly organising the chromosome inside the nucleus. For this purpose, there are positively charged histone proteins that serve as factors on which DNA is wrapped around to form nucleosomes, which are in turn folded into chromatin fibres. These are further folded into higher-order structures, yielding a very high degree of compaction that enables the DNA to fit inside the confined space of the nuclear compartment. Our understanding of these higher-order structures is poorly developed. Similarly, bacterial chromosome organisation into higher-order structures is still a matter of intensive research. Nucleoid-associated proteins (NAPs) can be termed analogous to histones in the sense that they organise the bacterial chromosome (Lopez-Garćia et al, 2006). NAPs are known to influence DNA topology in various ways (Martire et al, 2020). For instance, the the DNA-bridging histone-like nucleoid-structuring protein (H-NS) is able to bridge different DNA regions (Gill et al, 2022), whereas the integration host factor (IHF) (Ellenberg et al, 1997) causes hairpin-loop formation (Krogh et al, 2018) and the curved-DNA-binding protein CbpA upon binding to DNA causes the formation of protein-DNA aggregates that protect the DNA from nucleases. NAPs are ubiquitous and bind DNA nonspecifically (Cosgriff et al, 2010). Some of these nucleoid-associated proteins may contribute to the formation of large scale-structures such as topologically isolated supercoiled domains and transcription foci.

SMC complexes are another group of factors that play an important role in DNA compaction and structural maintenance in many species across the bacterial kingdom (Nolivos et al, 2014). Eukaryotes have as many as six SMC proteins per species that can form three distinct heterodimers with specific functions. They are known to be involved in a variety of processes such as chromosome segregation (Yoshinaga et al, 2000), condensation (Hirano et al, 2005), repair (Wu et al, 2012), and cohesion (Yoshigana et al, 2000, Wu et al, 2012). Bacteria usually have one SMC protein per species, which forms a homodimer. Bacterial SMC consists of a long antiparallel coiled coil with a hinge domain that is also involved in dimerization at one end and an ATPase domain at the other end (Wu et al, 2012). Bacterial SMC exists as a homodimer that associates with the two accessory proteins ScpA and ScpB to form a ring-like structure that can be clamped onto the DNA in an ATP-dependent manner (Hirano et al, 2006) (Figure 1.3). The bacterial SMC complex is analogous to condensin (the eukaryotic SMC complex involved in DNA condensation) and is known to be involved in chromosome condensation (Wilhem et al, 2015) and segregation. In the case of *E. coli*, the absence of SMC (also called MukB in this species) (Burmann et al, 2015) causes severe chromosome segregation defects (Hirano et al, 2006).

As mentioned before, the chromosome segregation machinery found in bacteria, the ParABS system is also involved in chromosome organisation, that is in the tethering of the *ori* region to the pole via interaction with polar organisation proteins, such as PopZ in *C. crescentus* (Ebersbach et al, 2005), bactofilin in *M. xanthus* (Lin et al, 2017) or DivIVA in *Actinomycetes* (Letek et a, 2008). It has been shown that SMC and ParB protein clusters overlap or are in close proximity. Studies in *B. subtilis* revealed that the SMC complex is recruited to the *ori* region in a ParB-*parS*-dependent manner (Sullivan et al, 2009). Besides, chromosome conformation capture analysis revealed that the ParB-*parS*-dependent recruitment of SMC to several *parS* sites is essential for the condensation of the origin domain (Kamada et al, 2018). It has also been found that deletion of SMC in *C. crescentus* also resulted in decreased inter-arm interactions, validating the global importance of SMC protein as a chromosome organisation tool. In the case of *B. subtilis*, SMC was also found to be involved in individualising the newly replicated origins by its loading on to the *parS* sites where it encircles the DNA.

*In vitro* and *in vivo* studies have provided evidence of SMC complexes being loaded at the ParB binding site close to *ori* and they move along the DNA towards the terminus by loop extrusion. This tethers the two chromosomal arms, thus bringing them into contact. Some studies have also shown that SMCs may be involved in DNA bridging (Kamada et al, 2018).

In the case of *E. coli* and other γ-proteobacteria, a protein complex called MukBEF is present, in which MukB (Mäkelä et al, 2020) is a functional homolog of the SMC protein, while MukE and MukF play the same role as the SMC accessory proteins ScpA and ScpB. MukB colocalizes with the origin region like SMC does in the case of *B. subtilis* (Danilova et al, 2007). Deletion of the corresponding genes results in the generation of anucleate cells and a disruption of the transverse organisation of the chromosome, which indicates that

they play a role in chromosome organisation as well as segregation (Nicolas et al, 2014). This can be explained by the fact that MukBEF complexes are involved in recruiting the topoisomerase TopoIV to the *ori* region to mediate the decatenation of newly replicated chromosomes (Nicolas et al, 2014). It is hypothesised that the MukBEF complex also triggers the decatenation activity of TopoIV. Apart from the *ori* region, the Muk proteins are also associated with the *ter* region, where they interact with MatP. MatP recognizes and binds to *matS* sites clustered around *ter* and organises the *ter* macrodomain (Mercier et al, 2008). Additionally, MatP removes Muk proteins from the *ter* region to avoid untimely activation of TopoIV (Nolivos et al, 2014).

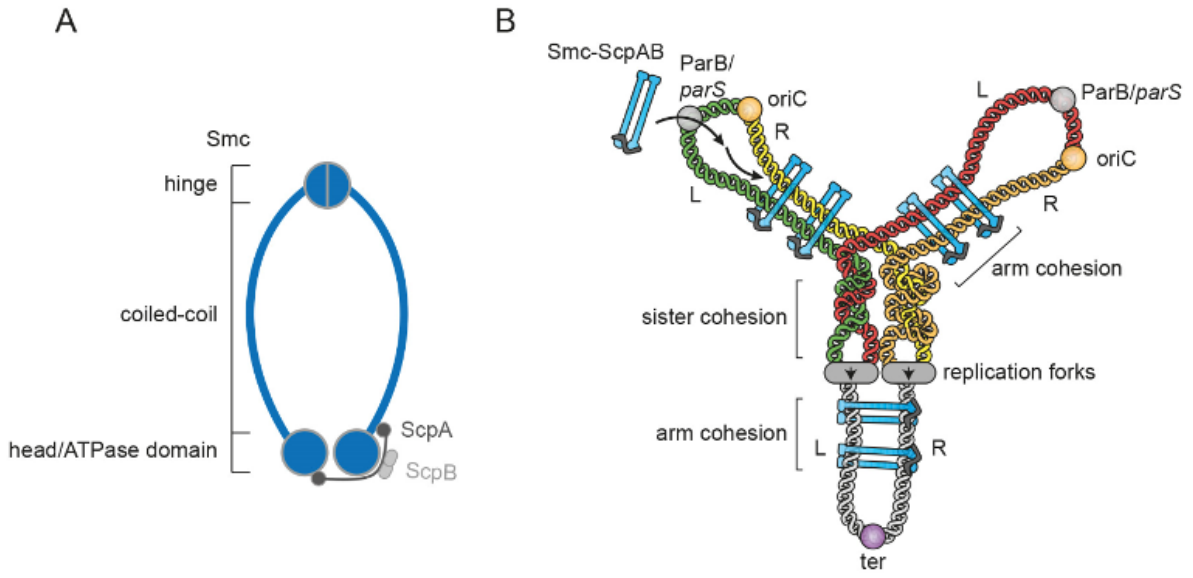


**Figure 1.3: SMC complex.** A. Schematic representation of the architecture of the SMC-ScpAB complex. B. Model showing the role of the SMC-ScpAB complex in *ori* separation and chromosome organisation in *B. subtilis*. Adapted from (Bürmann et al, 2015).

## Bacterial chromosome replication

DNA replication is a process in which a DNA molecule is duplicated into two by unwinding of the two strands and synthesis of complementary new strands (Figure 1.4) (Mott et al, 2007). Several enzymes such as DNA helicase, primase, DNA polymerase, RNA exonuclease and single-stranded DNA-binding protein catalyse these processes and they need to be tightly coordinated. Hence, this process is very intricate and needs to be executed with high precision and accuracy. Most bacterial genomes consist of one circular chromosome whose size ranges from 1 to 9 Mb (Land et al, 2015). However, some species may contain two or more circular chromosomes (such as *V. cholerae*) (Rasmussen et al, 2001).

Bacterial chromosomes have a single origin of replication (*ori*), in contrast to eukaryotes, which have multiple origins of replication (Méchali et al, 2010). Consequently, the single *ori* in bacteria results in a single replication eye upon new DNA synthesis. Initiation is achieved by the initiator protein DnaA, which cooperatively binds to specific recognition

sites called DnaA boxes within the *ori* region (Katayama et al, 2017). Upon ATP binding, this interaction triggers the separation of the DNA strands at the AT-rich DNA unwinding elements (DUE). This provides the entry site for the replisome to assemble. First, the helicase is recruited in a DnaA-dependent manner and the replication forks are established. Subsequently, the other replisome components are recruited and the forks proceed on either arm until they meet in the *ter* region and replication ends. As the helicase unwinds the DNA, separating the two complementary DNA strands, the leading strand is synthesised continuously, while the lagging strand is synthesised in 1-2 Kb fragments, starting from primers added by the primase (Beattie et al, 2015). The core polymerases are loaded into each replication fork by the clamp loader. These three proteins bind to the sliding clamp, ensuring processive activity of the replisome. Upon termination of DNA replication, the replisome disassembles and the interlinked sister chromosomes are resolved, thus marking the completion of replication (Duderstadt et al, 2014).

The subcellular position of the replisome depends on the organisation of chromosomes within the cell. To ensure that chromosome replication is regulated such that only one replication event occurs per cell cycle, several factors play a role. For example, as DnaA binding is the first step, the binding of DnaA is regulated such that it occurs only once per cell cycle in bacteria such as *C. crescentus* (Collier et al, 2012). This is ensured by the presence of competitors that bind to the *ori* region, thereby preventing the access of DnaA to the *ori*. Besides, the ATP-binding activity of DnaA adds another layer of regulation to this event. Furthermore, *dnaA* transcription is also regulated in a cell cycle-dependent manner. For instance, in the case of *C. crescentus*, chromosome replication is restricted to a specific cell type, the stalked cell. DNA replication initiates specifically and only once during the swarmer-to-talked cell (G1-S) transition (Gorbatyuk et al, 2004, Wortinger et al, 2000) which marks the onset of the replicative phase of the cell cycle, thus ensuring the tight control of chromosome replication and restricting it to once per cell cycle. The global cell cycle regulator CtrA plays a major role in the initiation of the G1-S transition and acts as a response regulator that restricts chromosome replication to the S phase. CtrA binds to *ori* and thus physically blocks DnaA boxes, preventing the initiation of replication (Frandi et al, 2019). Active, phosphorylated CtrA accumulates only in swarmer cells and late pre-divisional cells by a combination of regulated synthesis, phosphorylation and proteolysis, whereas it is absent throughout S phase. It also regulates the synthesis of various other proteins, thus making it essential to demarcate the G1 and S phases (Collier et al 2012, Gorbatyuk et al, 2004). Active CtrA is distributed in a gradient within the cell, which ensures that the future stalked cells contain much less phosphorylated CtrA, while the swarmers contain a high concentration of phosphorylated CtrA. In stalked cells, an additional mechanism is at work to regulate chromosome replication such that it happens only once per cell cycle, once CtrA has been cleared from the cell. It is mediated by the HdaA protein, a DnaA homolog that converts DnaA to its inactive, ADP-bound state and thus ensures that the chromosome replication does not start a second time after the first initiation event (Wargachuk et al, 2015).

Owing to recent advances in microscopic techniques and live-cell imaging, replisome dynamics can be directly studied, for example by detecting the location of the replisome and the duration of replication at a single-cell level. The visualisation of replication can help us understand the coordination of this process with other major cell cycle events and is hence a very useful tool. Replication is visualised by the fusion of different replisome subunits, such as DNA polymerase III, to a fluorescent protein. The choice of subunit to create the fusion protein is dependent upon the specific application and the specific bacterial species. The β-sliding clamp is one of the replisome components that can be used to create a fusion protein for visualisation purposes. Single-stranded DNA binding protein (SSB) has also been tested in several studies for the same purpose.

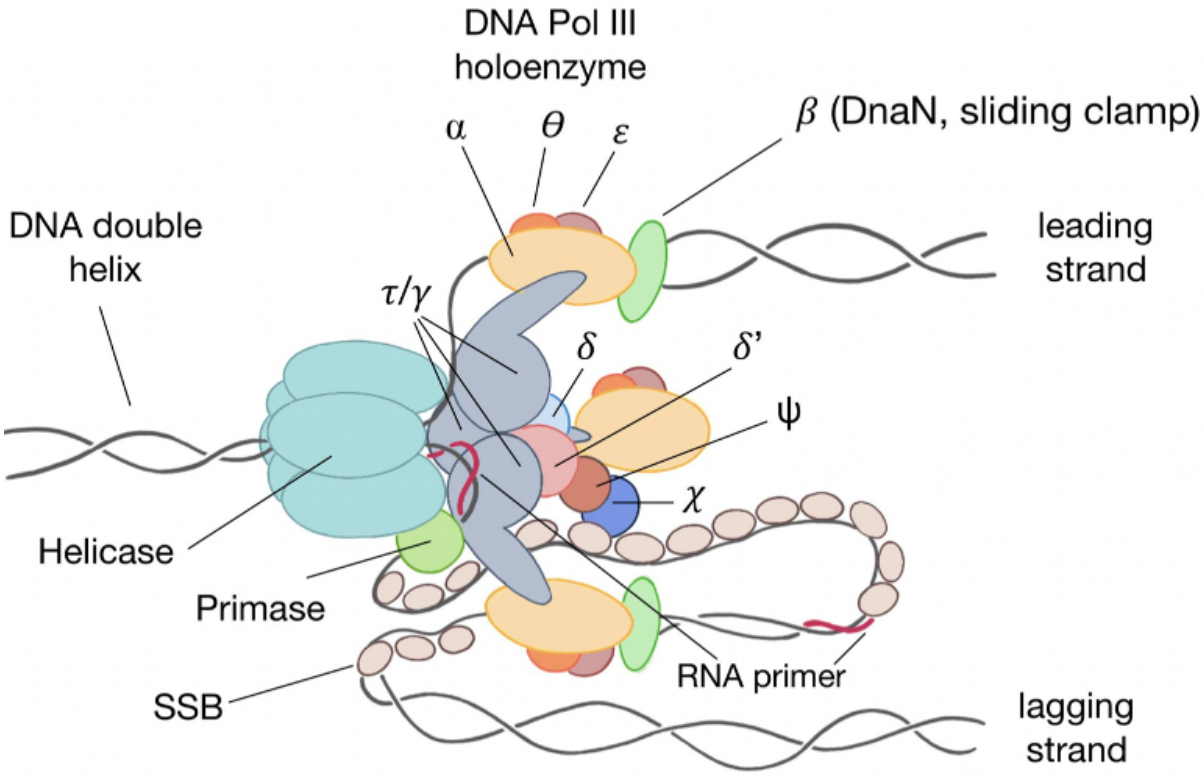


**Figure 1.4: Cartoon representation of the replisome at *ori*.** Helicase is shown unwinding the double helix, while DNA polymerase is seen synthesising new strands. The leading and lagging strands can be seen separately and primase and RNA primer can be found on the lagging strand. Adapted from (Trojanowski et al, 2018).

## Bacterial DNA segregation – the ParAB*S* system

The accurate segregation of genetic material in bacteria was initially studied in low-copy-number plasmids, which are segregated by active DNA partition processes (Austin et al, 1981). High-copy-number plasmids, by contrast, are distributed in the bacterial cell by passive diffusion. The maintenance of low-copy-number plasmids is mediated by dedicated partition (*par*) systems, three-component systems that include centromere-like site and a closely located *par* operon encoding two protein, a nucleotide triphosphatase (NTPase) and

a centromere-binding protein (CBP) (Nördstorm et al, 1980). There are three main types of *par* systems, based on the type of NTPase they employ (Schumacher et al, 2012). The most common are the type I systems, whose function relies on a Walker-type ATPase, as is the case for the chromosome partitioning ParAB*S* system. The type I family is further divided into types Ia (usually chromosomally encoded) and Ib (usually plasmid-encoded), based on the size and sequence of the ParA proteins. Whereas type I systems were found to segregate both chromosomes and plasmids, the remaining types have so far only been reported in the context plasmid segregation. Type II systems use actin-like NTPases, and type III systems use a tubulin-like GTPase (Gerdes et al, 2000). Partition operons are autoregulated at the transcriptional level by the Par proteins (the CBP proteins in Ib, II and III systems, and the NTPase in the type Ia systems).

As mentioned above, most plasmids use the ParAB*S* system for proper segregation. It is encoded in an operon comprising genes for a Walker-type NTPase (ParA) and a DNA-binding protein (ParB) that binds to both ParA and the third component, a centromere-like DNA sequence called *parS* (Gerdes et al, 2000). The centromere-binding protein uses either a helix-turn-helix (HTH) (such as by ParB), a ribbon-helix-helix (RHH), or a winged HTH motif for binding to *parS*. Even though there are structural differences between the ParAB components of plasmid-encoded ParAB*S* systems among different bacteria, the basic mechanism of plasmid segregation is conserved. Operons encoding Walker-type ATPases and HTH motif-containing DNA-binding proteins homologous to plasmidic ParAB proteins were later also discovered in bacterial genomes as well (Jensen et al, 2001). In fact, the presence of these operons is almost universal in the bacterial kingdom, since 75-80 % of all bacteria possess *parAB* operons to segregate their chromosomes (Jalal et al, 2020). Chromosomal *parAB* operons are usually located in the immediate vicinity of the replication origin. The cognate *parS* sites are typically 16 base pairs long palindromic sequences, generally placed in the origin region (Jalal et al, 2020(b)). The number of *parS* sites can vary from species to species, ranging from one in *Xanthomonas* species (Ucci et al, 2014) to as many as 22 in *Myxococcus xanthus* (Osorio et al, 2019). *parS* sites are highly conserved and have the consensus sequence TGTTNCACGTGAAACA (Gerdes et al, 2000). Notably, *par* genes have so far not been found in the chromosomes of two families of γ-proteobacteria, namely the *Enterobacteriaceae* (e.g. *E. coli*) and *Pasteurellaceae* (e.g. *Haemophilus influenzae*) (Gerdes et al, 2000). It has also been noted that a few species lack particular *par* elements, including *Streptococcus pneumoniae*, which does not have a *parA* homolog (Pinho et al, 2013). The chromosomal *par* operons were shown to stabilise plasmids that were otherwise unstable when containing a single *parS* site in a heterologous host (Yamaichi et al, 2000).

## The chromosomal ParAB*S* system

The chromosomally encoded ParA homologs cluster in a distinct subgroup (type Ia) compared to their plasmidic counterparts (type Ib), as they lack the N-terminal DNA-binding domain that autoregulates *par* operon expression in plasmidic systems (Jensen et al, 2001). Other properties such as their non-specific DNA-binding activity, their ability to interact with ParB, and their classification as Walker-type P-loop ATPases are conserved

(Lutkenhaus et al, 2012). When bound to ATP, ParA forms a dimer that interacts nonspecifically with DNA and thus associates randomly with the nucleoid. Upon interaction with ParB, it hydrolyses ATP to ADP and dissociates into monomers, which lack DNA-binding activity and are thus released from the DNA. There are cell pole-associated ParA-sequestering proteins, such as PopZ or TipN in *C. crescentus*, that capture monomeric ParA and thus prevent its immediate re-dimerisation and reloading onto the DNA (Schofield et al, 2010). Collectively, this reaction cycle creates a gradient of dimeric ParA, with the lowest concentration close to the duplicated *ori* region that carries ParB bound to *parS* and the highest concentration at the adjacent cell pole. The *parS*-bound ParB proteins follow this gradient by interacting dynamically with ParA dimers, thus gradually moving one of the *ori* regions to the opposite pole and setting the basis for the segregation of the duplicated chromosomes (Figure 1.5). Several models have been proposed to explain the mechanism underlying this process. One of the earlier suggestions was that ParA forms filaments that can exert mechanical force on the replicated sister chromosomes and segregate them by pulling on the ParB-*parS* complexes in a mitotic-like process (Iniesta et al, 2014). According to this model, ParA polymerizes into thin filament bundles when bound to ATP. Depolymerization of ParA filaments through ParB-induced ATP hydrolysis then pulls the ParB-*parS* complex and its associated chromosomal origin region. However, there was no solid evidence that ParA formed long filaments *in vivo* or *in vitro*. Recent experimental advances combined with theoretical modelling studies have led to alternative models, including the diffusion-ratchet model (Hu et al, 2017) or the DNA relay model (Lim et al, 2014). According to the diffusion ratchet model, the ParB-*parS* movement follows a gradient of ATP-bound ParA. *In vitro* reconstitution studies showed that ParA-ATP dimers binds DNA nonspecifically and that the binding of ParB to the DNA-bound ParA dimers triggers the ATPase activity of ParA, releasing ParA from the DNA. This sequence of events causes a local depletion of ParA dimers around the ParB-*parS* complex. As a consequence, the ParB-*parS* complex becomes mobile and starts to diffuse within the cell, until it reattaches to adjacent ParA dimers and is immobilised again. Repeated cycles of ParA binding, ATPase stimulation and ParA release are thought to cause the directed diffusion of the *ori* region towards higher concentrations of DNA-bound ParA dimers, eventually leading it to the opposite pole of the cell. However, mathematical modelling suggested that directed diffusion alone was too slow to enable the rapid movement of the *ori* regions during segregation. Hence, another model, the DNA relay model, was proposed (Lim et al, 2014). It suggests that the elasticity and dynamic motion of chromosomal DNA, caused by energy-consuming processes such as transcription, helps to speed up the translocation of the ParB-*parS* complex. This model explains the rapid and directed segregation of sister chromosomes without having to assume that ParA formed long filaments.


**Figure 1.5: The ParAB*S* system of *C. crescentus.*** PopZ (pink) is located at the cell pole and interacts with ParB (green). TipN localises to the pole opposite the *ori* region. Dimeric ParA (yellow) is randomly associated with the nucleoid, which in *C. crescentus* extends throughout the entire cell. The chromosome is represented by a blue line. As the cell cycle progresses, the newly formed ParB-*parS* complex moves to the new pole in a ParA-dependent manner. The concentration of dimeric ParA is decreased upon contact with the new partition complex. Finally in the daughter cells, the typical longitudinal organisation of the chromosome is restored (Adapted from PhD thesis, A.Jung).

Chromosomal ParB proteins are highly conserved among bacteria (Jalal et al, 2021) and have three distinct domains, including (i) an N-terminal non-structured region that interacts with ParA, (ii) a conserved domain that has recently been found to bind and hydrolyse CTP (Figure 1.7), (iii) a HTH-containing DNA-binding domain, (iv) a non-structured linker region, and (v) a C-terminal dimerisation domain, which in some species (such as *B. subtilis*) also has non-specific DNA-binding activity (Osorio-valeriano et al, Soh et al).


**Figure 1.6: Schematic representation of ParB.** The N-terminal CTPase domain (NTD), the DNA-binding domain (DBD) with the HTH motif (highlighted in orange) and the C-terminal dimerization domain (CTD) of ParB are shown.

ParB recognises and binds to the *parS* sequences and further spreads to adjacent DNA regions, creating a large nucleoprotein complex called the “partition complex” (Funnell et al, 2014). It has been shown that ParB variants defective in DNA spreading are also defective in chromosome segregation (Graham et al, 2014). Until recently, it remained enigmatic how even a single *parS* site can mediate the accumulation of hundreds of ParB molecules in the origin region. Recent studies have revealed that apart from representing a HTH-containing DNA-binding protein, ParB is also a cytidine triphosphate (CTP)-binding molecular switch that can bind and hydrolyze CTP (Osorio-valeriano et al, 2019, Soh et al, 2019, Jalal et al, 2020). The nucleotide-binding site includes a highly conserved arginine patch (GERRFRA), which had already been known to be important for chromosome segregation and ParB spreading. It was shown that upon CTP binding to the NTD and interaction of the DBD with *parS*, the two NTDs of a ParB dimer homo-dimerise, thereby closing the ParB dimer into a ring that embraces the *parS* site (Figure 1.7). Closure of the ring induces a conformational change that reduces the affinity of the HTH domain for the

*parS* site, inducing its release from *parS*. As a consequence, the bound DNA is moved to the space in between the non-structured linkers of the dimer, thus allowing the ParB ring to diffuse away from the *parS* site and facilitate ParB spreading. This allows new ParB molecules to bind to the *parS* site again. The residence time of ParB rings on DNA, and thus the degree of spreading, is controlled by the CTPase activity of ParB, as the hydrolysis of the CTP molecules opens the ring, causing it to dissociate from the DNA (Osorio-valeriano et al, 2021). The open ParB dimers are now free to reassociate with CTP and enter the cycle again. Spreading may be restricted by road blocks formed by NAPs (Jalal et al, 2021). ChipSeq studies have shown that, interestingly, the extent of ParB spreading varies from species to species depending on the nature of the NTD of the ParB protein they possess.

Recent studies have suggested that ParB loaded at *parS* can, at low frequency, recruit new ParB molecules independently of the *parS* site. Thus, not every ParB molecule may have to be loaded through *parS* (Tišma et al, 2021). This further strengthens the importance of ParB-ParB interaction in partition complex formation. It has also been shown that the nonspecific DNA-binding activity of ParB may also play a role in the condensation of DNA within partition complexes (Jalal et al, 2021).

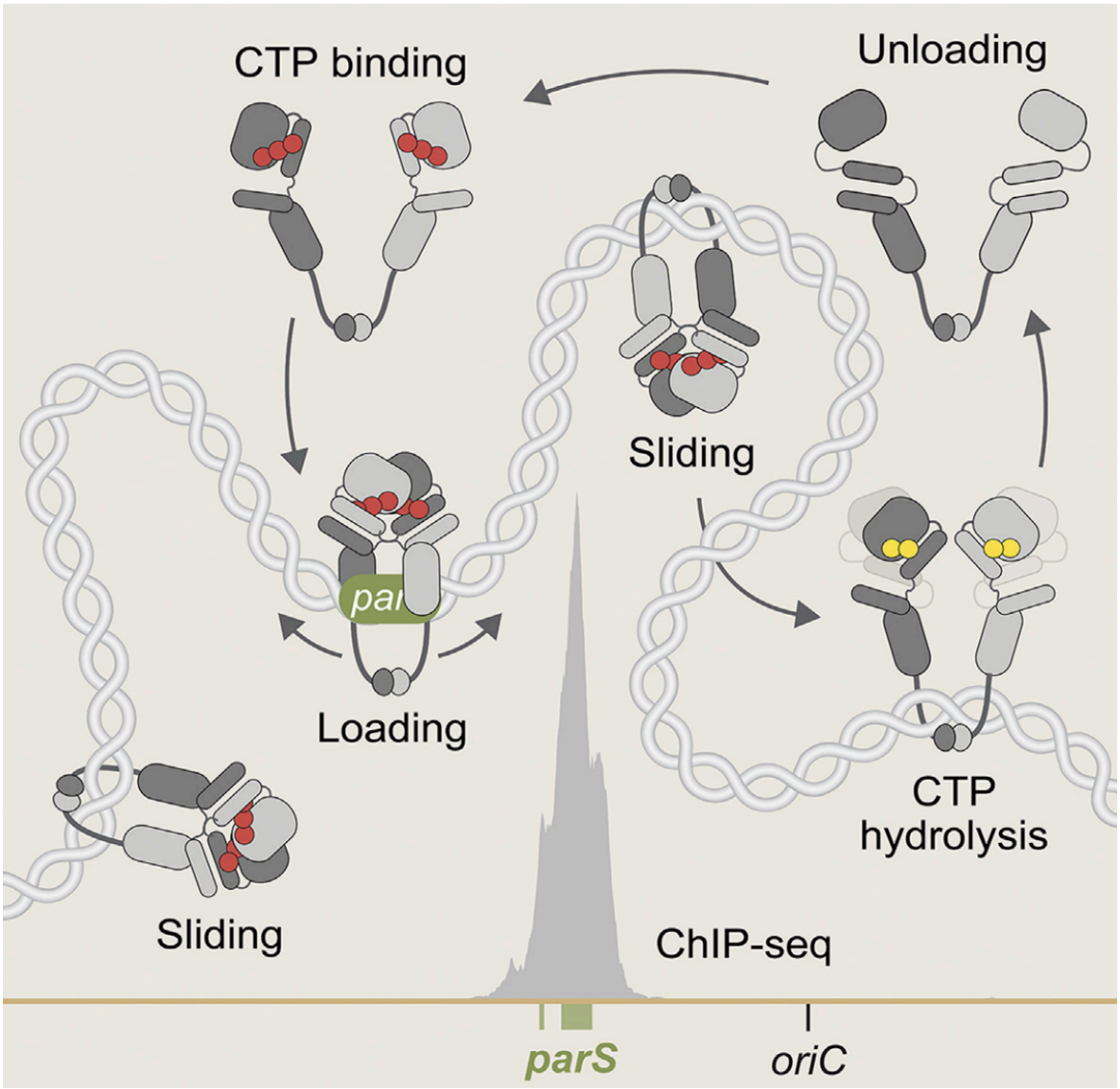


**Figure 1.7: CTP-binding cycle of ParB.** The cycle of ParB binding and spreading to the DNA depending on CTP/CDP association is represented. ParB dimerises at the C-terminal, each monomer represented as blue and grey, CTP is represented by the red dots, CDP by the yellow dots. *parS* site is highlighted in orange. The amino acids represent the residues that abolish the respective functions upon mutation. (Figure taken from Osorio et al, 2021).

Interestingly, recent studies on *Pseudomonas aeruginosa* revealed that apart from binding to the canonical *parS* there are several half-*parS* sites across the genome that ParB can recognize (Kawalak et al, 2018). This is not exclusive for *P. aeruginosa* as 6 different ParBs have been found to recognize half-*parS* sites (mainly GTTCCAC or GTTTCAC) in heterologous hosts as well (Kawalek et al, 2018). It is conceivable that the presence of hundreds of half-*parS* sites may be involved in enabling ParB to regulate the topology of the chromosome or in providing space for ParB to bind to and facilitate ParB-ParB interaction at distant DNA positions playing a role in global DNA condensation.

## ParB and divisome positioning

Cell division in bacteria takes place by means of the formation of a functional divisome at the site of cell division. The major protein involved in divisome assembly is FtsZ (Silber et al, 2020). This protein is a prokaryotic homologue of tubulin and can polymerise head to tail, forming filaments that assemble into a ring-like structure at the division site (Bi et al, 1991). It also recruits other divisome components and thus mediates cell constriction (Corbin et al, 2007). FtsZ can bind to and hydrolyse GTP (Scheffers et al, 2002). Studies have revealed that FtsZ treadmilling is essential to condense the filaments into a dense ring and facilitate septal constriction, thus bringing about cell division (Whitely et al, 2021). The robust placement of the Z-ring thus plays a crucial role in the spatial regulation of cell division.

It has been found out that in several bacteria, the ParB component interacts with proteins implicated in cell division. For example, in bacteria like *Streptococcus pneumoniae*, *Deinococcus radiodurans*, *Bacillus subtilis* and *Mycobacterium smegmatis*, the ParB (or equivalent) proteins interact with DivIVA (or equivalent) proteins, implicating a connection between chromosome segregation and cell division (Kawalek et al, 2020). Similarly, in *D. radiodurans*, the ParB protein also interacts with the MinC protein, which is involved in the regulation of FtsZ ring placement (Maurya et al, 2016). Apart from that, in *Magnetospirillum gryphiswaldense*, *Rhodobacter sphaeroides*, *H. neptunium* and *C. crescentus*, the ParB protein interacts with MipZ, a negative regulator of Z-ring positioning. Thus, it is known that the ParAB*S* system interacts with the regulators of cell division directly or indirectly. These regulators of Z-ring positioning can be positive regulators or negative regulators. Interestingly, many of these regulators are, like ParA, P-loop ATPases.

## The P-loop ATPases that regulate the division site placement

A combination of nucleoid occlusion factors and dedicated FtsZ placement machinery facilitate the division site placement in bacteria. The most commonly studied systems such as *E. coli* and *B. subtilis* possess the negative regulator of Z-ring positioning, the Min system. The Min system comprises the MinC, MinD and MinE proteins that inhibit FtsZ polymerization in the polar and subpolar regions, restricting it to the mid-cell. MinD is a P-loop ATPase that upon ATP binding, forms a dimer that associates via its C-terminal amphipathic helix (Park et al, 2011) to the cytoplasmic membrane. The MinC protein directly interacts with FtsZ and inhibits its polymerisation. The C-terminal domain of MinC interacts with MinD that activates its FtsZ inhibitory activity and thus the N-terminal domain of MinC blocks the ring formation (Zhou and Lutkenhaus, 2005, de Boer et al,1989, Cordell et al, 2001). The ATP-bound MinD causes the MinCD complex to remain attached to the membrane near where it inhibits the FtsZ ring formation. In the case of *E. coli*, a third component, MinE binds to the MinCD complex and stimulates the ATPase activity of MinD causing the MinCD complex to dissociate from the membrane (Loose et al, 2008). Subsequently, the MinCD proteins occupy the opposite pole, where MinE is absent. The

iteration of this process causes the pole-to-pole oscillation of the MinCD complex, effectively blocking Z ring formation at the poles.

In the case (Schumacher et al, 2017) of the delta proteobacterium *Myxococcus xanthus,* It has been shown that the Z ring positioning is regulated by the positive regulator system, the PomXYZ system. The PomX and PomY proteins function together with the ParA/MinD-type ATPase PomZ to stimulate and position the FtsZ ring at the midcell region. It has been noticed that the PomXYZ complex may directly recruit FtsZ to the division site. Like ParA, PomZ is a monomer in the ADP-bound form, forms ATP-bound dimers and exhibits ATP-dependent non-specific DNA binding activity as a dimer. It is also noted that its partner proteins, PomX and PomY, stimulate independently the ATPase activity of DNA-bound PomZ. Interestingly, neither MinE nor PomX/Y are homologues of ParB.

Similar to these mechanisms, the P-loop ATPase that negatively regulated the Z-ring positioning in *C. crescentus* is MipZ, which undergoes an ATPase-dependent monomer-dimer switch similar to that of ParA.

## The mid-cell positioning of FtsZ by MipZ

In the case of the *C. crescentus*, the ParA-like protein MipZ is responsible for the mid-cell positioning of the FtsZ ring, tightly coupling division site placement to the dynamics of chromosome segregation. MipZ interacts with ParB and thus coordinates cell division with chromosome segregation. Similar to ParA, MipZ can exist as a ADP-bound monomer and ATP-bound dimer (Figure 1.7), and it binds to DNA nonspecifically as a dimer. MipZ monomers interact with ParB, which forms *ori*-associated partition complexes that are tethered to the cell poles (both poles for pre-divional cells and only one pole in the case of non-replicative swarmer cells). Unlike in the case of ParA, where ParB stimulates ATP hydrolysis and dissociation of the ParA dimer, MipZ monomers are thought to be stimulated to dimerize upon interaction with the partition complex by an as-yet unknown mechanism. Thus, ParB acts as a source of dimeric MipZ and thus promotes the formation of a MipZ dimer gradient, with the MipZ concentration being highest at the cell pole and gradually decreasing with increasing distance from the cell pole. The formation of this gradient is facilitated by the capture and immobilisation of MipZ dimers on the meshwork of chromosomal DNA extending throughout the *C. crescentus* cytoplasm. In predivisional cells, which have completed chromosome replication and segregation, a bipolar gradient is formed, with a concentration minimum at the mid-cell (Figure 1.9). DNA-associated MipZ dimers interact with FtsZ and inhibit its polymerization, preventing the formation of a functional Z ring. Consequently, cell division occurs only at the mid-cell, where the MipZ concentration is the lowest. The intrinsic ATPase activity of the MipZ dimers ensures that they are monomerised. Since monomers no longer bind to the DNA, they fall off from the DNA. Thus, dimers of MipZ are mostly concentrated in the polar and subpolar regions, where, consequently, the Z-ring formation is inhibited. The monomers find their way back to the poles where it interacts with ParB and re-enters the ATPase cycle as dimers. Thus,

the interaction of MipZ with ParB at the pole coupled with its intrinsic ATPase activity and DNA-binding property as dimers causes the gradient formation of the MipZ dimers that regulates the position of the Z-ring and thus, of the cell division in the case of *C. crescentus*.

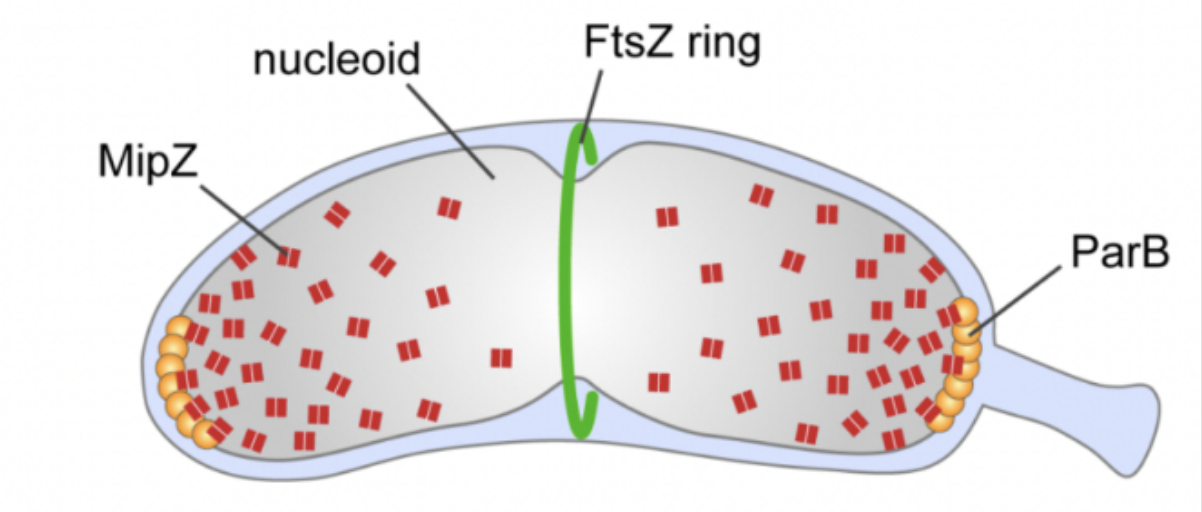


**Figure 1.8: Schematic representation of bipolar gradient formation by dimeric MipZ in a ParB-dependent manner in *C. crescentus*.** ParB is localised at both poles (yellow) in the pre-divisional cell. The green ring represents the stable Z-ring that has formed in the middle of the cell. It can be noticed that the red colored boxes that represent dimeric MipZ form gradients, with the lowest concentration at the mid-cell and highest concentration at the poles. Adapted from (Kiekebusch et al, 2012).

In another alphaproteobacterium, *Rhodobacter sphaeroides*, a MipZ gradient was not observed. Instead the dimers are localised at the mid-cell (Thanbichler et al, 2006, Kiekebusch et a, 2012). Studies revealed that *R. sphaeroides* MipZ interacts with ParB as a monomer. However, unlike *C. crescentus*, where MipZ is involved in Z-ring positioning, dimeric *R. sphaeroides* MipZ seems to be involved in Z-ring assembly, as dimeric forms are present at the mid-cell.

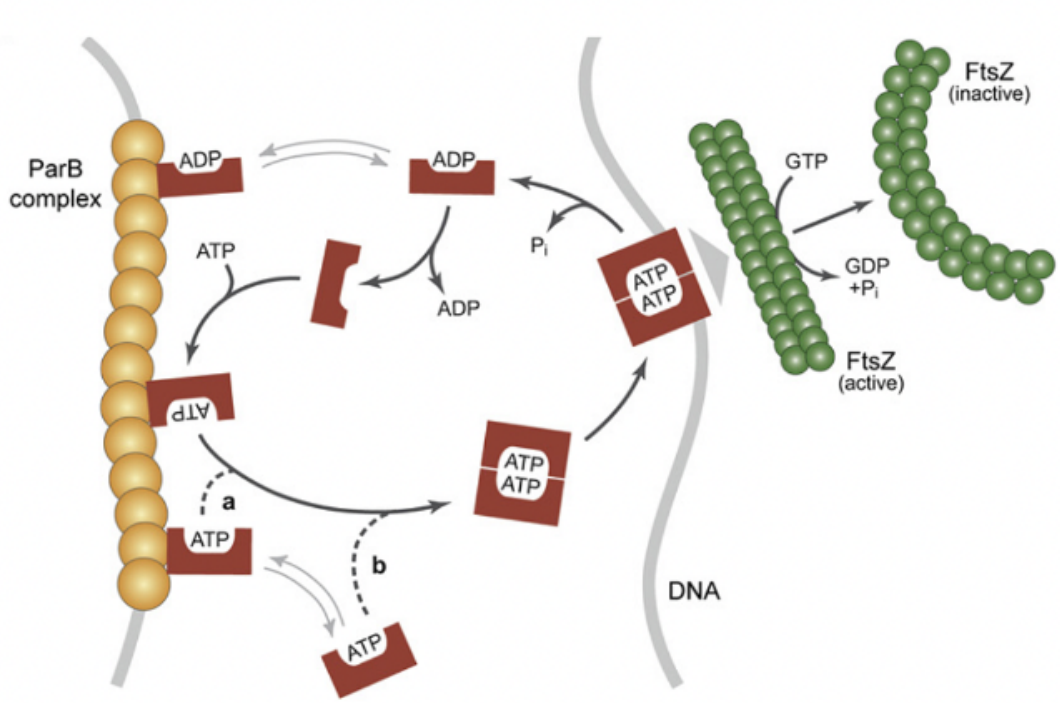


**Figure 1.9: Schematic representation of the ATP-dependent monomer-dimer cycle of MipZ and its interaction with its interaction partners ParB, DNA and FtsZ.** In red, monomeric ADP-bound or dimeric ATP-bound MipZ can be seen. The dimers can be seen interacting with the DNA (grey) and the FtsZ ring (green). Both monomers and dimers interact with the ParB complex (yellow). Adapted from (Kiekebusch et al, 2012).

In *Magnetospirillum gryphiswaldense*, there are two MipZ proteins, MipZ1 and MipZ2. While MipZ1 has a crucial role in cell division by positioning the Z-ring, the absence of MipZ2 only causes minor cell division defects (Toro-Nahuelpan et al, 2019). MipZ1 interacts with ParB and forms a bipolar gradient like the MipZ homologue of *C. crescentus*, while MipZ2 localises to the cell division site similar to the MipZ of *R. sphaeroides* (Dubarry et al, 2019).

Thus, in conclusion, the essential cellular processes of chromosome segregation and cell division are tightly coordinated in the bacterial cell by means of various strategies. In this study, we focus on two alphaproteobacteria, *H. neptunium* and *C. crescentus*, and investigate how their ParA (and ParA-like) proteins and ParB homologues function together to support their cell biology and cell cycle events, with a focus on chromosome segregation and cell division.

## Aims of this study

Chromosome organisation and segregation are mainly studied in established model organisms such as *E. coli*, *C. crescentus*, *B. subtilis* that are mostly rod-shaped. In our lab, a stalked budding bacterium, *Hyphomonas neptunium*, was established as a new model organism. Recent studies have shown that *H. neptunium* possesses a ParABS system and organises its chromosome in a longitudinal manner. Chromosome segregation proceeds in a unique two-step manner. In the first step, the chromosome segregates within the mother cell. After a time lag, the second step, the segregation through the stalk, commences. In this study, we aim to understand the dynamics of the *ori* region during segregation by tagging the region close to *ori* and comparing its movements with *ori*. Chromosome loci tagging followed by microscopy points to the fact that the chromosome is longitudinally arranged in the cell. We also aim to complete this analysis by tagging one more region to complete this dataset to conclusively prove that the chromosome is indeed longitudinally organised in the cell. Most importantly, we aim to understand the implication of chromosome replication in the second step of chromosome segregation. We aim to systematically dissect the temporal relationship between chromosome replication and segregation using microscopic methods and data analysis. The second step of segregation is co-ordinated by a protein so-far not known. Interestingly a ParA-like protein in *H.neptunium*, HNE-0708 is found to be a novel protein with unknown functions. This protein shares similarities with ParA in possessing the characteristic Walker A and B motifs. This study aims to contribute to the understanding of this protein and its potential role in chromosome segregation in *H.neptunium*. We aim to characterise this protein biochemically and test its interaction with DNA. Finally, we also aim to understand the interaction of the ParA-like protein MipZ that is indispensable for the robust placement of the FtsZ ring in *C.crescentus* with that of the chromosome segregation protein ParB. We aim to understand the molecular interfaces involved in this interaction. The dimerisation of MipZ, which occurs at the cell pole, is crucial for the establishment of its interaction with DNA, its gradient formation and its inhibition of a functional Z-ring formation. The interaction of MipZ with ParB is thus of central importance as this interaction connects cell division and chromosome segregation. In this study, we aim to analyse the ParB binding interface of MipZ and whether this interface is shared between DNA and ParB to competitively bind dimeric MipZ. We also aim to understand the interaction interface of MipZ on the surface of ParB. As the ParB molecule interacts with both ParA and MipZ, we aim to understand if there is any overlap between these regions. Finally, we also aim to study the residues that are involved in MipZ-ParB interactions to shed light into the molecular mechanism by which MipZ dimers are formed in the presence of ParB.

# Chapter 2: Replication dynamics and chromosome segregation in *Hyphomonas neptunium*

## Introduction

As mentioned in the previous section, chromosome replication and segregation occur simultaneously in bacteria, unlike in their eukaryotic counterparts. Chromosome segregation in bacteria has largely been studied in rod-shaped model organisms such as *E. coli, C. crescentus* or *B. subtilis* (Gobou et al, 2021). However, only little information is available on the dynamics of this process in species with more complex cell shapes, such as the stalked budding bacterium *Hyphomonas neptunium* (Jung et al, 2019). *H. neptu*nium proliferates by budding off new offspring from the distal end of its stalk. This creates a challenge for the replication machinery, as it must not only segregate the sister chromosomes within the mother cell but also translocate one of the copies through the stalk and organise the chromosome in a longitudinal manner once it has arrived in the daughter cell. Therefore understanding chromosome segregation in *H. neptu*nium will add to our understanding of how morphologically diverse bacteria carry out chromosome segregation.

### *H. neptunium* as a model organism

*H. neptunium* is a marine alpha-proteobacterium that replicates via stalk-terminal budding (PhD Thesis A.Jung, Jung et al, 2019) and its cell cycle share similarity to that of *C. crescentus*. *H. neptunium* cells can be either motile swarmer cells or sessile stalked cells (Figure 2.1) (Badger et al, 2006). At a certain stage of their developmental cycle, the swarmer cells undergo a non-reversible transition to stalked cells, during which they shed their unipolar flagellum. The stalked cells synthesise a stalk at the pole opposite the previously flagellated pole and are replication-competent, so they can duplicate and segregate their chromosomal DNA. The new cells are formed at the distal end of the stalk via budding and, therefore, one of the chromosomal copies needs to be translocated through the stalk to reach the daughter cell (Jung et al, 2019). Once the duplicated chromosome reaches the daughter cell, the daughter cell separates from the stalked mother cell. The stalked mother cell then immediately enters the next reproductive cycle, whereas the swarmer offspring first needs to undergo the transition to a stalked cell to start cell division.

*H. neptunium*, like its relative *C. crescentus*, organises its chromosome in the cell in a longitudinal manner. The replication origin is placed at the flagellated pole and the terminus is at the future stalked pole. Furthermore, this bacterium possesses a putative chromosomal ParAB*S* system placed in an operon close to *ori*. The identified *parS* sites correspond to the global consensus sequence for chromosomal *parS* sites (Jung et al, 2019).

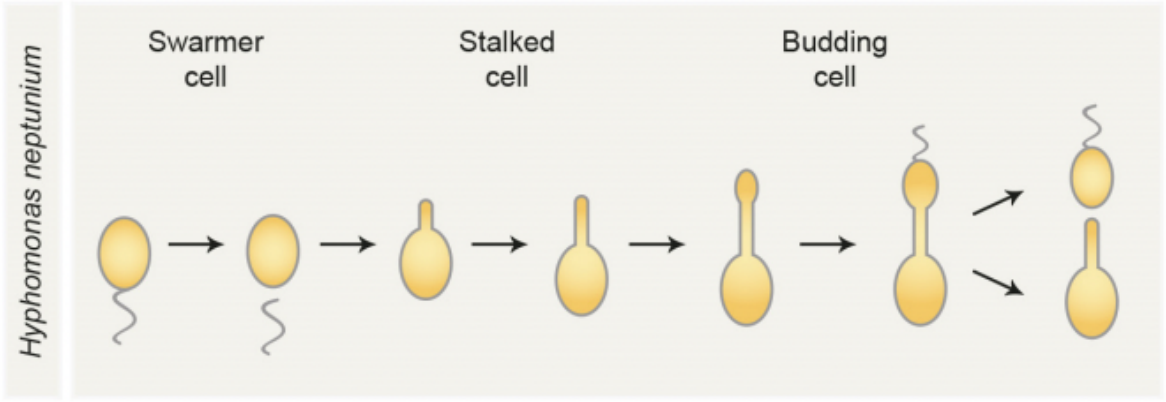


**Figure 2.1: Cell cycle of *H. neptunium*.** From left to right: the swarmer cell sheds its flagellum and develops a stalk at the opposite cell pole. A new swarmer daughter cell develops from the distal end of the stalk and buds off at the end of the cycle. Each division cycle gives rise to one swarmer cell, which must undergo the same cycle and one stalked cell, that can re-enter the budding and division process immediately. Adapted from (PhD thesis, A Jung).

## The ParAB*S* system of *H. neptunium*

*H. neptunium* possesses a single circular chromosome with a size 3.7 Mb, whose replication is limited to one round per cell cycle. Marker frequency analysis revealed the position of *ori.* The chromosome encodes a putative *parAB* operon in the *ori* region (Figure 2.2). Two *parS* sites were identified upstream of the *parA* gene.

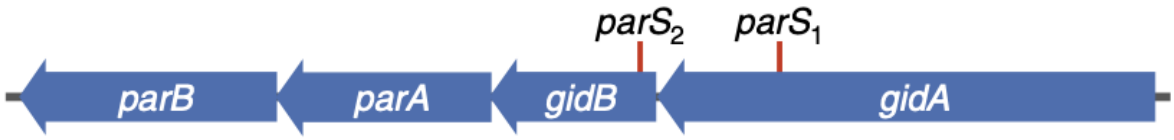


**Figure 2.2: Schematic representation of the chromosomal *parAB* operon.** The two *parS* sites in *H. neptunium* can be seen placed close to the *parAB* operon (Jung et al, 2019).

Unlike in most characterised bacterial systems, where replication is concomitant with segregation, *in vivo* studies in *H. neptunium* showed that the segregation of the ParB-*parS* complex is a two-step process. In the first step, one of the duplicated ParB-*parS* complexes moves to the stalked pole of the mother cell and remains there until a visible bud is formed at the tip of the stalk. In the second step, the chromosome is transported through the stalk to the bud. Data from long-stalked *H. neptunium* cells, generated by incubation in low-phosphate medium (Cserti et al, 2017), show that this transport occurs rapidly and in a directed manner, which indicates that it is driven by an active segregation mechanism. Time-lapse analysis of ParB revealed that sister chromosome segregation within the mother cell takes on average 30±13 minutes, with an average speed of 0.05±0.03 µm/minutes. Once the ParB-*parS* complexes are segregated within the mother cell, the complex at the stalked pole remains there for an average of 58±24 minutes before it traverses the length of

the stalk to reach the bud. The segregation through the stalk itself only takes 3-4 minutes, at a speed of ~1 µm per minute) (Figure 2.3).

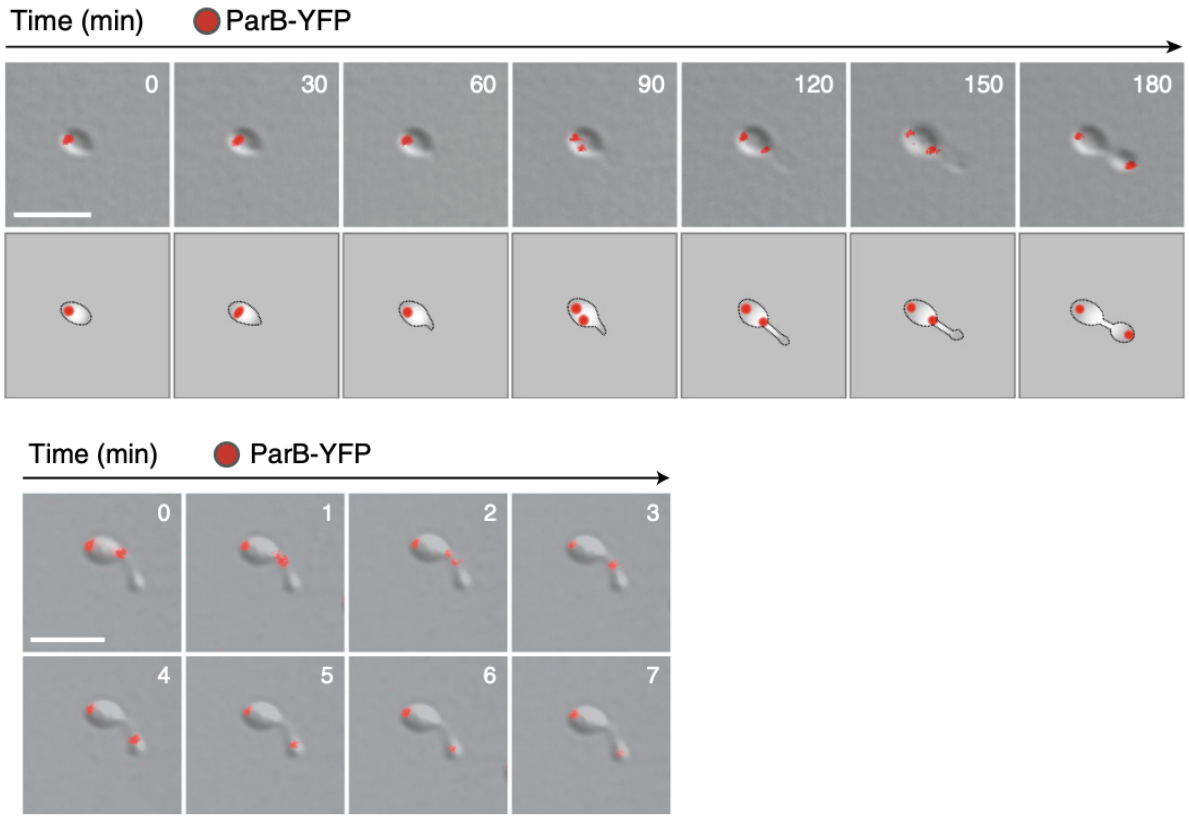


**Figure 2.3: ParB-YFP segregation is a two-step process.** Time-lapse analysis (overlay of DIC and fluorescence images) of an *H. neptunium* strain producing ParB-YFP. The lower panel shows the segregation through the stalk with a time resolution of 1 minute. Scale bar: 3 µM. Adapted from (PhD thesis A.Jung).

It was observed that the segregation through the stalk does not commence before a visible bud is formed. In order to find out if the size of the bud is the trigger for the second step of chromosome segregation, the relative size of the bud was analysed with respect to the size of the mother cell at the stage where ParB just moved through the stalk. The data reveal that there is no specific range of bud sizes, which correlates with the ParB segregation. However, there is a critical minimal bud size, which is approximately 55% of the width of the mother cell below which ParB was never observed to be segregating through the stalk (Figure 2.4). Another possible reason for the waiting time before the segregation though the stalk could be the coupling of segregation to replication itself, which will be analysed later.

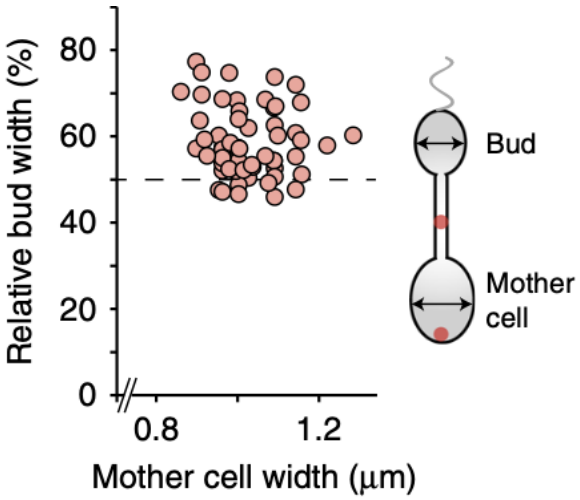


**Figure 2.4: The second step of segregation is limited by a critical bud size.** The relative width of the bud cell compared to the mother cell was approximately 60 ± 7%. A schematic representation of the dividing cell with segregating ParB foci is shown on the right. Taken from (Jung et al, 2019).

To study the effect of the lack of ParA function in *H. neptunium*, a strain producing a defective, dominant negative ParA variant under an inducible promoter was used, whereas it was not possible to construct a ParB depletion strain. Upon ParA depletion, the cells showed severe morphology, cell division and chromosome segregation defects, and ParB foci accumulated in the mother cell, unable to move to the buds. Moreover, in the cells stained with DAPI, no DNA was found in any of the stalks (Figure 2.5), suggesting that ParA and ParB are essential in *H. neptunium*. The pole-organising protein PopZ might play a role in capturing the segregated ParB at the flagellated pole of the bud cell. However, the deletion of *popZ* does not severely impair the phenotype.

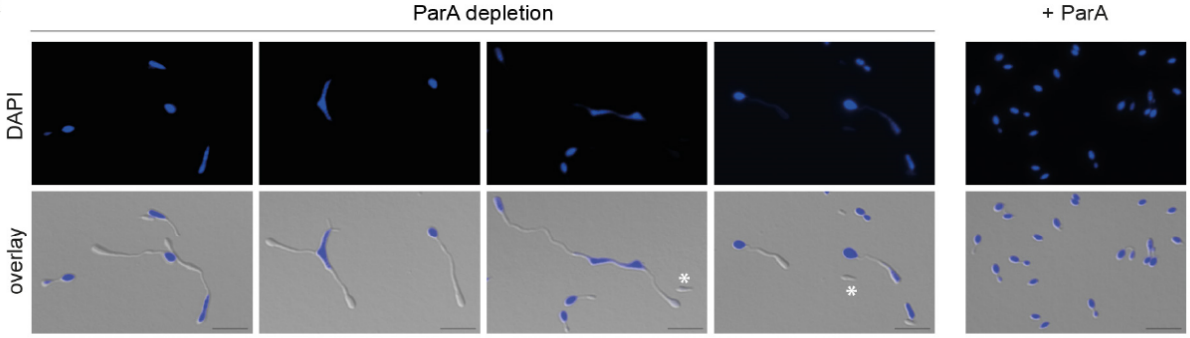


**Figure 2.5: ParA is essential in *H.neptunium*.** DIC and fluorescence images of DAPI-stained cells depleted of ParA for 45 hours. The DAPI signal is shown in blue. Adapted from (PhD thesis A. Jung).

# Results

## Chromosome organisation and dynamics in *H. neptunium*

A systematic analysis of the arrangement of chromosomal loci in *H. neptunium* was previously performed by making use of the ParB-*parS* system of *Yersinia pestis* plasmid pMT1 (Lindler et al, 1998). A plasmid carrying the *parS* site of *Y. pestis* pMT1 is integrated at a specific chromosomal locus to which the corresponding fluorescently labelled ParB binds, making it possible to visualise the tagged locus. Importantly, *Y. pestis* ParB is divergent enough to not bind to the endogenous *parS* sites of *H. neptunium*. In addition, the native ParB protein of *H. neptunium* tagged with a different fluorescent tag was used to mark the chromosomal *ori* region. The use of this strategy revealed that the chromosome has a longitudinal arrangement.

Towards this, several strains with different chromosomal loci tagged with $parS_{pMT1}$ were generated. Each strain can thus express fluorescently labelled ParB-YFP that labels the *ori* region and an inducible $ParB_{pMT1}$-mCherry fusion that labels the different chromosomal loci. With this set up, the distance of different loci in comparison with the *ori* were measured using ImageJ. The relative position of these loci were mapped with respect to the *ori*, that showed that the loci mapped near *ori* on the chromosome starting from 5° position, are placed at the pole, closer to the *ori* and as the chromosomal distance of the loci increase, they are placed farther away from the old pole where. Further, the regions after the *ter* site are progressively located closer, eventually bringing back the 357° position closer to the *ori* tracing the complete circular chromosome.

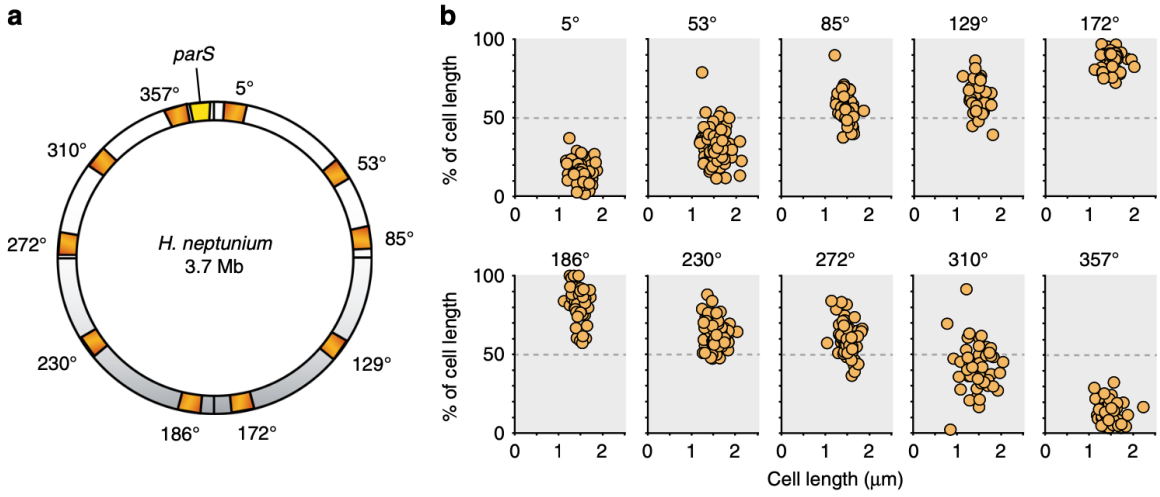


**Figure 2.6: Spatial arrangement of the *H. neptunium* chromosome.** The first figure is the schematic representation of the circular chromosome with several loci that were tagged for this study represented in orange. The chromosomal origin region is indicated in yellow. The second figure shows the subcellular distribution of the indicated loci relative to the origin region. As indicated, the 5° position and 357° position

are closest to the origin region and regions close to *ter* is placed at the opposite pole. Thus, this shows that the chromosome is longitudinally placed in the cell.

In order to complete this dataset on the subcellular positions of chromosomal loci in *H. neptunium* (Figure 2.6), a locus at position 310º was tagged as done previously using the ParB-*parS* system of *Y. pestis.* The analysis of snap-shots showed that the segregation dynamics of this locus were similar to a locus at the 53º position, which is equidistant to the tagged locus at 310º from the *ori* on the opposite arm of the chromosome. In both cases, the tagged loci showed an intermediate localization between the flagellated pole and the mid-cell. Moreover, the origin region moves to the bud before the 310º position does.

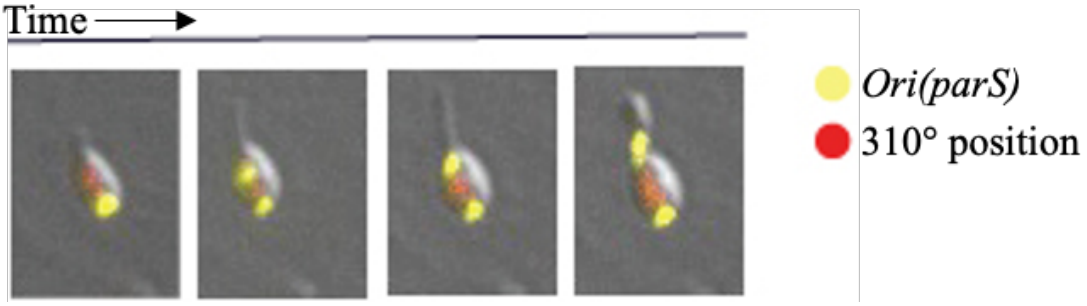


**Figure 2.7: Segregation dynamics of a locus at the 310° position of the *H. neptunium* chromosome.** Shown are overlays of DIC and fluorescence images of strain SRE15 (*parB-yfp* $P_{Zn}$::$P_{Zn}$-*mCherry-ParB*$_{pMT1}$ at 310°position) arranged according to their cell cycle stage.

This finding adds to the result that chromosome organisation indeed is longitudinal (Figure 2.6). The *ori* and *ter* regions are placed at opposite cell poles and the two arms of the chromosome stretch between the two poles across the length of the cell.

## Dynamics of the 2° position of the *H. neptunium* chromosome

The dynamics of the *ori* and *ter* regions were analysed in previous studies using time-lapse microscopy in cells harbouring a system called fluorescent repressor/operator system (FROS), in which a *lacO* array is integrated at the locus of interest, to which a fluorescently labelled LacI repressor can bind, making it possible to visualise the position of this locus. Snap-shot analyses showed that when regions close to *ori* (357º) and *ori* itself (359º) were labelled, either *ori* moves to the bud first or both regions move together, but the region at 357º never moved first. In the case of the *ter* region, it mostly localised at the stalked pole but during bud formation, it was also seen near the mid cell region. To confirm that it is indeed the *ori* region that segregates first within the mother cell and through the stalk, it was important to track *ori* movement in comparison with the proximal regions. To this end, we imaged cells that produced ParB-YFP as a proxy for the *ori* region and additionally carried a FROS label at the *ori-proximal* region at 2º. Time-lapse analysis demonstrated that the *ori* region indeed segregated through the stalk before the 2º position (Figure 2.8).

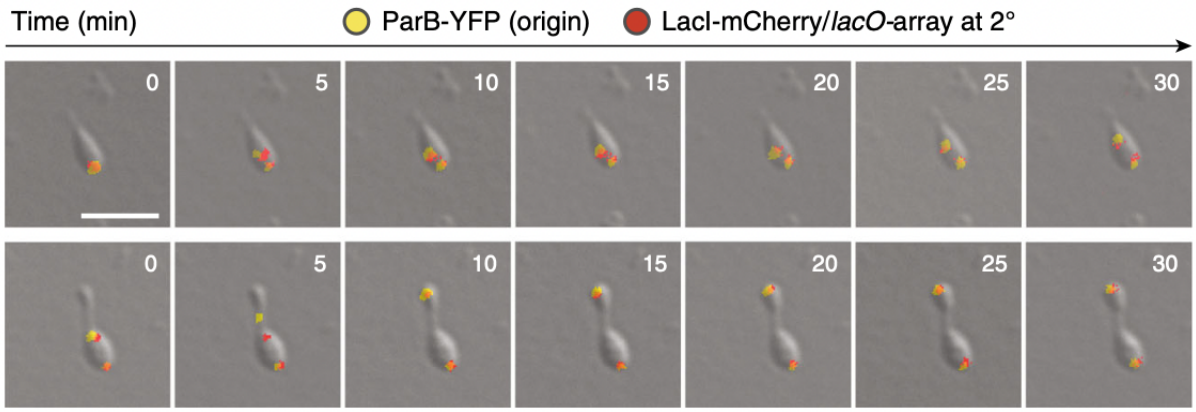


**Figure 2.8: Origin dynamics during the two-step chromosome segregation.** The upper panel shows the first step of segregation and the lower panel shows the second step of segregation. ParB-YFP bound to *parS* (in yellow) served as a proxy for the *ori* region, and LacI-mCherry induced for 1.5-3 h (in red) marked the chromosomal region at the 2°position.

## Dynamics of the replisome in *H. neptunium*

Analyses of the segregation dynamics of fluorescently tagged chromosomal loci (Jung et al, 2019) suggested that, unlike in other bacteria, chromosome replication and segregation in *H. neptunium* are to some degree temporally uncoupled, reminiscent of eukaryotic chromosome replication. To confirm this assumption and analyse how replication and segregation are coordinated, the dynamics of the replisome was studied. Towards this end, we fluorescently labelled the β-sliding clamp of the replisome complex, encoded by the *dnaN* gene, by replacing the endogenous *dnaN* gene with a *dnaN-yfp* fusion by means of double homologous recombination. During replication, the DnaN molecules condense to form a tight focus that moves within the cell as replication progresses. To understand the dynamics of the replication process, we proceeded to analyse these cells by time lapse microscopy. Swarmer cells are replication-incompetent and hence cannot produce a replisome. In such cells, the replisome is disassociated. The DnaN protein is hence distributed everywhere in the cell body. As the cell progresses through the cell cycle the swarmer-stalk transition happens. Microscopically the beginning of the stalk formation is not distinguishable. However, as cells grow further, a clear formation and elongation of stalks can be seen. During the swarmer to stalk transition, we observed that the DnaN signal condensed into one tight focus close to the old cell pole, aligning with the origin. As time progresses, the focus moves away from the old pole towards the opposite pole. Sometimes, two foci were also visible, indicating the two replication forks. Finally, the foci/focus reached the middle-subpolar region of the opposite pole before the signal became diffuse again. This indicated the completion of replication and the dissociation of replisome. The replisome does not react to the opposite pole, but halts somewhere between the middle of the cell and the subpolar region at the distal end. This is because the duplicated origin region must have displaced the *ter* from the stalked pole to the mid-cell region where the replisome disassembles. During the course of replication, it was observed that simultaneously, the cell synthesised the bud and after approximately 118 minutes the replisome was seen either

disassociating indicated by diffused signal or directly starting another round of replication indicated by a shift of focus to the old pole. (Figure.2.9).

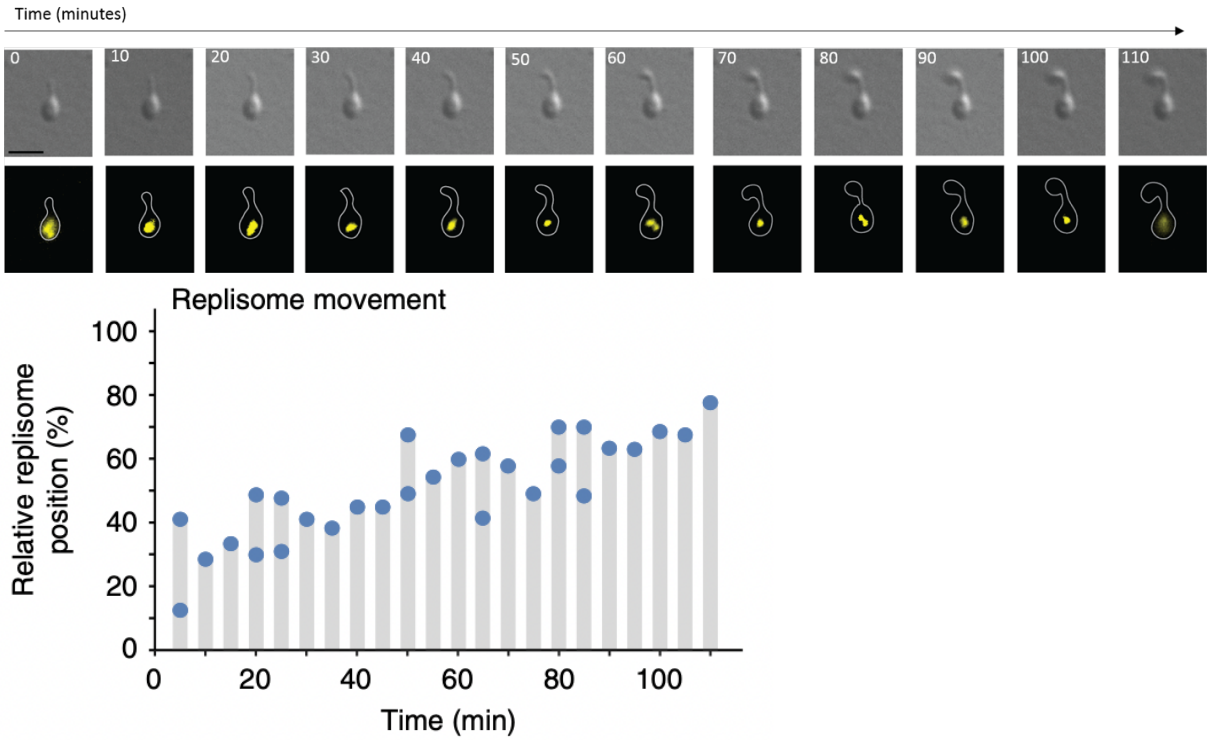


**Figure 2.9: Replisome dynamics in *H. neptunium*.** Shown are DIC and fluorescence images of a single cell of strain RP4 (*dnaN-venus*), observed at different stages of the replication cycle. Images were taken at 10 min intervals. Scale bar: 2 µm.

## Timing of chromosome replication and *ori* segregation through the stalk

In order to determine if there was a defined correlation between the timing of chromosome replication and *ori* segregation through the stalk, we set out to analyse the localization of both DnaN and ParB by means of a strain in which the native *dnaN* and *parB* genes were replaced with *dnaN-venus* and *parB-cerulean* fusions, respectively. This strain (JR47) was used for time-lapse analysis, but under standard imaging conditions using cells on agarose pads prepared in rich medium, a strong background signal was observed that prevented proper visualisation of the ParB-Cerulean fusion. To reduce the background signal, we therefore chose to image the cells on pads prepared in dilute (25%) medium. This approach considerably reduced the background noise, making it possible to obtain clearly defined ParB-Cerulean signals.

An analysis of time-lapse series recorded on strain carrying ParB-Cerulean revealed that the movement of the ParB-*parS* complex through the stalk occurred towards the end of the replication cycle, that is after at least half of the chromosome appeared to be replicated. In order to obtain quantitative data, we set out to measure the time lag between the start of ParB-*parS* translocation through the stalk and the end of chromosome replication.

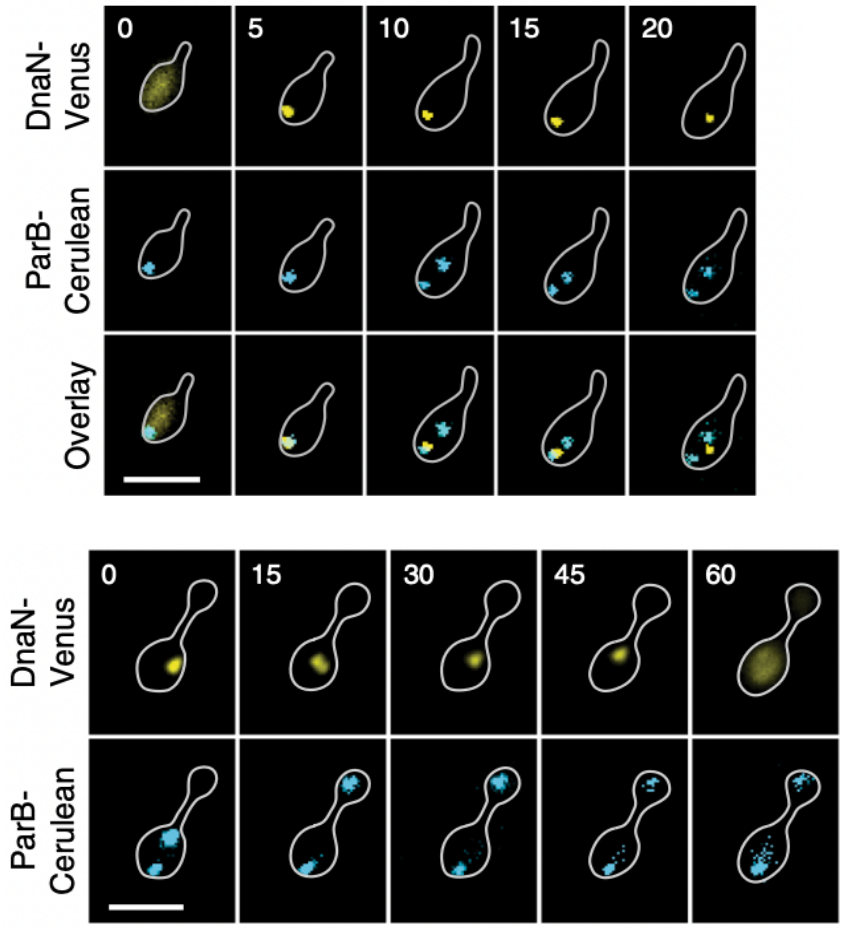


**Figure 2.10: Chromosome replication and segregation in *H. neptunium.*** YFP and CFP images from time-lapse series of strain JR47, producing ParB-Cerulean (indicated by blue foci) and DnaN-Venus (indicated by yellow foci), at time intervals of 15 min. The upper panel shows a cell during chromosome segregation in the mother cell body. The lower panel shows a cell during translocation of the *ori* region through the stalk. Scale bar: 2 μm.

To this end, we first quantified the duration of replication itself, using time-lapse microscopy (Figure 2.10, upper panel). We analysed stalked cells that at the beginning of the time-lapse series showed a diffuse signal for DnaN-Venus, indicating that the replisome had not yet assembled and started replication. The formation of a clear focus at the old cell pole marked the assembly of replisome and thus the initiation of a replication cycle. The time point when the DnaN-Venus signal dispersed again marked the completion of the replication cycle. In this manner, the time interval between replisome assembly and disassembly, i.e. the total duration of chromosome replication, was quantified in 50 cells. The results reveal that the replication lasts for 117.5 min with an RMS error of 15.97.

To determine at which point during the replication cycle the moving ParB-*parS* complex is translocated through the stalk, we colocalized DnaN-Venus and ParB-Cerulean in strain JR47 in replicating cells. We found that the replisome disassembles consistently after the onset of the second step through the stalk. The time gap between ParB segregation through the stalk and the replisome disassembly was quantified in 30 cells (Figure 2.10, lower

panel). The data showed that the time gap between the start of ParB-*parS* movement and the chromosome replication varied, ranging from 10 min up to 80 min. Nevertheless, most of the cells showed a time gap of around 40 min between the start of the second segregation step and DnaN-Cerulean dispersal. This indicates that in a majority of the population, *ori* translocation through the stalk commences only during the second half of the replication process, on average when 67% of the chromosome is replicated. This further corroborates previous findings supporting the notion that there is a partial temporal uncoupling between chromosome replication and segregation (Figure 2.11).

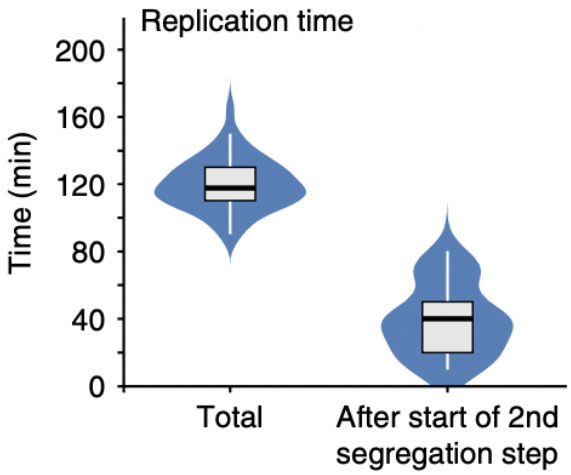


**Figure 2.11: Quantification of replisome movement.** The graph indicates the relative average subcellular locations of the DnaN-Venus signals, with 0% indicating the old (previously flagellated) pole and 100% the future stalked pole of the mother cell. For frames in which the two replication forks were clearly separated, the positions of both DnaN-Venus foci were included (B) Quantification of the total replication time (n = 50 cells) and the interval between the start of the second segregation step and replisome disassembly (n = 30 cells)

In conclusion, we could conclusively prove that the chromosome is organised in a longitudinal manner inside the cell. In the unique two-step mechanism of chromosome segregation, the *ori* (tagged by ParB) is the first region to enter the stalk. Hence, this step cannot be ParA-mediated (as there is no DNA in the stalk before the *ori* enters). The second step of segregation of chromosomes in *H neptunium* occurs after a time-lag. Although the exact reason for this lag is unknown, it is found out that on an average 67% of the chromosome is replicated before the second step of segregation begins. In the future it will be interesting to understand the exact mechanism of the segregation through the stalk and the molecular mechanism that regulates the stalling of the ori at the stalked pole and the time gap between the two steps.

# Chapter 3: Characterisation of a ParA-like protein in *H. neptunium*

## Introduction

Our understanding of the chromosome segregation in *H.neptunium* as a two-step process opens up several questions, such as the identity of the unknown trigger that initiates the second segregation step, or the factors that potentially anchor the duplicated *ori* at the stalked pole of the mother cell. Since the first step of chromosome segregation is ParA dependent, the *ori* translocation occurs by following the dimer gradient of ParA that is attached on the chromosome non-specifically. Since the duplicated *ori* is the first region to translate through the stalk, it is understandable that the second step of segregation is ParA independent. However this led us to investigate other ParA homologues present in *H. neptunium* to test whether any of these proteins can be a potential player in the second segregation step. Many proteins involved in almost all crucial aspects of life including ParA-like proteins are capable of binding and hydrolyzing nucleotide triphosphates (Fung et al, 2001). In general, these proteins belong to several chain folds including the mononucleotide binding fold (p-loop NTPases). The p-Loop NTPases comprise 10 to 18 % of all gene products (Liepe et al, 2002). These proteins are characterised by an N terminal Walker A motif consisting of a flexible loop between a beta strand and an alpha helix. The loop has a sequence pattern of GxxxxGK that plays a role in positioning the triphosphate moiety of the NTP. At the distal end, there is a Walker B motif that typically contains an aspartate (sometimes glutamate) residue that binds to $Mg^{2+}$ ion.

Phylogenetic analyses show that the GTPase superclass can be divided into two large classes on the basis of structural and sequential similarities. The first class includes the majority of well-known GTPases such as the heterotrimeric G proteins (HTGP), Ras family etc, since a large number transcription factor related proteins are included in this class, this class is designated as TRAFAC GTPases. The second class consists of signal recognition particle associated GTPases, the MRP/MinD/ParA related superfamily, and many BioD-related enzymes involved in metabolism among others. This class is called SIMIBI suggesting the three main subclasses that constitute this class (Figure 3.1) (Lutkenhaus, 2012). The ParA/Soj subfamily is represented by the ParA ATPase, which, together with the *parS* binding protein ParB, is involved in partitioning of newly replicated chromosomes and low-copy number plasmids (Figure 3.1).

For this study, we set out to investigate the ParA-like proteins of *H. neptunium*. As described in chapter 2, this species exhibits a dimorphic life cycle that starts with the birth of a swarmer cell that is flagellated and thus free to move around in the medium. As it develops, it terminally differentiates into a sessile stalked cell that is replication competent. The cell multiplies by budding off new offspring from the distal end of the stalk. This mode of reproduction makes the translocation of duplicated DNA to the bud cell compartment a challenge that leads us to the central question of investigating the potential roles of other ParA-like proteins in this process.

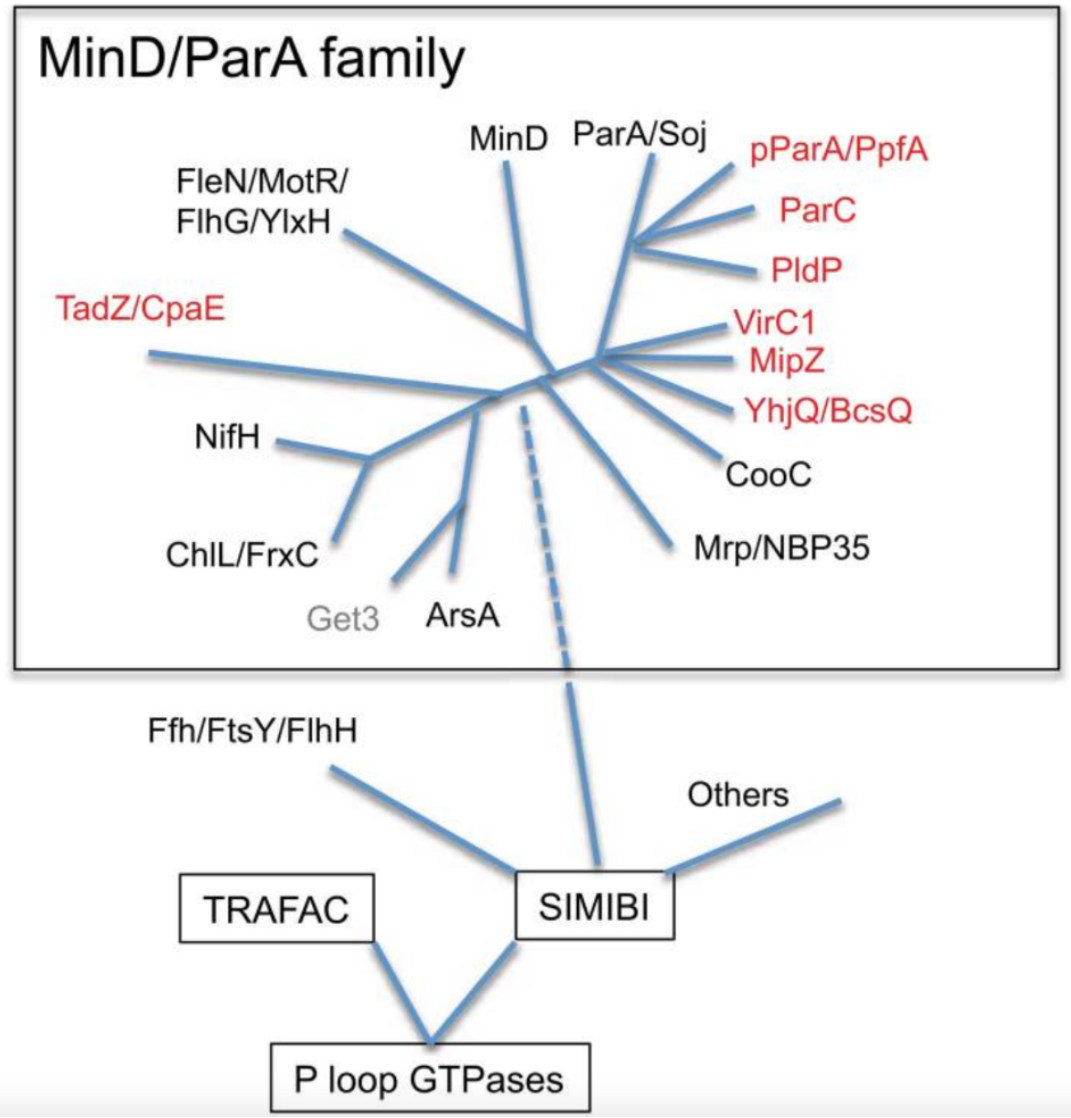


**Figure 3.1: Classification of P-loop GTPases.** The phylogenetic tree shows that the Mrp/MipZ/MinD/ParA families belong to the SIMIBI class of P-loop GTPases. Shown in red are the members discovered recently (before 2012). Taken from (Lutkenhaus, 2012).

# Results

## HNE_0708 belongs to a previously uncharacterized family of ParA-like proteins

A BLAST analysis with the ParA amino acid sequence of *C. crescentus* revealed that the proteome of *H. neptunium* includes six ParA-like proteins. A phylogenetic analysis of these proteins shows that all of these ParA homologs belong to the Mrp/MinD superfamily of P-loop ATPases (Figure 3.2). The members of this superfamily perform a variety of functions, ranging from positioning of the chromosome (ParA/Soj), the regulation of division site placement (MinD, MipZ), nitrogen fixation (NifH), arsenite resistance (ArsA) and flagellar regulation (MotR/FlhG), Fe-S cluster translocation (Mrp family), light-dependent chlorophyll biosynthesis (ChiL) (Shi et al, 2006) and the uncharacterised AF2380 family as shown in figure 3.2.

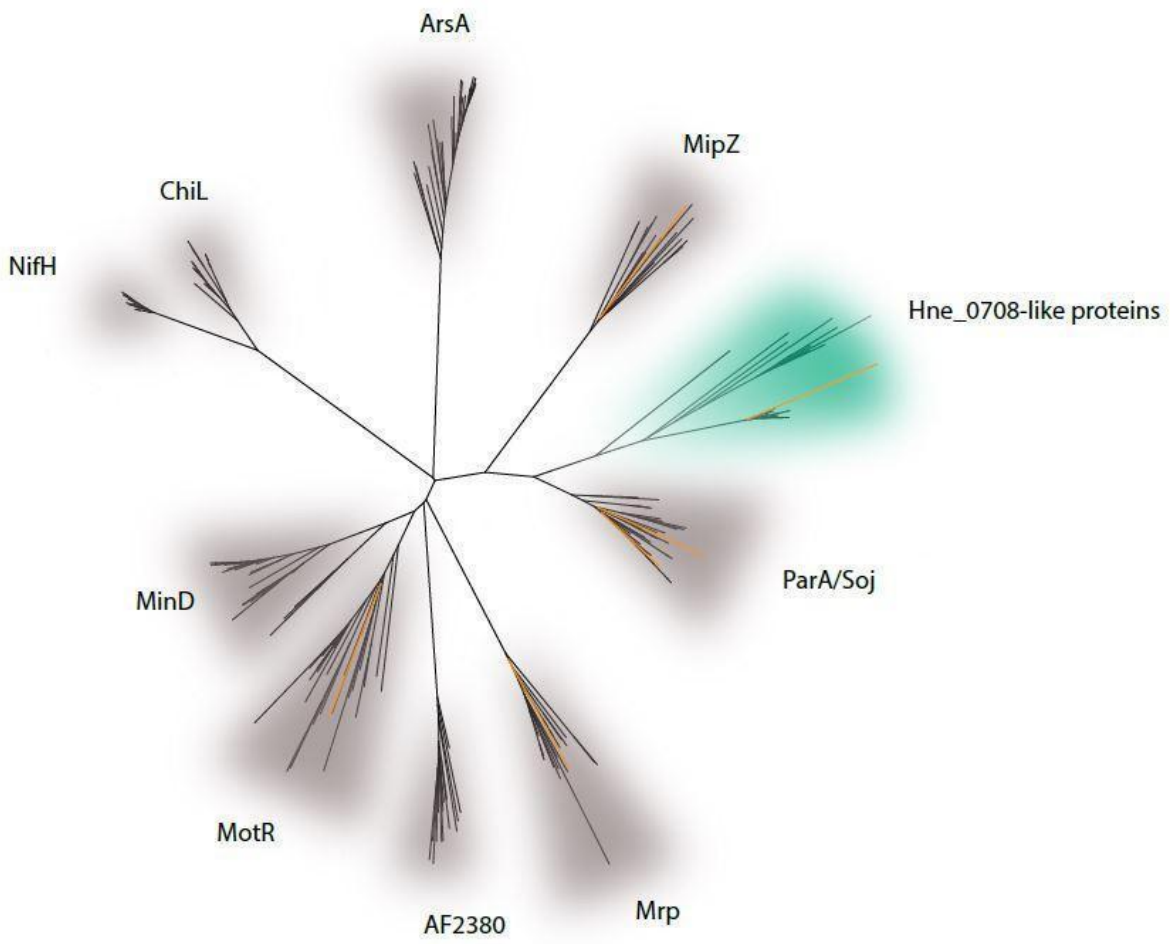


**Figure 3.2: Phylogenetic tree of representative ParA-like proteins from the Mrp/MinD superfamily constructed using the maximum likelihood method.** The ParA homologs of *H. neptunium* are indicated in orange. The green cluster corresponds to a new family of ParA-like protein that includes HNE_0708.

*H. neptunium* has a member in the MotR family (HNE_0468), the homologue of which is involved in flagella biosynthesis in *Pseudomonas aeruginosa* (2). HNE_0468 was grouped into the Mrp/MBP35 subfamily. The members of this family are involved in the formation of FeS clusters in many bacteria (Esquilin-Lebron et al, 2021). HNE_3561 is annotated as chromosome partition protein ParA, the gene of which is found together with *parB*, *gidA* and *gidB* close to the GC skew of the *H. neptunium* chromosome. It is known from recent studies that the ParAB*S* system is involved in the first step of chromosome segregation, that is the segregation of the sister *ori* regions within the mother cell (Jung et al, 2019). Apart from the canonical ParA(HNE_3561), HNE_1300 is also annotated as a part of the ParA family. While HNE_0943 is annotated as a part of the MotR family, HNE_0468 is annotated as an Mrp family protein. HNE_0708 and HNE_1128 (MipZ) are annotated as orphan *parA* homologs as there are no obvious partner proteins and are not found in an operon. As opposed to other ParA homologues, HNE_0708 has a long N-terminal region with a TIR domain (Figure 3.3). TIR domains were shown to be responsible for protein-protein interactions in other bacteria (Spear et al, 2009). HNE_0708 is a member of a new class of ParA-like proteins, positioned between the ParA/Soj subfamily and the MipZ subfamily, which makes this protein interesting to study further.

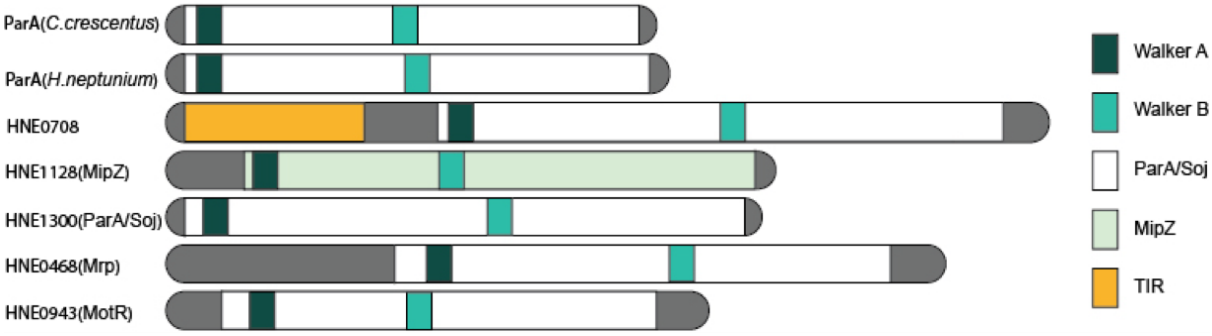


**Figure 3.3: Domain architecture of the ParA-like proteins of *H. neptunium*.** Shown are the domain architectures of the canonical ParA and the homologues, HNE0708, HNE1128 (MipZ), HNE1300, HNE0468 and HNE0943 in *H. neptunium* in comparison with the ParA protein of *Caulobacter crescentus.* HNE_0708 is characterised by an N-terminally located TIR domain (marked in yellow).

## HNE_0708 shows a diffuse and patchy localization

For the initial characterization of HNE_0708, the protein was fused C-terminally to Venus and expressed from the zinc-inducible $P_{Zn}$ promoter in *H. neptunium* (Anne Raßback, unpublished). The HNE_0708-Venus fusion showed a diffuse localization in the cytoplasm and a patchy localization in the stalk (Figure 3.4). Notably, cells producing the fusion protein displayed phenotypic defects, including bulges in the stalk in stalked and budding cells. It was possible that the pattern observed and the morphological aberrations were caused by the overproduction of the fusion protein, as the fusion construct was expressed in addition to the endogenous HNE_0708 gene.

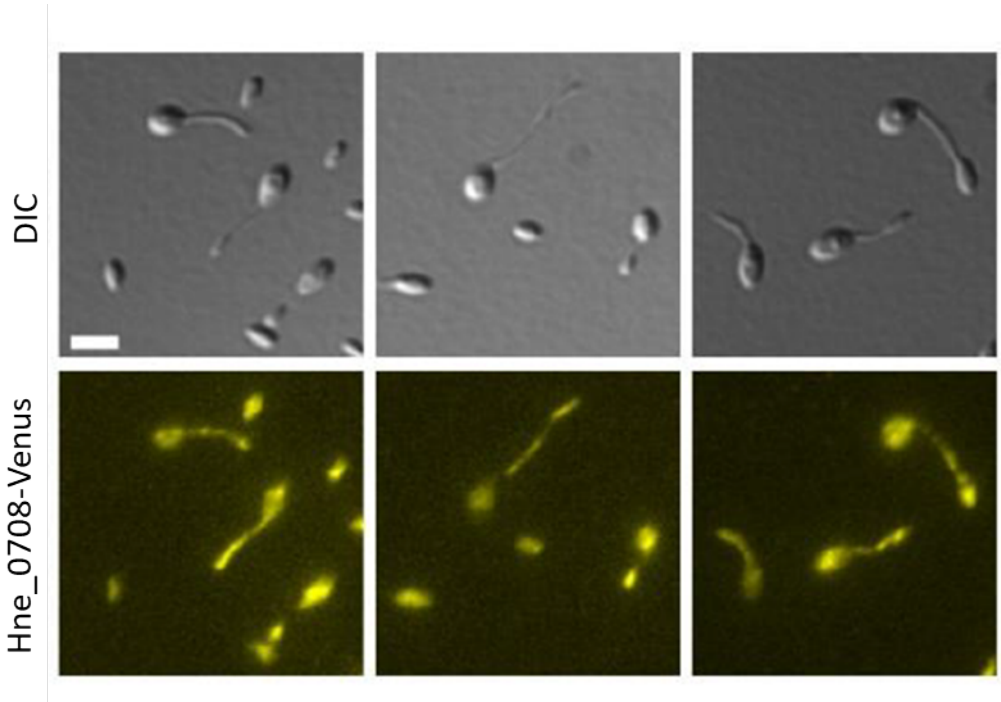


**Figure 3.4: Localization of HNE_0708-Venus.** The fusion protein was produced under the control of the zinc-inducible $P_{Zn}$ promoter in the wild-type background (strain AR37). Adapted from (PhD thesis, A. Raßbach).

## ΔHNE_0708 cells show bulged stalks with chromosome accumulation in the bulges

To further characterise HNE_0708, an in-frame deletion mutant was generated by double homologous recombination, using a derivative of the *sacB*-containing pNPTS138 plasmid. The deletion resulted in a phenotypic defect in stalked and budding cells. At least 22 % of the budding cells showed atypical bulges close to the buds (Figures 3.5 and 3.8). The bulges were noticeable only in stalked cells that had already produced a conspicuous bud, suggesting that this defect could potentially arise during the process of budding. In this context, it remains elusive whether the mother cell recognises the bulges as future buds or as a part of the stalk. To this end, a closer understanding of the structure of the bud is required. Towards this, a cryo-electron microscopy analysis was performed. It reveals that there could be DNA accumulation in the bulges. DAPI staining also revealed possible DNA accumulation in the stalks of mutant cells (Figure 3.5). This could mean that chromosome segregation is stalled at the bulges. However, since the buds contained DNA as well, it may be that either the newly replicated chromosome moving to the bud compartment now occupies both the bud and the bulges, pointing towards a segregation defect, or there are supernumerary chromosomal copies that no longer fit in the bud and thus accumulate in the bulges, pointing towards a replication (in addition to a segregation) defect. In the case of swarmer cells, the cell shape varied such that they appeared to be elongated with tapering ends instead of the robust wild type buds.

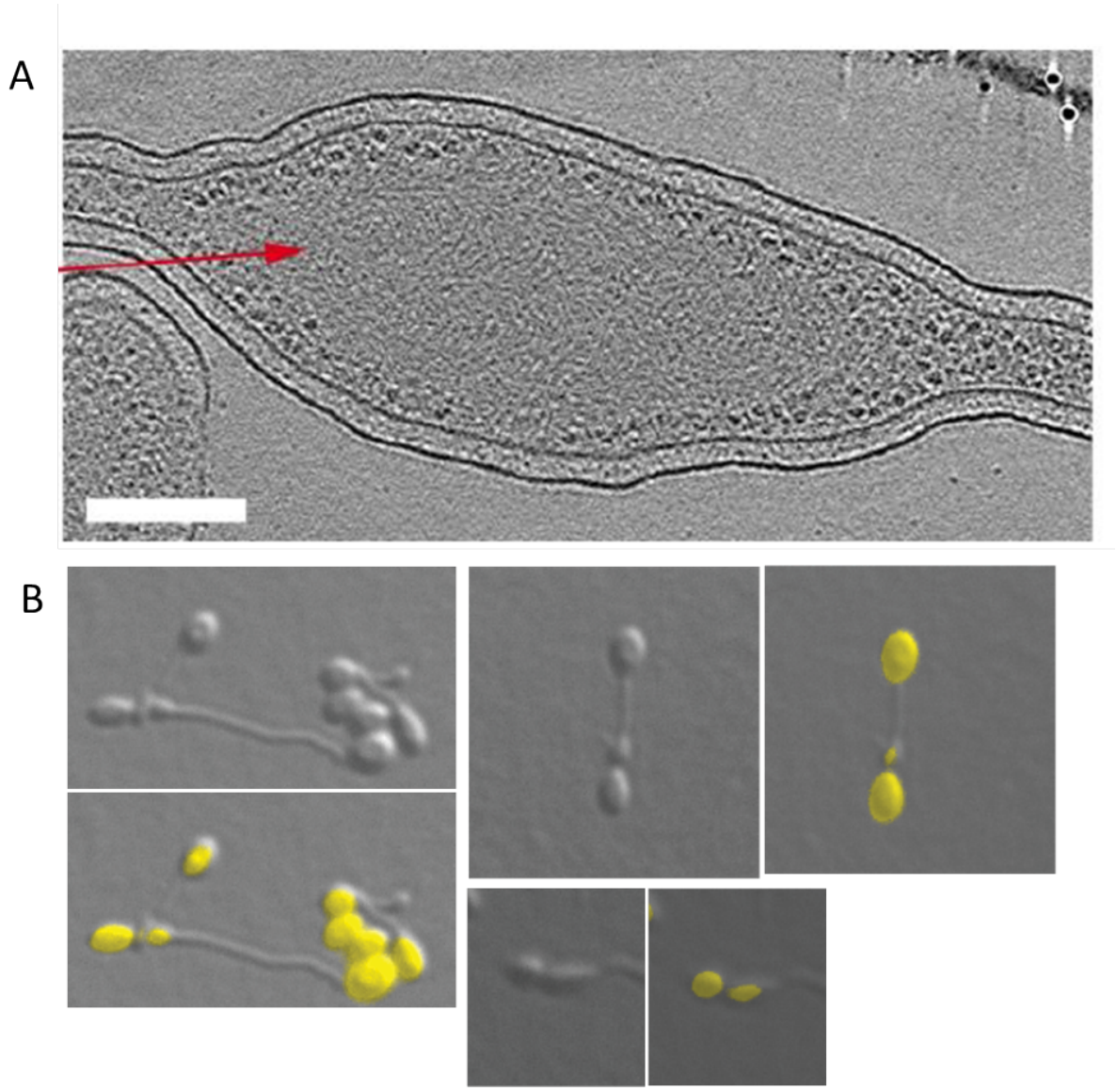


**Figure 3.5: Morphological and DNA segregation defects of Δ*HNE_0708* cells.** (**A)** Cryo-EM image showing DNA accumulation in a bulge (indicated by a red arrow). Adapted from (PhD thesis, A. Raßbach). **(B)** DIC images and overlays of DIC and fluorescence images of cells of DAPI-stained cells of strain RP10 (Δ*HNE_0708*). The DAPI signal is false-colored in yellow.

## ΔHNE_0708 cells hyper-initiate chromosome replication

It has been found out that the bulges in the stalk of Δ*HNE_0708* cells contain chromosomal DNA. Whether stalk bulging is the cause or consequence of DNA accumulation is a question that needs to be answered. To this end, we decided to investigate chromosome replication and segregation in the mutant background. For that, a ParB-Venus fusion was produced in place of the native protein in cells lacking HNE_0708. Initial observations suggest that there are multiple ParB foci in the mother cell. To clarify whether the effect observed was indeed due to the absence of HNE_0708, we performed the same analysis in

the wild-type background. We found that under this condition, cells also showed an increased number of ParB foci and morphological defects (Figure 3.6, lower panel). These findings indicate that the ParB-Venus fusion is not fully functional and thus not suitable to analyse origin duplication and segregation.

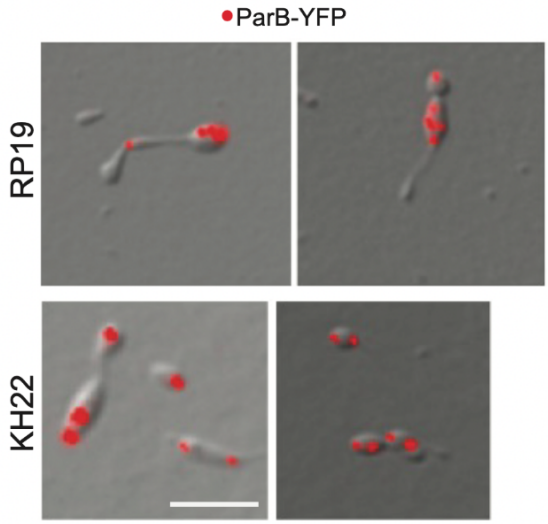


**Figure 3.6: ParB-YFP expression causes defective replication.** The ParB-YFP signal as represented by the red foci shows defective origin replication in cells in Δ*HNE_0708* (RP19) and wild-type (KH22) backgrounds. scale bar represents 3 µm.

To clarify the involvement of HNE_0708 in chromosome replication or segregation, we went on to construct strains producing a ParB-Cerulean fusion in place of the native protein in the wild-type and Δ*HNE_0708* backgrounds. In the wild-type background, the cells showed negligible phenotypic defects, indicating that the fusion protein is, at least largely, functional. A quantification of the number of ParB-Cerulean foci in the mutant background revealed that there is an elevated number of stalked and budding cells that possessed more than three ParB foci in the absence of HNE_0708 (Figure 3.7). In ~23% of the budding cells, more than two foci were observed, out of which more than half had more than three foci. However, even in the wild-type background, a small fraction of cells showed multiple ParB foci, but their proportion was significantly lower than in the Δ*HNE_0708* background. This may be explained by the re-initiation of chromosome replication in the mother cell once the bud has become physiologically separated from the mother cell compartment, which may occur before its actual physical separation from the stalk. At the swarmer cell stage, both wild-type and ΔHNE_0708 cells showed at most two ParB-Cerulean foci, with two foci likely observed for cells that have just transitioned to the stalked stage and thus initiated chromosome replication. While most of the swarmer cells have one ParB focus, we quantified only those cells with two foci, that is, cells that have just transitioned to S phase but not yet developed a visible stalk to gauge a potential effect of HNE_0708 on replication initiation or DNA segregation in the mother cell. Thus, in the absence of HNE_0708, there could be a hyper-initiation of replication or a defect in chromosome segregation.

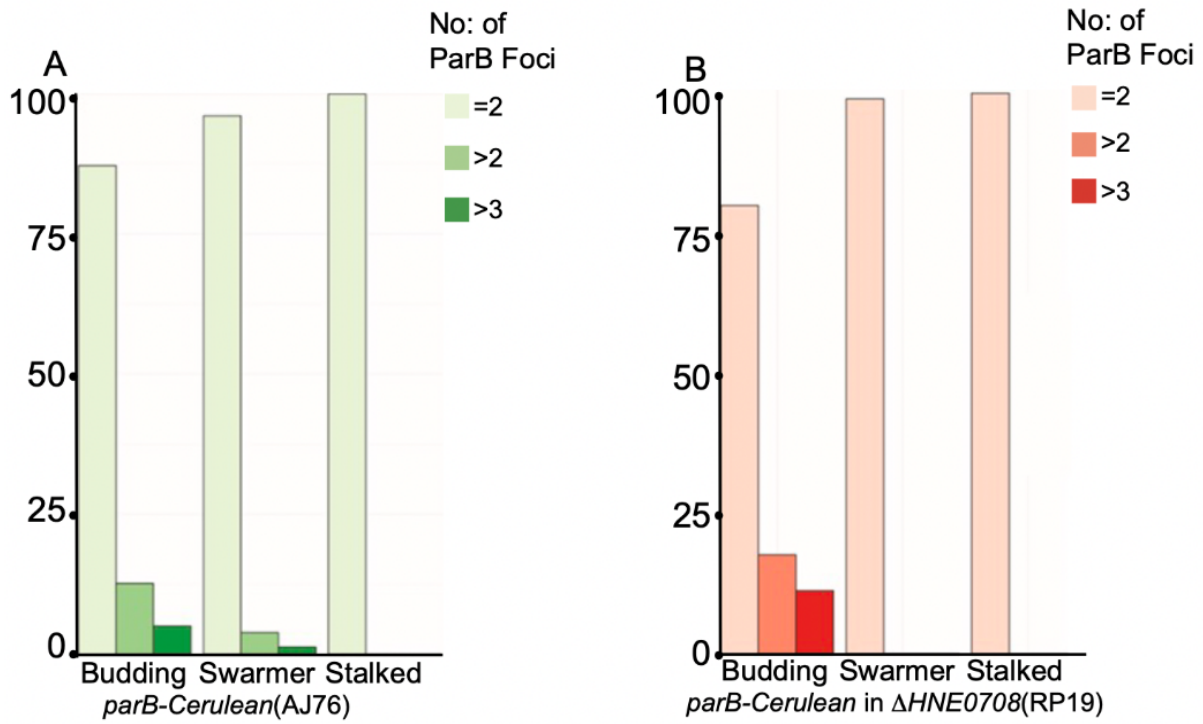


**Figure 3.7: The number of ParB foci in the Δ*HNE_0708* mutant is higher than that in the corresponding control.** Quantification of number of ParB foci in budding, stalked and swarmer cells carrying a *parB-Cerulean* fusion in **(A)** the wild-type background (AJ76) or the **(B)** Δ*HNE_0708* background (RP19).

To understand whether there is any correlation between the accumulation of ParB-Cerulean foci and the stalk-bulging phenotype, cells that showed stalk bulges were analysed in more detail. Specifically, we aimed to clarify whether the bulging of the stalk correlated with increased origin firing or whether bulges develop because there are more ParB foci. The presence of multiple ParB foci alone cannot be the reason why bulges appear, since we clearly see a significant accumulation of ParB foci in the *parB-Venus* background that does not specifically result in a stalk bulging phenotype, although it does result in morphological aberrations. It is conceivable that the loss of HNE_0708 links aberrant chromosome replication or segregation with the formation of bulges. To understand the chronology of the appearances of these defects, we needed to follow the development of the cell under the microscope.

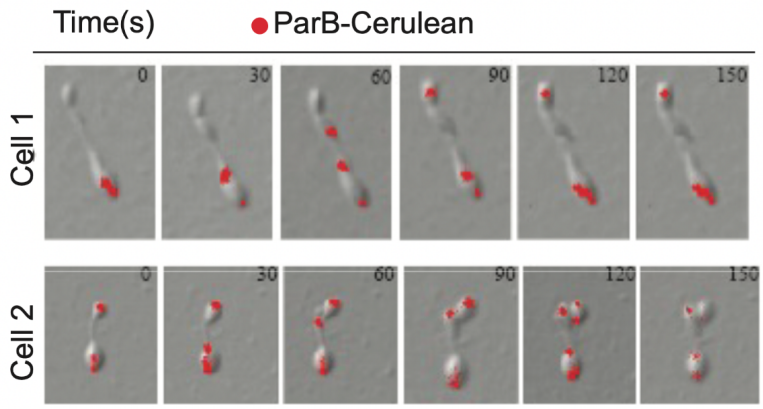


**Figure 3.8: Time lapse analysis of ParB-Cerulean in the Δ*HNE_0708* and wild-type backgrounds.** Shown are the localization dynamics of ParB-Cerulean in Δ*HNE_0708* for two cell types, that have the bulging phenotype and that do not. Both cell types show defective replication and segregation.

To this end, a time lapse analysis of cells producing ParB-Cerulean instead of native ParB was carried out. It was observed that, in Δ*HNE_0708* cells, bulges started to appear before the ParB-Cerulean signal reached the stalk. In Figure 3.8, the mutant stalked cell shows two ParB-Cerulean foci that segregated within the mother cell in a wild-type manner. During this process, a bulge forms at the terminal end of the stalk. As segregation through the stalk proceeds, the cell still shows two ParB foci within the mother cell. At 30 minutes, the focus at the stalk pole of the mother cell looks brighter than the opposite pole indicating that it may contain two foci. At 60 minutes, one of these foci segregates and reaches the bulge. At 90 minutes, it reaches the bud cell. In the meantime, the two foci that were already separated in the mother cell seem to merge together at the old pole again, which may be because the segregated partition complex cannot be anchored at the stalked pole. At 120 min, the ParB focus at the stalk end of the mother cell seems to be brighter than that of the focus at the old pole. This could be because of the merging between the two foci in the mother cell. Although at this time resolution it is difficult to pinpoint the exact time point when replication hyper initiation begins, these findings reveal a severe defect in the dynamics of DNA replication and segregation that, collectively, may result in the improper segregation and organisation of chromosome in the buds including the clogging of DNA in the bulges. In the second panel another cell that does not have the stalk-bulging phenotype can be observed. Here also we see that despite not having a stalk bulging, the defect in ParB replication and segregation exists in this cell and is comparable to the stalk-bulging cells. This could mean that the defect in replication and segregation is directly linked to the absence of HNE_0708.

From snapshot images of cells carrying ParB-Cerulean in the absence of HNE_0708, it is revealed that, out of the stalked cells that show a bulging phenotype, 63% of the cells had at least three ParB foci and 37% of the cells had more than three ParB foci, further confirming a connection between these defects (Figure 3.9). There was a slight delayed growth in the cells lacking HNE_0708, whereas in the *parB-Cerulean* background the differences in the growth rate seem to be abolished. It is possible that the ability to form

biofilm could be different, which could be the reason for different growth rates. Further analyses are needed to account for the differences in biofilm formation.

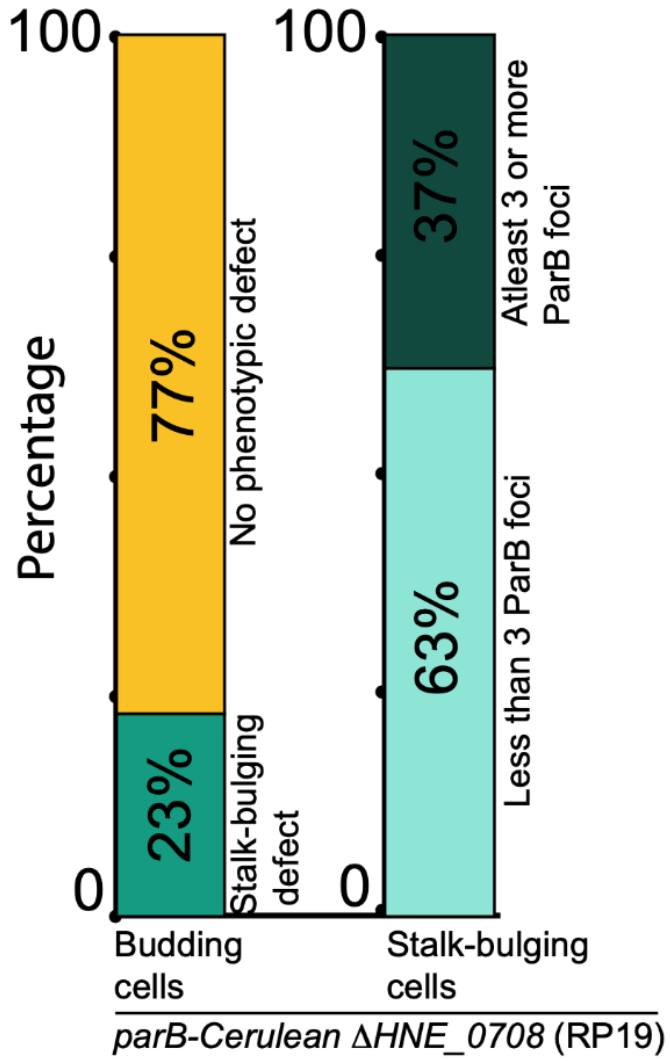


**Figure 3.9: Defects in growth and replication in ΔHne-0708.** Quantification of snapshots of DIC-CFP overlay images of RP19 cells that carry ParB-Cerulean in the absence of HNE_0708 show that 23% of budding cells showed a stalk-bulging phenotype out of which 37% cells have more than 3 ParB foci.

## A subpopulation of swarmer cells shows a defect in cell shape

A subpopulation of the swarmer cells in the Δ*HNE_0708* background showed a phenotypic defect where they did not show the typical ovoid morphology but instead appeared thinner and more elongated, with tapered ends (Figure 3.10). They likely represent offspring released from cells with bulged stalks. Notably, mother cells that underwent this kind of cell division may look similar to the wild-type cells, making their physiological defect less conspicuous. Apart from that, since not all cells with a morphological defect have multiple ParB foci.

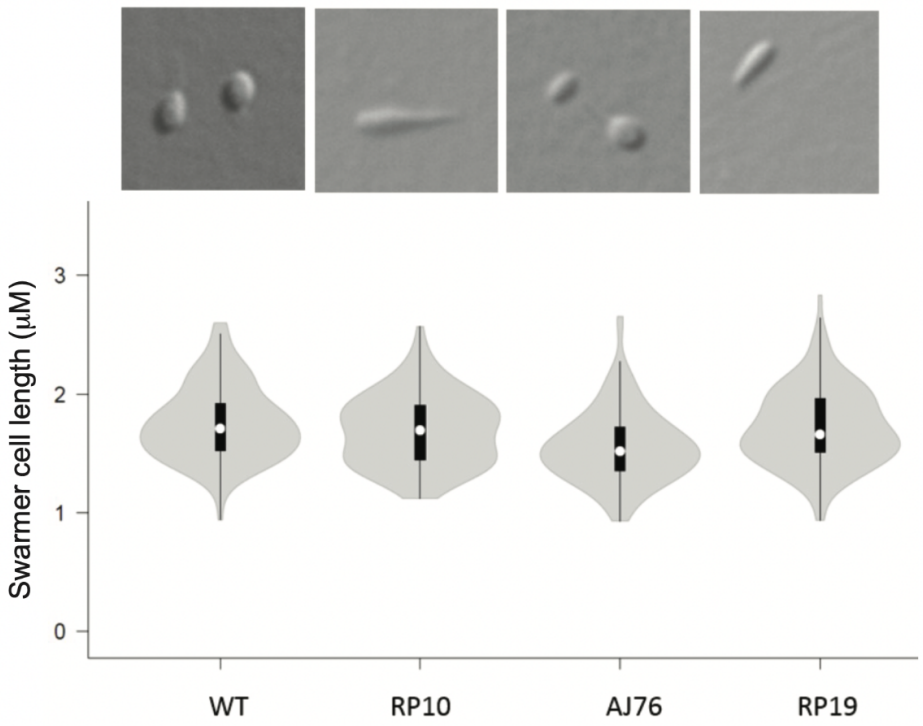


**Figure 3.10: A subpopulation of newborn Δ*HNE_0708* swarmer cells show a morphological defect.** RP10 (Δ*HNE_0708*) and RP19 (*parB-Cerulean* Δ*HNE_0708*) swarmer cells show a possible subpopulation of cells with longer cell length and a difference in cell shape as represented by the microscopy images as opposed to Wild type and AJ76(*parB-Cerulean*) cells that are more robustly oval shaped. (The number of cells quantified are 111(WT), 101(RP10), 58(AJ76) and 38(RP19)).

## HNE_0708 can bind to DNA and hydrolyse ATP

To further our understanding of the physiological role of HNE_0708, we first aimed to determine how different it was structurally from ParA and MipZ family proteins. Figure 3.11-A shows the predicted Alpha Fold structure of HNE_0708. Apart from the ParA domain that contains the deviant walker A and walker B motifs, the N-terminal is additionally characterised with the presence of a TIR domain that is absent in other ParA proteins like MinD or MipZ. Similar to canonical ParA, the dimer interface is occupied by a patch of positively charged amino acids that can potentially bind to DNA.

Next, we set out to purify HNE_0708 to determine its biochemical properties. For this purpose, we fused the protein to a cleavable N-terminal $His_6$-SUMO tag to increase its accumulation and solubility. The protein was purified in a HEPES-based buffer at pH 7.5. However, upon cleavage of the $His_6$-SUMO tag, the resulting native HNE_0708 protein turned out to be insoluble and precipitated. Therefore, the tag was retained and biochemical experiments were performed with the fusion protein.

Since ParA proteins are known to bind and hydrolyze ATP, we set out to perform an ATPase assay to determine if HNE_0708 had any hydrolytic activity, using a coupled-enzyme assay as HNE_0708 consists of the sequence LKGGVGKTT corresponding to the

deviant walker A motif. This analysis revealed that HNE_0708 hydrolyzed ATP with a $k_{cat}$ of 0.155 $min^{-1}$.

Previous studies of ParA and MipZ showed that these proteins interact non-specifically with DNA. Their DNA-binding site is characterised by a series of positively charged amino acids at the rim of the dimer interface that interact with the negatively charged phosphate backbone of DNA. Given the defects in DNA replication and/or segregation observed in the absence of HNE_0708, we aimed to determine whether this new type of ParA-like protein may also have DNA-binding activity. Calculating the electrostatic surface potential of a predicted HNE_0708 dimer, we observed a putative highly positively charged region at the dimer interface that could potentially mediate interactions with DNA. To test this possibility, we investigated the ability of HNE_0708 to interact with a double-stranded DNA oligonucleotide using biolayer interferometry (Figure 3.11 B).

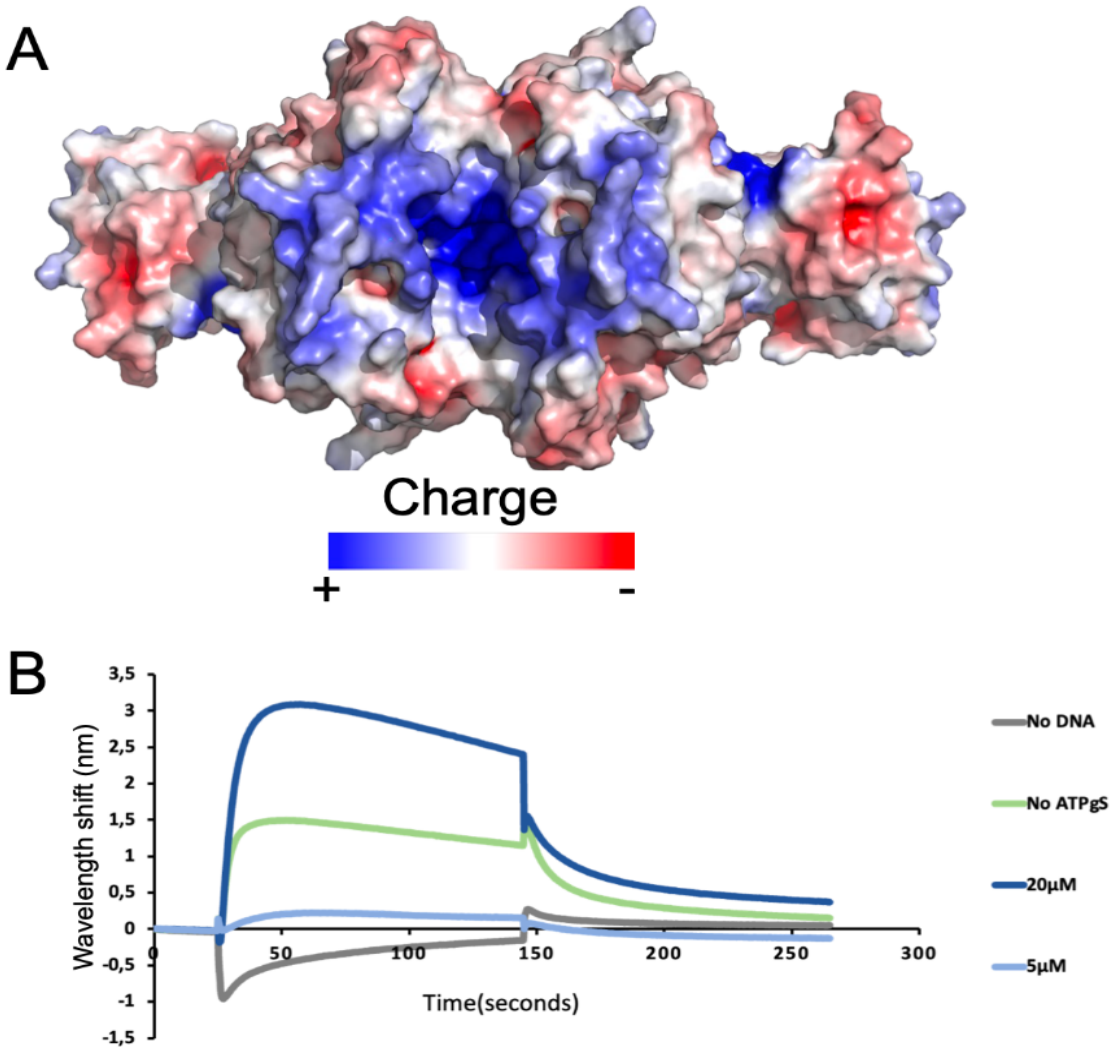


**Figure 3.11: HNE_0708 can potentially bind DNA.** **(A)** Predicted electrostatic surface potential of an HNE_0708 dimer. The positively charged patch indicated in blue could potentially bind to DNA non-specifically. **(B)** Biolayer interferometry analysis of the interaction of HNE_0708 with DNA. Biotinylated

DNA(3.7μM) was immobilised on streptavidin sensor chips and 5 or 20 μM concentrations of HNE_0708. It can be noted that in the absence of ATP$\gamma$S the binding affinity is reduced.

DNA was biotinylated, immobilised on a sensor and probed with varying concentrations of protein. While the HNE_0708 protein alone did not bind to a sensor lacking DNA, it showed a marked interaction with the DNA-modified sensor. At a protein concentration of 5 $\mu$M, only moderate binding was observed, but at 20 $\mu$M a significant interaction was observed, which was enhanced in the presence of ATP$\gamma$S, a slowly hydrolysable analogue of ATP that effectively locks ParA-like ATPases in the dimeric state. The buffer that was used to purify HNE_0708 contained ATP to increase the solubility of HNE_0708. Even though the purified protein was dialysed against the same buffer without ATP, it is possible that trace amounts of ATP were still present. This might account for the binding of the protein to the DNA without ATP$\gamma$S. Altogether, these results suggest that HNE_0708 is a genuine ParA-like ATPase that is able to hydrolyze ATP and to bind DNA.

This study thus concludes that Hne-0708 is a ParA-like protein with a N-terminal TIR domain known for protein-protein interaction in bacteria. This protein is a part of a previously unknown subfamily of ParA like proteins. The characteristic stalk-bulging defect as well as the chromosome segregation defects point to the fact that this protein potentially plays a crucial role in recognising the identity of the bud and consequently the chromosome segregation.

# Chapter 4: Coordination of MipZ-dependent division site placement and chromosome segregation in *C. crescentus*

## Introduction

Chromosome segregation needs to be carefully coupled with cell division to ensure faithful inheritance of the genetic material by the daughter cells. In this study, we focused on a segregation system commonly found in the bacterial kingdom, the ParAB*S* system. It is known that the components of the ParAB*S* system interact with proteins that take part in other essential functions such as cell division (Figure 4.1) (Kawalet et al, 2020).

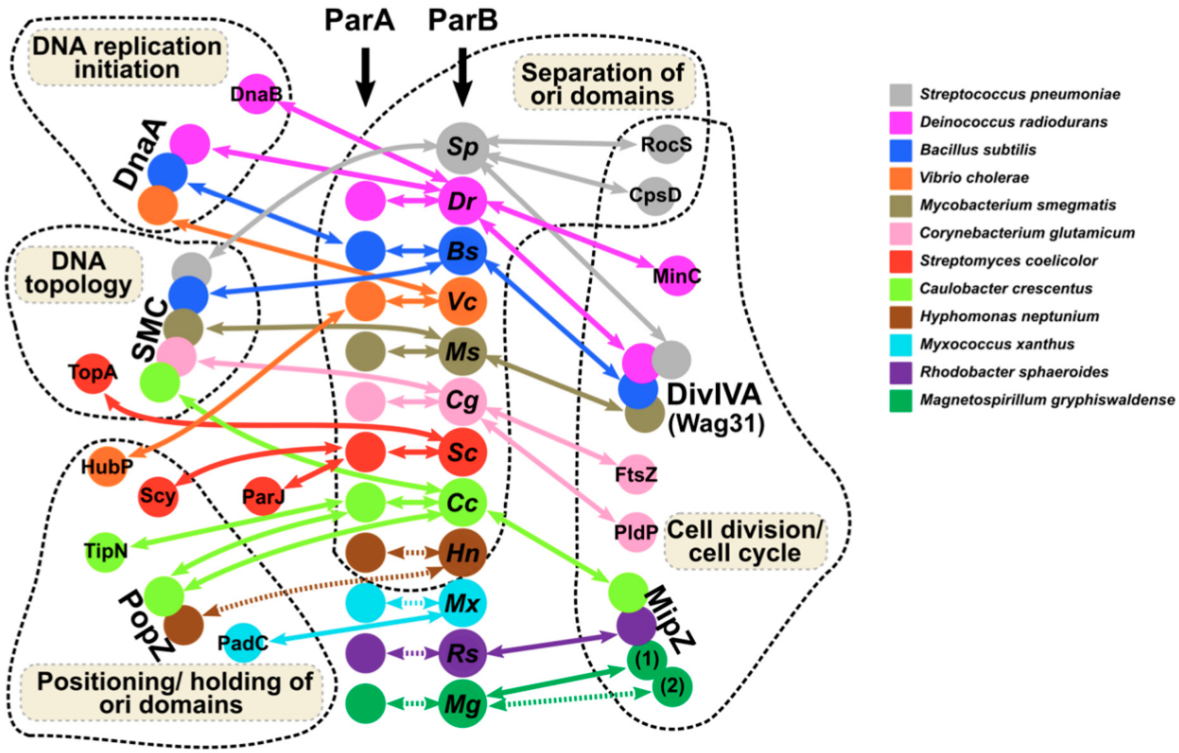


**Figure 4.1: ParA and ParB of different species and their interaction partners.** Interaction of different ParB and ParA components of ParABS systems belonging to different species of bacteria with other proteins involved in important cellular processes. Taken from (Kawalek et al, 2020).

In the case of the alpha proteobacterium *C. crescentus*, ParB is found to be interacting with another ParA-like protein, MipZ (Thanbichler et al, 2006), which is involved in division site placement, thus linking chromosome segregation and cell division. This interaction is crucial for establishing a bipolar gradient of MipZ, which in turn is essential for the proper spatiotemporal regulation of cell division. Here we look into the details of this interaction and how it coordinates cell cycle events in *C. crescentus*.

## MipZ - a negative regulator of division site placement

As introduced in chapter 1, cell division is brought about by the assembly of a functional FtsZ ring at the midcell position. Hence it is important that the Z ring is positioned at the right place and at the right time. Cells have evolved various mechanisms to ensure that this happens. Oftentimes, dedicated protein machinery is involved in the positioning of the Z ring such as the prototypical MinCDE system found in *E. coli* (Lutkenhaus, 2012). *C. crescentus* possesses a ParA-like P-loop ATPase, MipZ, that has evolved to regulate Z ring positioning by interfering with the polymerisation of the FtsZ ring. MipZ is an ATP-dependent molecular switch. It exists as a dimer when bound to ATP. Upon spontaneous ATP hydrolysis, the dimers fall apart into monomers (Figure 4.2). MipZ has multiple interaction partners, including FtsZ, the chromosome partitioning protein ParB and non-specific DNA. It is known that, *in vivo*, MipZ interacts with ParB only when in its monomeric form. By contrast, only dimeric MipZ can bind to DNA and regulate Z ring positioning.

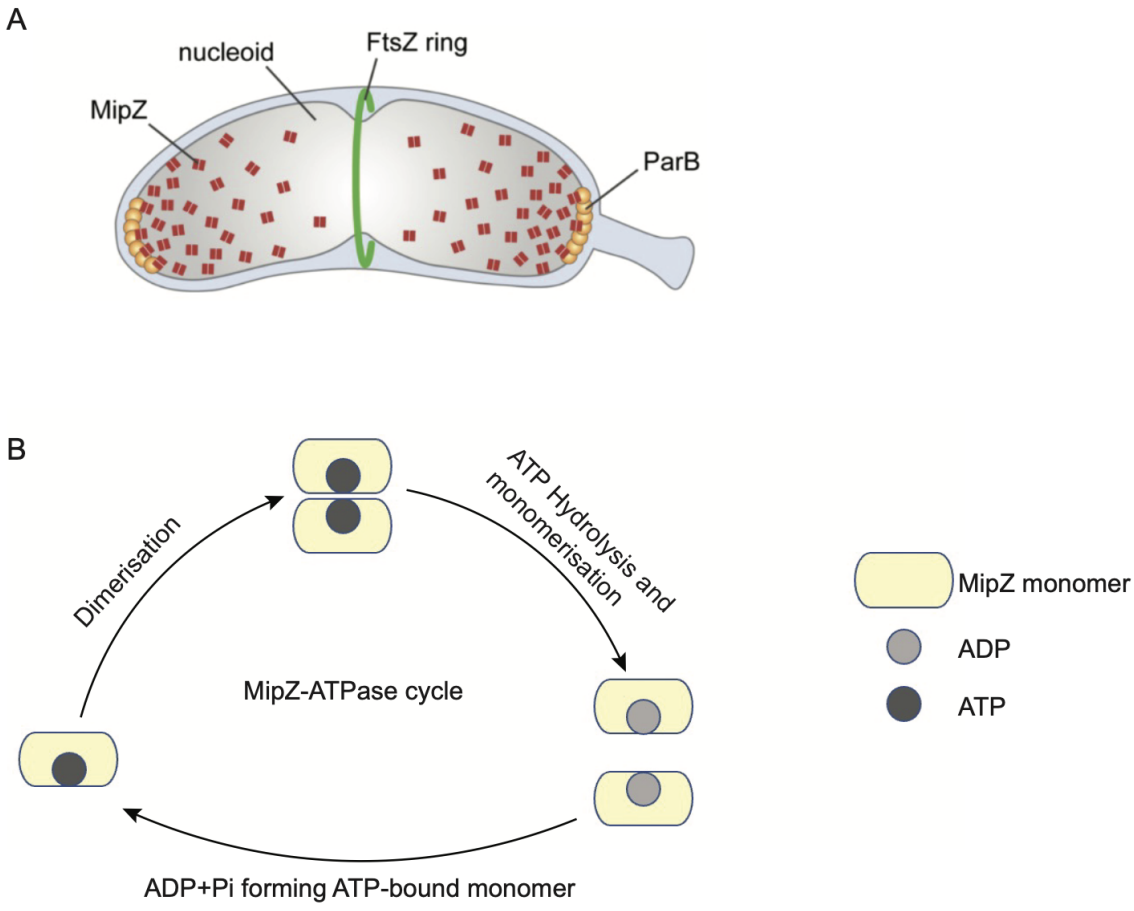


**Figure 4.2: The ATPase cycle of MipZ.** Panel A shows the bi-polar distribution of dimeric MipZ(red) that allows a functional FtsZ ring(green) to be formed only at the mid-cell. Panel B shows the ATPase cycle of MipZ. Monomeric MipZ can interact only with ParB. Upon ATP-binding, MipZ dimerises and thus gains affinity for DNA and FtsZ. The intrinsic ATPase activity then converts the ATP-bound dimers to ADP-bound monomers, which re-enter the cycle.

MipZ dimers are distributed in a bi-polar gradient within the pre-divisional cell, with the highest concentration at the poles and the lowest at the midcell. They act as an inhibitor of FtsZ polymerization and thus prevents Z ring formation close to the cell poles, thereby effectively limiting cell division to the midcell region. The MipZ dimer gradient is thought to be established by a dynamic localization cycle driven by the oscillation of MipZ between the monomeric and dimeric state that is accompanied by a switch in the interaction pattern of MipZ molecules (Figure 1.9).

## The DNA-binding interface of MipZ

To understand how the MipZ surface is made available for all the three interaction partners, a much closer look into the residues involved in the interaction was needed. As a result, previous studies have identified several residues that are involved in ParB binding, DNA binding and FtsZ binding. This was initially done by systematically mutating residues on the surface of the MipZ dimer structure and analysing their effect on the localization behaviour and function of MipZ. This approach identifies several amino acids potentially involved in interactions with the interaction partners of MipZ. The DNA binding interface of MipZ was proven by microscopy and *in vitro* methods such as biolayer interferometry (BLI), an optical technique that measures real-time ligand binding as a function of shift in wavelength and hydrogen deuterium exchange followed by mass spectrometry (HDX-MS), a method that identifies regions blocked by ligand binding by assessing the accessibility of backbone amide hydrogens (Gallagher et al, 2016). ParA-like proteins are known to be involved in DNA binding. The amino acids that are conserved as DNA binding residues on canonical ParA homologs are not found on MipZ which led to mutating surface-exposed bulky and hydrophobic amino acids to be mutated to test the interaction. In this method 9 residues were discovered (PhD thesis, Binbin He). They were mostly positively charged and hence can be presumed to be interacting with DNA non-specifically through its negatively charged phosphate backbone.

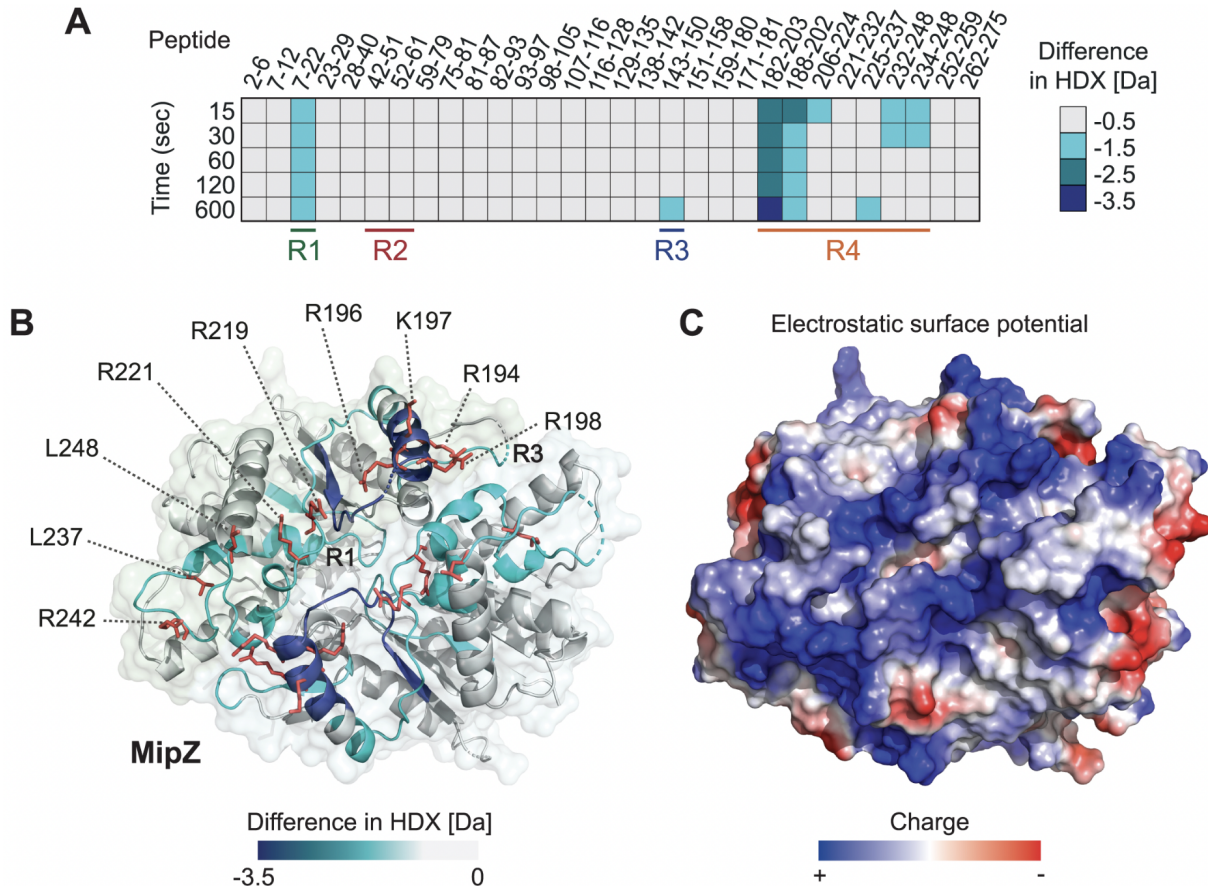


**Figure 4.3: MipZ interaction with DNA. (A)** HDX-MS result on the surface of MipZ mapped for the interaction of DNA. The region designated as R4 towards the C-terminal end is the maximum protected area that interacts with DNA. **(B)** Representation of the protected area on the surface of dimeric MipZ with the amino acids found to be important for DNA-MipZ interaction via biochemical methods marked. **(C)** The electrostatic surface potential shows the exposed patch of positively charged amino acids at the dimer interface that can bind nonspecifically to DNA(Corrales-Guerrero et al, 2020)

Previous studies have identified the ParB binding region of dimeric MipZ by Alanine scanning mutagenesis as well. As a result we can now map on the surface of MipZ the putative regions involved in ParB, DNA and FtsZ binding. The ParB-binding residues partially overlap with the previously identified DNA binding region on the MipZ surface, this would mean that the MipZ surface is shared between ParB and DNA. We need to further dissect these interfaces to find out how MipZ interacts with ParB and DNA.

As described in the introduction, the bipolar gradient distribution of dimeric MipZ is crucial for effectively placing the functional FtsZ ring at the mid cell. The poles act as a source of dimeric MipZ. The MipZ gradient formation critically depends on the interaction of MipZ monomers with the cell pole-associated ParB partition complexes. However, the molecular mechanism underlying this phenomenon is still unclear. Towards this end we set out to understand the interaction between these two proteins.

# Results

## MipZ binds to ParB via its C-terminal region

To understand the mechanism underlying MipZ dimerisation, it is crucial to identify the residues involved in its binding to ParB. Previous studies by alanine-scanning mutagenesis have identified some residues that could potentially be involved in this process, including W58, R221, D236, V246, L248, L172, D147. It was suggested that some of these residues may also be involved in DNA binding. To shed more light on the interaction of MipZ with ParB, we mapped the ParB-binding interface of MipZ by hydrogen/deuterium exchange mass spectrometry (HDX-MS). To this end, MipZ dimers formed in the presence of ATPγS, which locks the protein in the dimeric state, were incubated with ParB in a deuterated buffer. They were then subjected to fragmentation and analysis by mass spectrometry. The peptides that showed reduced deuterium uptake in the presence of ParB would be the putative regions blocked by ParB binding. As a result, we identified a total of 102 peptides, covering 99.7% of the protein sequence. Protected peptides were mapped to helices α13, α14, loops α12-α13 and α13-α14 as well as the β9 region (Figure 4.4). It is observed that the residues of MipZ that bind to ParB as represented by the blue coloured regions on the map can include R221, D236, L237, L248, L251, R254, R258 and they are present in the region designated as R4 (the C-terminal region) in the HDX map of the MipZ dimer interacting with DNA shown in Supplementary Figure S1. A representation of the HDX-MS results shed light into the region on MipZ where the protected residues are present.

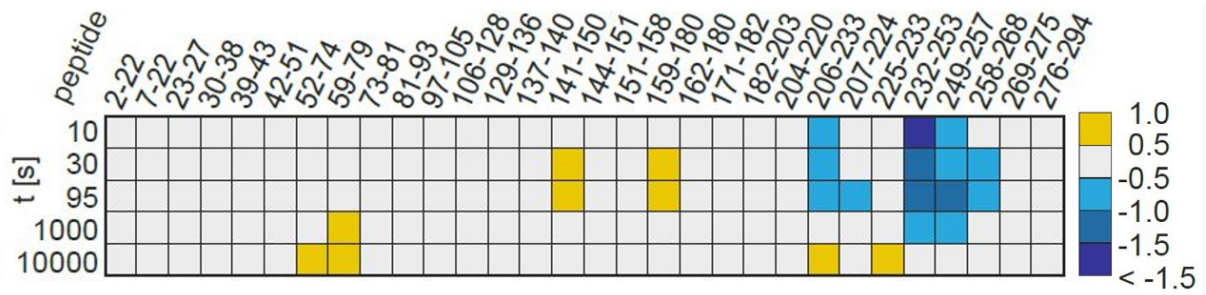


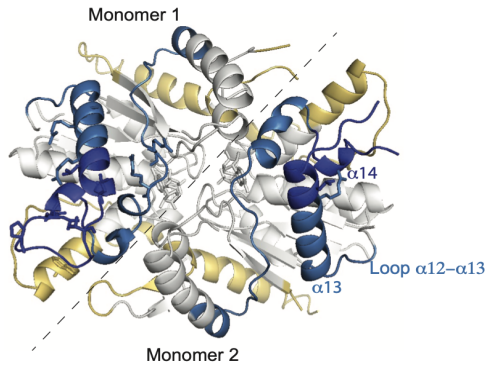

**Figure 4.4: HDX-MS of ParB dimer bound to MipZ dimer on the surface of MipZ dimer.** HDX-MS data mapped on the sequence wherein the C-terminal region is the primarily protected area in the presence of ParB The heat map represents the protected area in blue and the deprotected area in yellow colour. The sequences corresponding to the protected area are mapped on the surface of a MipZ dimer in the same colour as indicated in the lower panel. Similarly, the deprotected area is represented on the surface as yellow.

## ParB and DNA partially share their interaction interface on the surface of MipZ dimers

The HDX-MS results suggest that DNA and ParB could share similar or overlapping binding sites on the surface of MipZ dimers. As is evident from Figure 4.6, residues R242, R219, R196, R198, K197, R194 are protected exclusively upon binding DNA and residues R258, L251, R254, D236 are protected exclusively upon binding ParB. However, residues L248, L237, and R221 are protected in both DNA and ParB binding. Given the putative overlap of the binding sites, DNA and ParB should compete with each other for binding to MipZ. In the case of ParB it is known that ParB can bind both monomeric as well as dimeric MipZ. However, DNA can only bind dimeric MipZ as the dimer interface brings together positively charged residues of both monomers to form an overall positively charged patch that interacts with the negatively charged phosphate backbone of DNA.

Mapping the interaction interfaces of ParB and DNA binding on the surface show that the yellow region corresponding to the DNA binding in Figure 4.5 overlaps with the blue region that interacts with ParB at amino acids L248, L237, and R221 as represented in green.

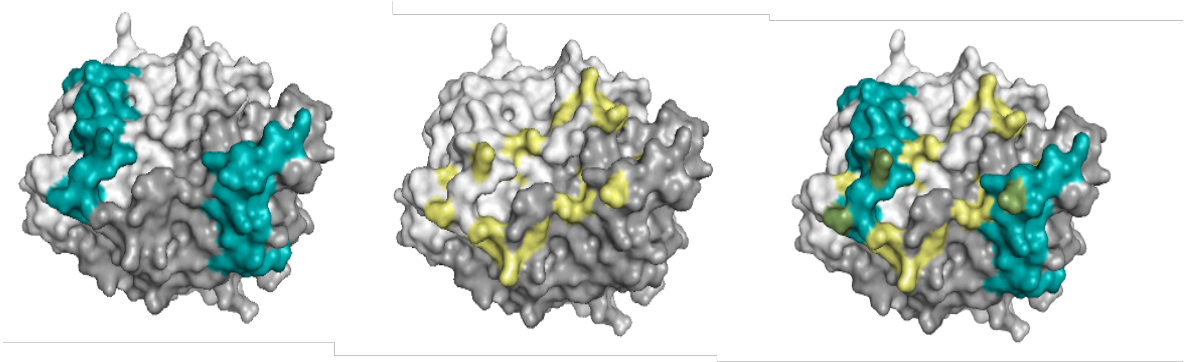

**Figure 4.5: Overlap of the ParB and DNA binding interfaces on MipZ.** Shown are the surface of dimeric MipZ with the two monomers colored white and grey, respectively. The coloured regions indicate the positions of the putative DNA binding interface (blue, left), the experimentally determined DNA binding interface (yellow, middle), and both the putative ParB and DNA binding interfaces (right), with shared amino acids colored green

In order to confirm whether ParB and DNA in fact compete with each other for dimeric MipZ, a biochemical experiment was carried out using biolayer interferometry. To this end, biotinylated double-stranded oligonucleotides were immobilised on SAX streptavidin biosensors and the binding reaction was monitored when either MipZ dimers or a mixture of MipZ dimers and ParB were added. If ParB competes with DNA, the availability of free MipZ dimers able to bind the immobilised DNA should decrease with increasing

concentrations of ParB in the ligand mixture, resulting in a gradual decrease in the binding signal. A series of binding experiments were done with 4μM MipZ (in the presence of ATPγS that locks it in dimeric state) and increasing concentrations of ParB ranging from 0 to 80 μM of ParB, with a control that contains only 80μM ParB as the binding cocktail (Figure 4.6).

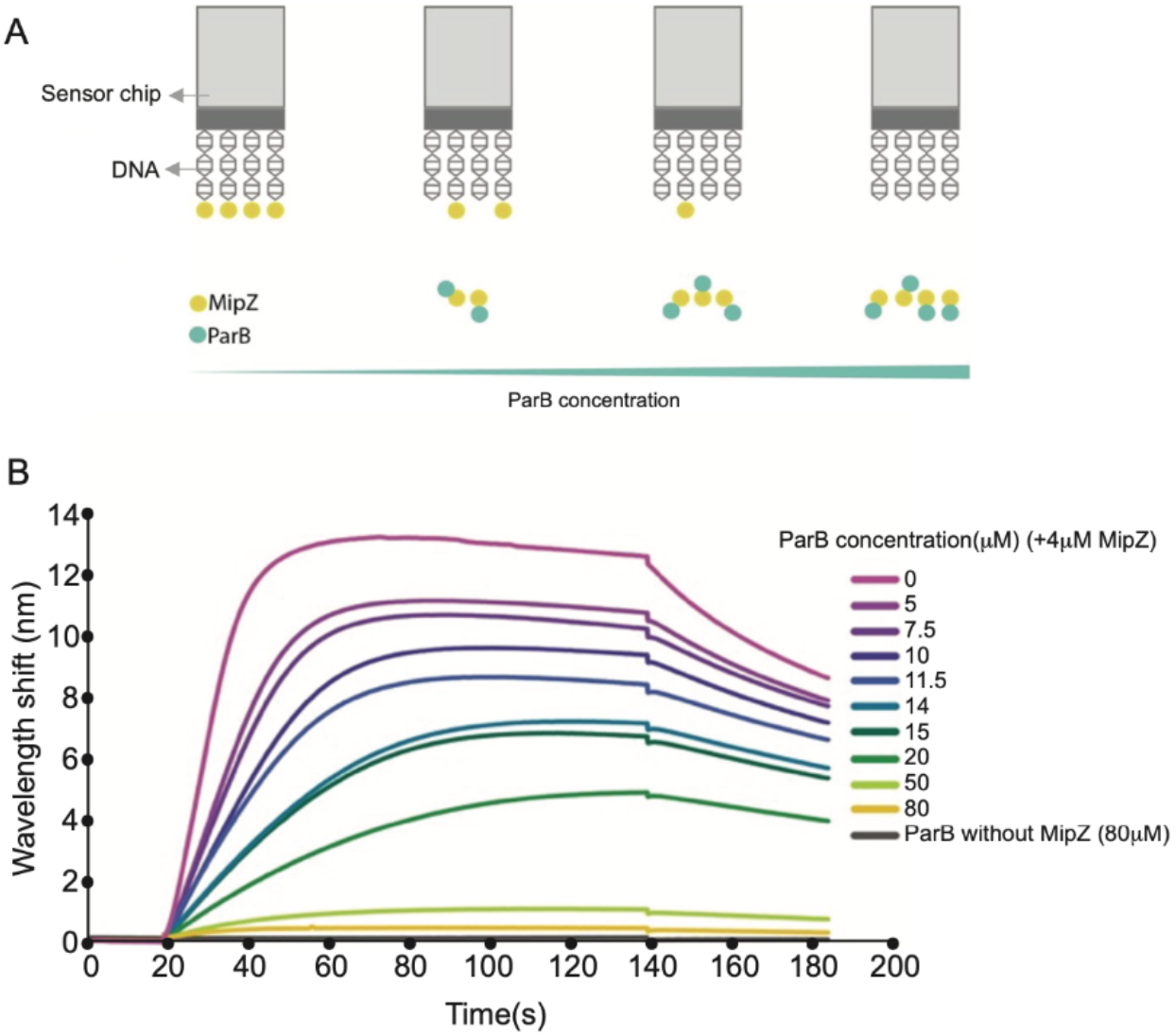


**Figure 4.6: ParB and DNA compete with each other for binding to dimeric MipZ.** The first panel(A) is the cartoon representation of the BLI experiment where the DNA is immobilised into the sensor chip and is seen interacting with MipZ. The second panel(B) shows the BLI result where DNA is immobilised on the sensor chip on which a cocktail of MipZ and ParB are added. Varying concentrations of ParB with constant concentration of MipZ as indicated in the figure were added. In the presence of ParB the MipZ dimers are sequestered, resulting in lower and lower binding with increasing concentration of ParB.

In accordance with the HDX-MS result, there is a clear decrease in the binding of MipZ dimers to DNA if ParB is present at increasing concentrations. Unlike some other ParB homologs, *C. crescentus* ParB lacks non-specific DNA binding activity, which makes it

possible to carry out this experiment without interference by direct association of ParB with the immobilised DNA. As is evident from the control run, even in the presence of 80 µM ParB, no DNA binding was detected, thus proving that the wavelength shifts correspond exclusively to DNA-MipZ interaction (Figure 4.7, black trace). This experiment thus provides biochemical proof that the interaction regions of DNA and ParB overlap on the MipZ surface.

To obtain further insight into the ParB-binding region of MipZ, we aimed to determine to what extent the surface region pinpointed by HDX-MS is conserved. To this end, MipZ homologs of species that also possess ParB were subjected to the Consurf server, which maps the degree of sequence conservation of proteins onto their molecular structure (Ashkenazy et al,2016). This analysis showed that the putative ParB-binding site of *C. crescentus* ParB is conserved among these proteins. This could mean that this region has specifically evolved in MipZ to mediate the interaction with ParB (Figure 4.7).

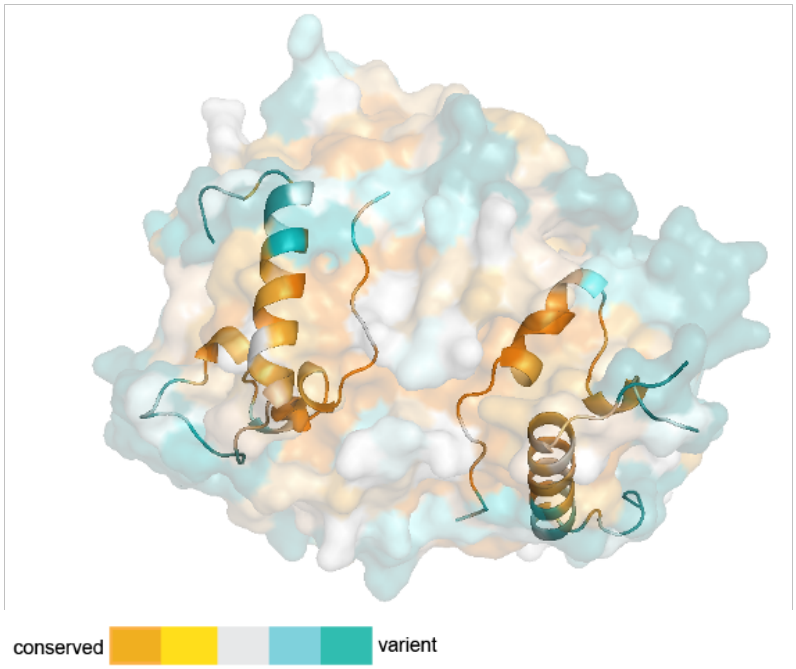


**Figure 4.7: The ParB binding area on the MipZ surface is conserved among bacteria that possess both ParB and MipZ.** The coloration of the MipZ dimer surface generated by the Consurf server indicates the degree of conservation of surface-exposed residues of MipZ among species that also possess ParB. Conserved regions are shown in orange, non-conserved regions are shown in blue. The regions in the C-terminal part of MipZ that exhibit reduced HDX in the presence of ParB (compare Figure 4.4) are shown in cartoon representation.

## ParB interacts with the C-terminal domain of MipZ

As mentioned in the introduction, ParB has recently been discovered to be a CTP-binding molecular switch that in the presence of CTP forms rings on DNA to form the partition complex. *C. crescentus* ParB not only interacts with ParA but also with the ParA-like ATPase MipZ, bringing together two crucial cell cycle events namely chromosome segregation (via its interaction with ParA) and cell division (via its interaction with MipZ).

To understand how ParB shares its surface with all its interaction partners, it is mandatory to obtain an understanding of interaction surfaces involved. Importantly, it is the interaction between ParB and MipZ that brings about the dimerization of MipZ, and it is crucial to identify the residues involved in this interaction on both ParB and MipZ surface to be able to understand the underlying mechanism of MipZ dimerization. We therefore analysed changes in the HDX pattern of ParB induced by the presence of MipZ. To this end, ParB was incubated with MipZ dimers in a buffer prepared with deuterated water. 77 ParB peptides that showed reduced deuterium uptake were identified, with a coverage of 95.4% of the protein sequence.

A detailed analysis of the HDX results revealed that to helices in the C-terminal dimerization domain of ParB, formed by amino acids V252-E261 and T289-I304, as well as amino acids E130-E135 in the N-terminal CTPase domain showed reduced HDX in the presence of MipZ dimers, suggesting that they are involved in MipZ binding. On the other hand, amino acids A184-I206 in the *parS*-binding domain of ParB showed increased deuterium uptake, possibly due to conformational changes induced by the interaction (Figure 4.8).

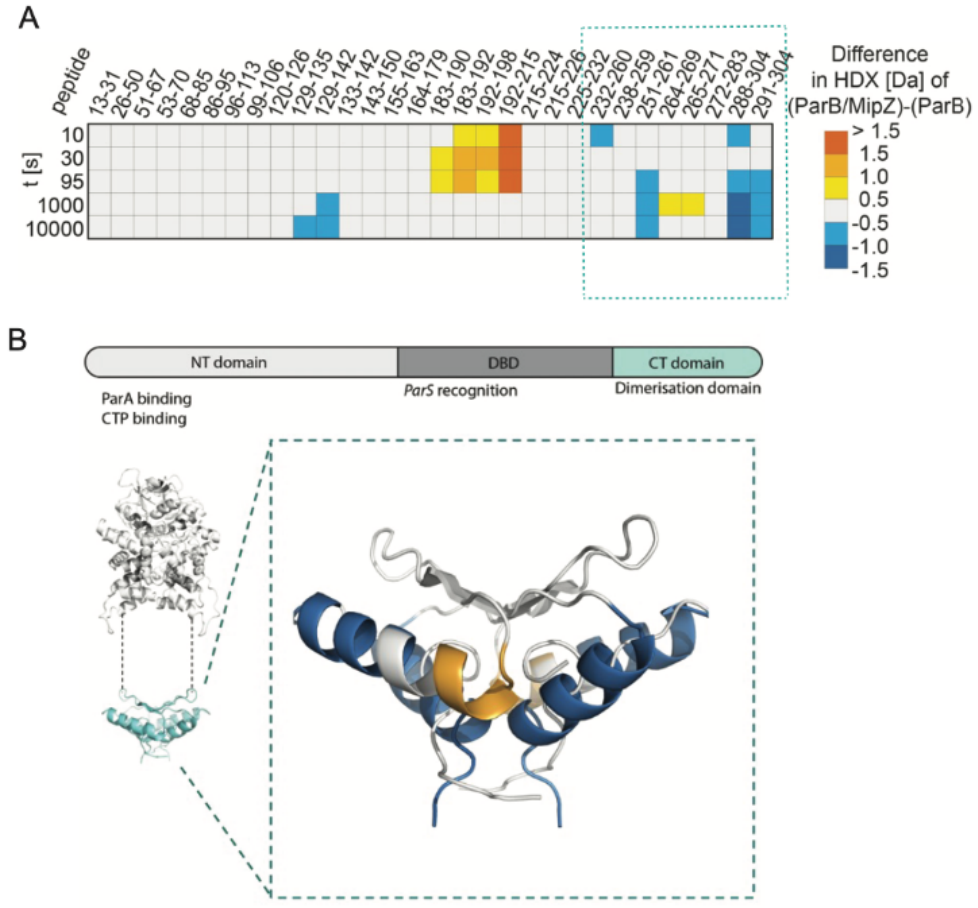


**Figure 4.8: Changes in HDX in the ParB dimer induced upon incubation with MipZ dimers.** The first panel represents the HDX result mapped on the ParB sequence, where the CT region has maximum coverage or reduced deuterium uptake as indicated in blue marked in the square. The lower panel shows the region

mapped on the surface where the CTD is predominantly represented as a region of higher protection as indicated in blue. The orange regions indicating lower protection could be because of some residues getting more exposed due to minor conformational changes induced by the interaction.

The observed interaction of MipZ with the C-terminal region of ParB is interesting, because this region of *Caulobacter* ParB has so far only been implicated in dimerization. In general, CTP-induced ring formation by ParB is brought about by the engagement of the two N-terminal CTPase domains of ParB (Soh et al, 2019, Osorio et al, 2019), whereby CTP and *parS* binding induces a conformational change in the CTPase domain and the adjacent *parS*-binding domain that facilitates the homodimerization reaction. By contrast, the C-terminal domain forms a stable dimer under all conditions (Madariaga-Marcos et al, 2019), thus closing the ParB permanently at the C-terminal end of the two subunits. In bacteria such as *B. subtilis*, this domain region was found to interact with DNA in a nonspecific manner, which is important for DNA condensation *in vitro*. *C. crescentus* ParB does not exhibit any strong non-specific DNA interaction. Thus, it is possible that apart from being the dimerization domain, the *C. crescentus* C-terminal domain may have specifically evolved to bind MipZ, thereby making it a protein-protein interaction domain as well.

## *In vitro* interaction between MipZ and a mini-partition complex

To further clarify the importance of the regions identified by HDX-MS for the MipZ-ParB interaction, we decided to analyse the binding of MipZ to DNA-loaded ParB rings using BLI. To this end, we used an experimental setup devised by Tung le, where a *parS*-containing DNA fragment that is biotinylated at both its ends is immobilised on a streptavidin-coated sensor chip, thereby generating closed DNA loops (Figure 4.9 A). Towards this, a DNA sequence of a total length of 196 bp that contains one of the *Caulobacter parS* sequences was amplified from genomic DNA using biotinylated primers. After immobilisation on the sensory chip, ParB was added in the absence or presence of nucleotides. We observed a clear binding signal when the reaction was performed in the presence of CTP or its poorly hydrolyzable analogue CTPγS, but not in the absence of CTP (Figure 4.10 B).

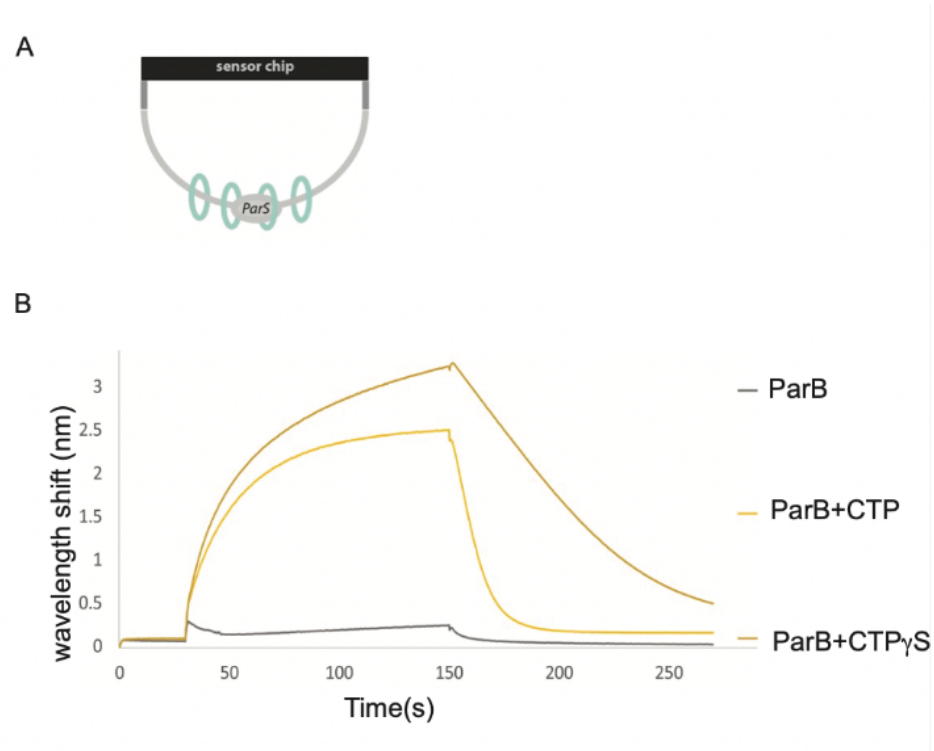


**Figure 4.9: Formation of mini-partition complexes to study the MipZ-ParB interaction by BLI.** (**A**) Cartoon representation of the set-up used for the BLI analysis, where a *parS*-containing DNA that is biotinylated at both ends and immobilised on a streptavidin-coated sensor chip forms a closed loop with *parS* in the middle of the sequence. In the presence of CTP, ParB rings (blue) are loaded forming a mini-partition complex. (**B**) Binding curves showing the association of ParB with *parS*-containing DNA in the presence or absence of CTP or CTPγS and its dissociation after transfer of the sensor into protein- and nucleotide-free buffer. Note that ParB rings are not stable in the absence of CTP.

Notably, in the presence of CTP, ParB binds well to the DNA loop but dissociates quickly once the complex is transferred to a buffer lacking the nucleotide during the dissociation step. In the presence of CTPγS, however, the rings are more stable and dissociate more slowly upon nucleotide removal. This finding suggested that CTPγS needed to be used and included in all buffers to stabilise mini-partition complexes. Given the high costs for this nucleotide analogue, which needed to be obtained by custom chemical synthesis, we decided to resort to a CTP hydrolysis-deficient variant of ParB (ParB-Q58A) that had previously been shown to form stable DNA-associated rings *in vitro* and *in vivo*. BLI analysis showed that ParB-Q58A indeed remained stably bound to the DNA loop if CTP was included during both the association and dissociation steps. This is because it hydrolyses CTP very slowly compared to the wild type protein. However, it has to be noted that in the absence of CTP, the ParB-Q58A dissociates from the DNA. Hence CTP was supplied along with the association step when MipZ was added. Thus, this setup was used for all further MipZ-ParB interaction experiments.

Having established the formation of mini-partition complexes, we next aimed to investigate the interaction of MipZ with the loaded ParB rings. Since MipZ binds non-specifically to DNA, it was necessary to use a mutant variant of MipZ, MipZ-R198A, which carries an

amino acid exchange in the DNA-binding pocket that specifically abolishes DNA binding while leaving other activities of MipZ unaffected (Figure 4.10). The ParB-Q58A variant could successfully recruit the MipZ variant in the presence of CTP, confirming that despite the point mutations the ParB-MipZ interaction is unaffected in this system and can further be used to analyse this interaction.

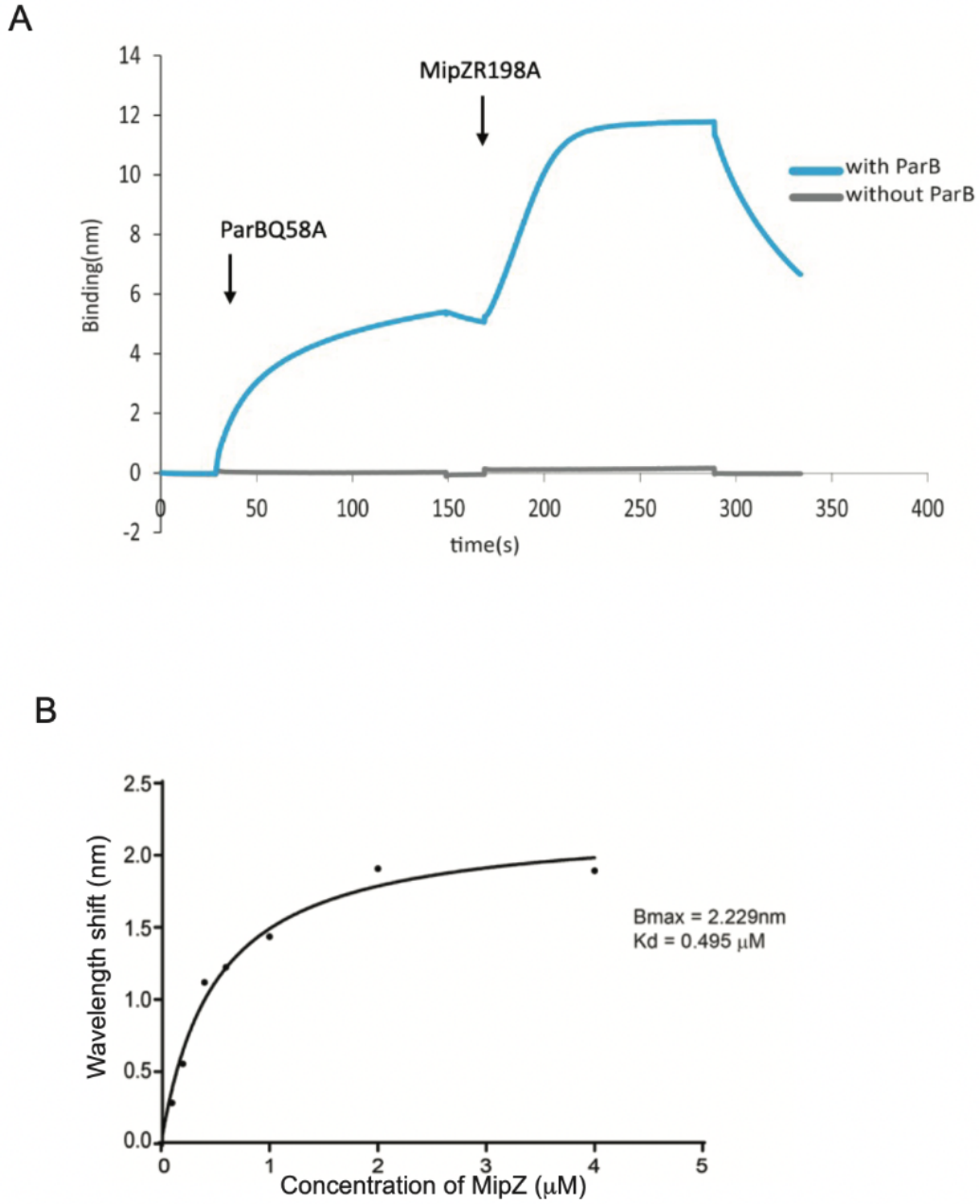


**Figure 4.10: Caulobacter ParB recruits MipZ *in vitro*.** Panel A shows sensors probed with biotinylated DNA loops that carry ParB-Q58A rings when exposed to MipZ-R198A, in the presence of CTP, shows binding. A representation curve of the titration is shown, in blue, MipZ-R198A(4μM) binding to ParB-Q58A(10μM) is shown whereas in grey MipZ binding (or lack thereof) in the absence of ParB variant is shown. The second panel shows $K_D$ of the titration of interaction between MipZ and ParB variants that is found out to be 0.495 μM.

## The analysis of chimeric ParB proteins identifies the C-terminal domain of ParB as a critical MipZ interaction determinant

With an *in vitro* system at hand to probe the ParB-MipZ interaction, we went on to narrow down the region(s) of ParB mediating MipZ binding. To this end, we generated chimera of *C. crescentus* ParB in which the C-terminal dimerization domain was replaced for the C-terminal domains of divergent ParB homologs that are distinct in sequence and from a species lacking the MipZ system. To this end, we first chose the C-terminal domain of ParB (Spo0J) from *B. subtilis*. It shares only with the *C. crescentus* counterpart and, unlike the *C. crescentus* domain, contains several lysine residues that were shown to mediate non-specific DNA binding activity.

Using the BLI set-up, we formed mini-partition complexes of the chimeric protein on a DNA fragment containing the *C. crescentus parS* sequence. The chimera bound more efficiently to DNA, likely because the non-specific DNA-binding activity of the *B. subtilis* C-terminal domain added to the specific loading of the protein at the *parS* site. In the presence of CTPγS during all steps of the analysis, the chimera remained stably bound to the DNA. However, upon addition of MipZ, no additional binding signal was observed, indicating the chimera is no longer able to interact with MipZ. This finding confirms a critical role of the C-terminal domain as a mediator of the ParB-MipZ interaction *in C. crescentus*. Notably, in the absence of CTPγS, the chimera also interacts with the DNA loop, likely based on its non-specific DNA-binding activity, but it dissociates rapidly from the DNA upon transfer into a MipZ-containing solution that lacks the chimeric protein. In control reactions with the wild-type ParB protein of *C. crescentus*, there is a clear interaction with MipZ in the presence of CTPγS. From these findings, we infer that the C-terminal domain of *C. crescentus* ParB is necessary for the interaction of ParB with MipZ.

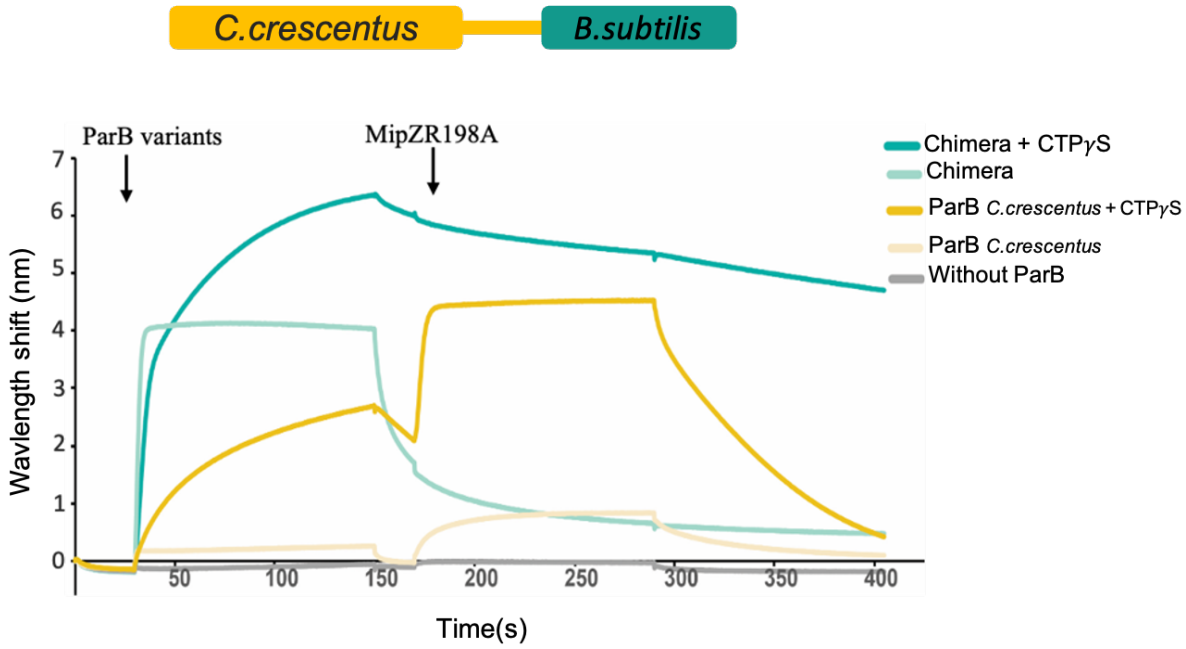

**Figure 4.11 : A chimeric variant of *C. crescentus* ParB containing the C-terminal domain of *B. subtilis* ParB cannot recruit MipZ.** On doubly biotinylated DNA that was immobilised in streptavidin sensor chips, the ParB chimeras (10µM) were added. To this 4µM MipZR198A was added to test the ability of the chimera ParB variants to recruit MipZ. The dark green curve represents the chimaera protein carrying the CT of Spo0J that does not recruit MipZ because of the absence of *Caulobacter* CT. The dark yellow curve represents the WT ParB of *Caulobacter* that recruits MipZ.

Since the strong non-specific DNA-binding activity of the C-terminal domain of *B. subtilis* ParB complicated the interpretation of the data, we decided to construct a similar chimera using the C-terminal domain of *M. xanthus* ParB, which does not bind DNA non-specifically (Osorio et al, 2021). At the same time, we also generated a reverse chimera, comprising the N-terminal region of *M. xanthus* ParB and the C-terminal domain of *C. crescentus* ParB to determine whether the latter would be sufficient to recruit MipZ to mini-partition complexes.

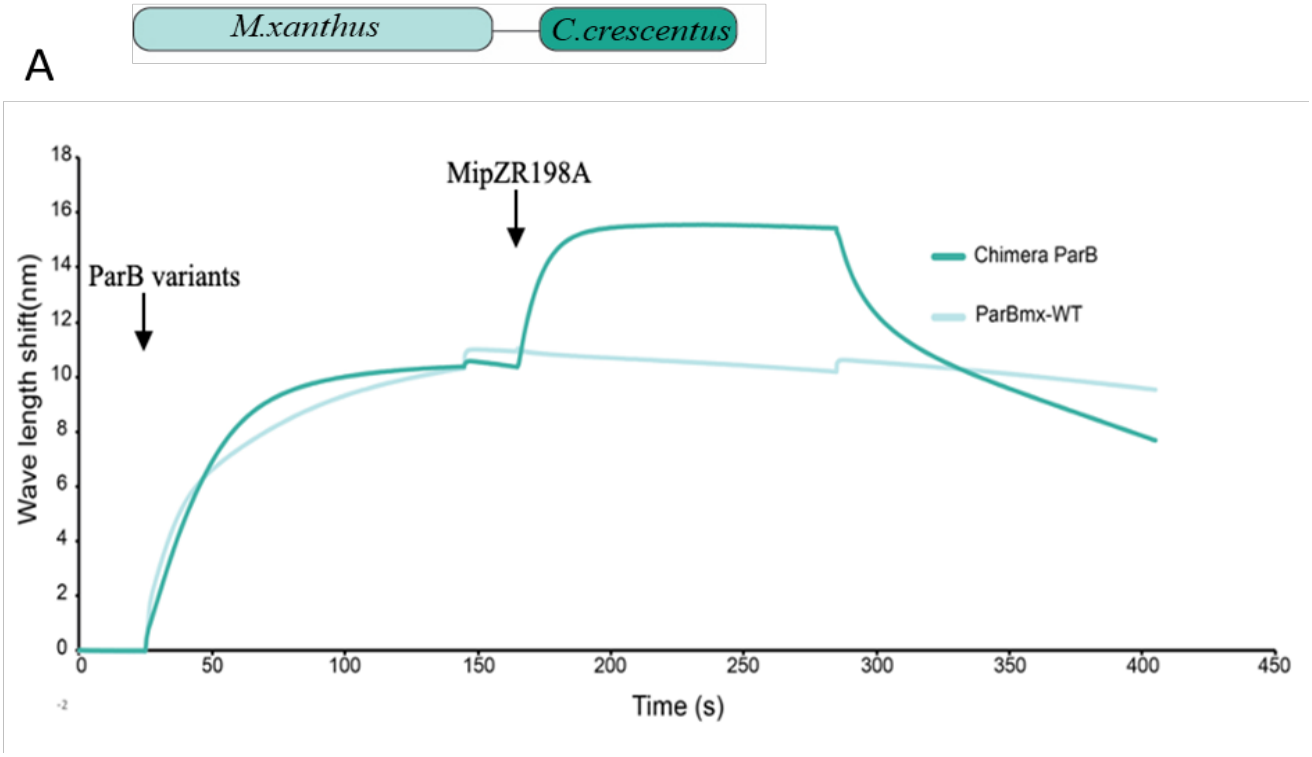


**Figure 4.12: The CTD of *Caulobacter* ParB is necessary and sufficient to recruit MipZ.** ParB chimera as indicated in the cartoon (10µM) immobilised on DNA supplied with 1µM CTP. To test its binding with MipZ, MipZR198A(4µM) supplied with 1µM ATP and CTP were added. With the CT of *C.crescentus* ParB present, the chimera is able to recruit MipZ

To analyze the binding characteristics of the new chimeras, we first immobilised a DNA fragment containing *C. crescentus parS* on a streptavidin-coated biosensor and incubated the DNA loops formed with the ParB chimera composed of the N-terminal region of *C. crescentus* ParB and the C-terminal domain of *M. xanthus* ParB to form mini-partition complexes. As expected, since the *parS* recognition region of the chimera was still intact,

the chimera was readily loaded on the DNA (Figure 4.13). The chimera carried the Q58A exchange, abolishing its CTPase activity, so that the ParB rings formed remained stably associated with the DNA loops after the association step. However, unlike the wild-type protein, this chimera did not show any interaction with MipZ, further proving that the CT region is necessary to recruit MipZ *in vitro*.

To analyse the reverse chimera comprising the N-terminal region of *M. xanthus* ParB and the C-terminal region *C. crescentus* ParB, we performed a similar experiment using biosensors that were derivatized with double-biotinylated DNA containing an *M. xanthus parS* site. Again, the protein contained a mutation (Q52A) that abolishes its CTPase activity (Osorio et al, 2021), thus stabilising its interaction with the DNA. (figure 4.12) Importantly, unlike the wild-type *M. xanthus* protein, the chimera was able to interact with MipZ. Collectively, these results obtained with the chimeric proteins demonstrate that the C-terminal domain of *C. crescentus* ParB is sufficient to bind MipZ.

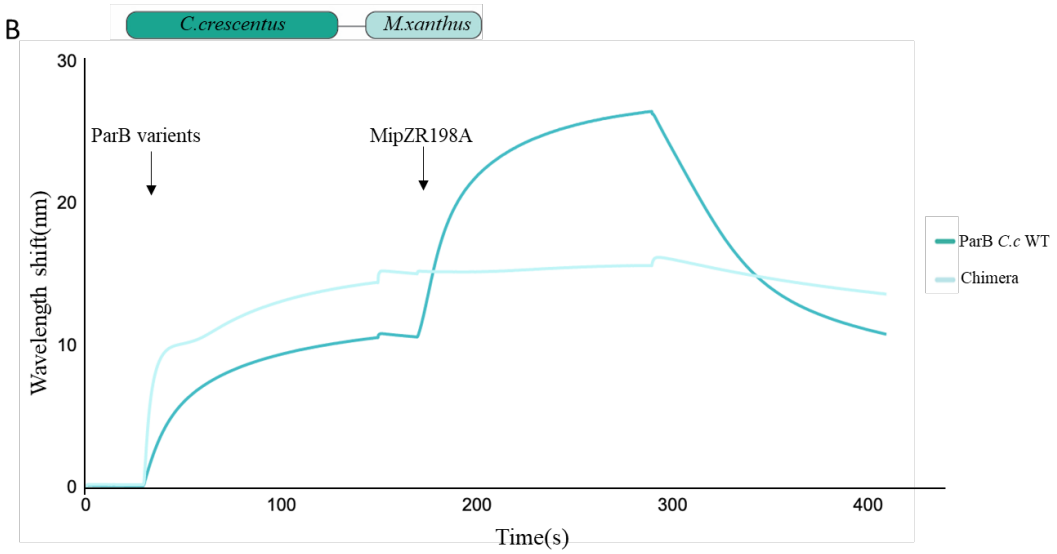


**Figure 4.13: The CTD of *Caulobacter* ParB is necessary and sufficient to recruit MipZ.** ParB chimera as indicated in the cartoon (10µM) immobilised on DNA supplied with 1µM CTP. To test its binding with MipZ, MipZR198A(4µM) supplied with 1µM ATP and CTP were added. The *C.crescentus* ParB, without its CT is unable to recruit MipZ

## The C-terminal region of *C. crescentus* ParB is sufficient to recruit MipZ

To conclusively show that the C-terminal domain of *C. crescentus* ParB is sufficient to recruit MipZ, we designed an experiment in which the C-terminal domain of ParB was directly immobilised on a streptavidin-coated BLI biosensor after in *vitro* biotinylation using an amine-reactive biotin derivative. Subsequently, the immobilised protein was again probed with increasing concentrations of wild-type MipZ in the presence and absence of ATPγS to mimic the monomeric and dimeric states of MipZ. We found that the isolated C-terminal domain was able to recruit MipZ dimers with a $K_D$ value of 0.36 µM. Its affinity is thus comparable with that determined for the interaction of MipZ-R198A to full-length

ParB in a mini-partition complex. This result proves that the C-terminal domain of ParB is necessary and sufficient to recruit MipZ *in vitro*.

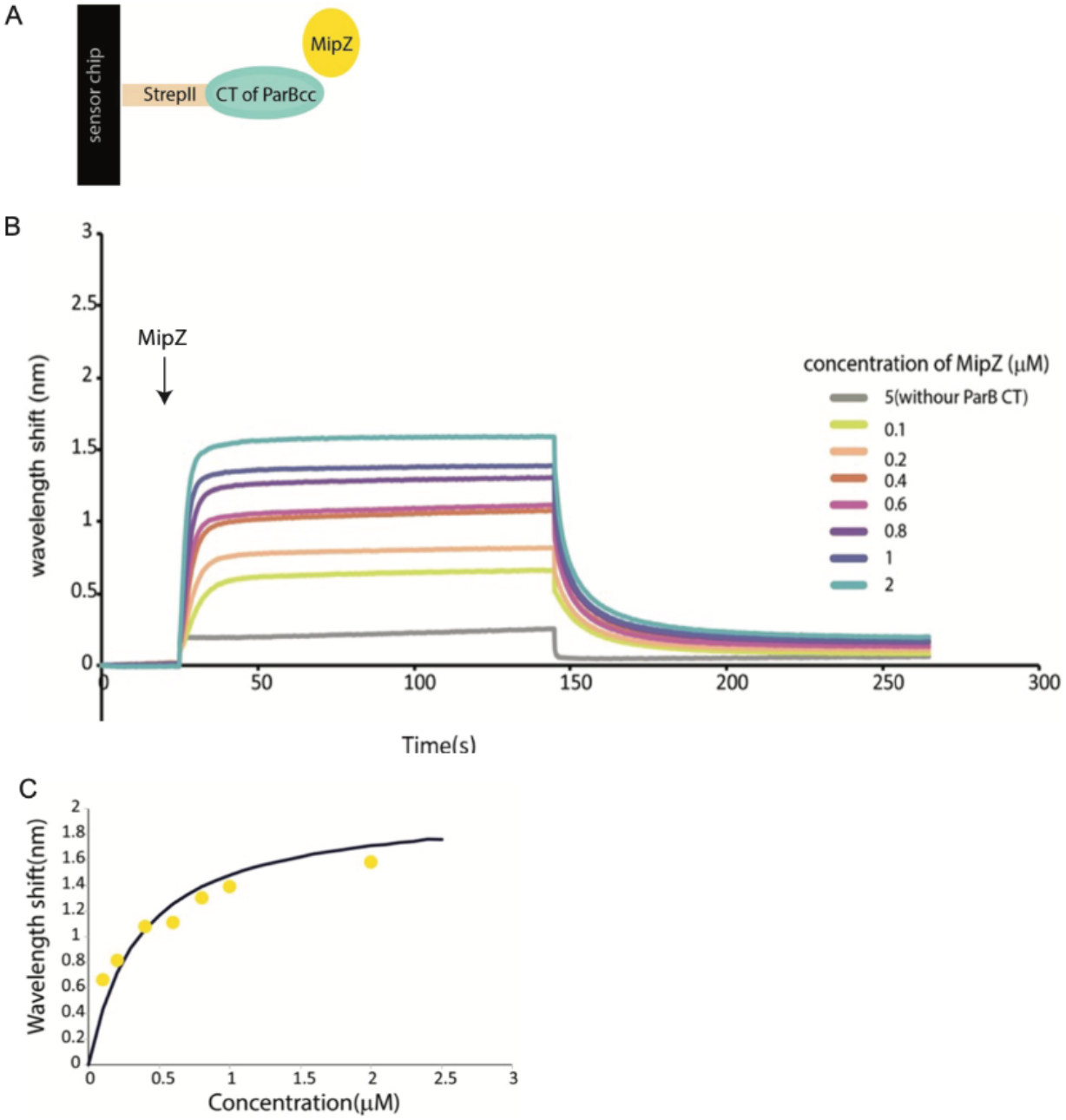


**Figure 4.14: The C-terminal domain of *C. crescentus* ParB is sufficient to recruit MipZ**. Panel A shows the cartoon representation of ParB-CT peptide binding to sensor chip set up that was used for BLI. Panel B shows the titration of increasing concentrations of MipZ that bind to the immobilised ParB fragment (5μM). Panel C shows the $K_D$ measurement obtained from the titration with a value of 0.36 μM.

## The predicted interaction interfaces of ParB-monomeric MipZ and ParB-dimeric MipZ

Our findings demonstrate conclusively a key role for the C-terminal domain of *C. crescentus* ParB in the recruitment of MipZ. The data obtained by HDX-MS analysis suggest that two helices in this domain, comprising amino acids V252-E261 and T289-I304, respectively, may contain the main interaction determinants, although future work is required to map the precise binding interface. The role of the short comprising amino acids E130-E135 that showed decreased deuterium uptake in the HDX experiment is likely not involved in the interaction with MipZ, as the CT alone was completely capable of recruiting MipZ. Each monomer of the ParB CT folds into these two helices at either ends and the central part folding into a beta hairpin motif. The amino acids in the hairpin motifs are highly conserved and are involved in the dimer formation. The helices fold outward in the dimers structure that could potentially interact with other proteins or DNA, consistent with this, it is the aminoacids in these helices that predominantly showed protection towards deuterium uptake in the HDX experiment.

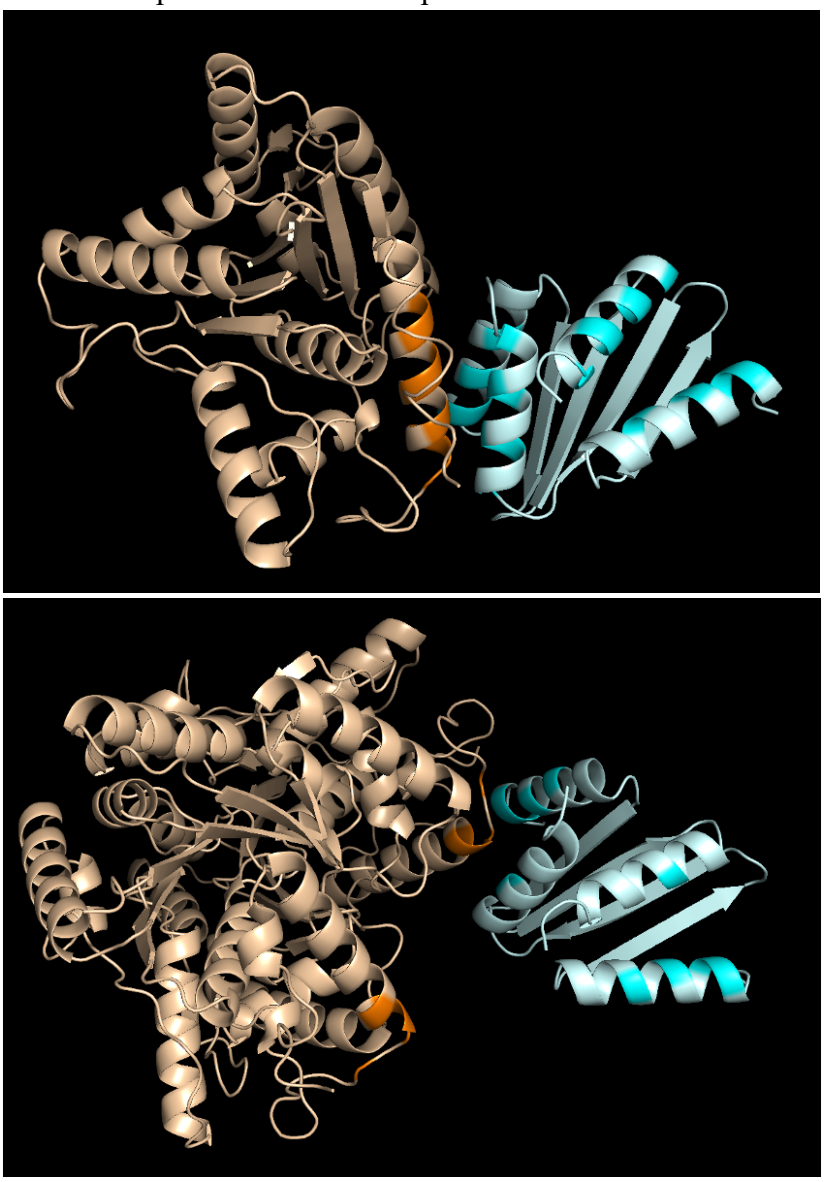

**Figure 4.15: The predicted interaction interfaces of monomeric and dimeric MipZ with ParB show variations**.The first figure shows the predicted structures of monomeric MipZ interacting with the dimeric CT of ParB. The second figure shows the dimeric MipZ interacting with the dimeric ParB CT.It can be seen that the interaction interfaces are slightly varied between both cases.

It can be seen that compared to the monomeric MipZ interacting ParB CT with that of dimeric MipZ, the region involved in the interaction is slightly varied. the potential residues involved in monomeric MipZ interaction on the surface of ParB CT peptides are D294, N298, D256, L293, C292, T301, T257, L260, L264 and L290 out of which L293, C292, N298, T301, L264 and L290 are exclusively involved in monomeric MipZ interaction. On the other had, the dimeric MipZ interacts with a smaller area on the parB surface and potentially engage the following amino acids: D256, T257, L260, D263, D294 out of which D263 exclusively interacts with the dimeric form. It could be that the conformational change induced by dimerisation caused a shift in the interaction interfaces of the proteins. It will be interesting in the future to understand the importance of this interaction in facilitating the dimerisation of MipZ.

# Chapter 5: Discussion

## Part 1: Replication dynamics and chromosome segregation in *Hyphomonas neptunium*

In this study we examined the role of replication in the two-step segregation of the chromosome of *H. neptunium.*

## The two-step chromosome segregation in *H.neptunium*

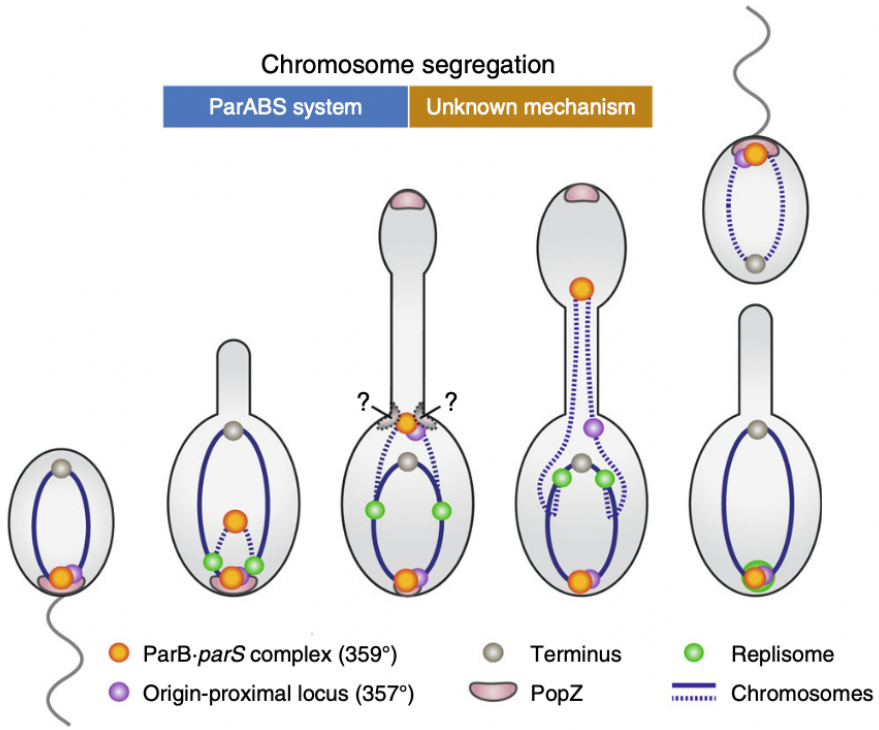


**Figure 5.1: Model of the two-step chromosome segregation process in *H. neptunium*.** The first cell is a swarmer cell with the partition complex (orange) tethered to the polar landmark protein PopZ (pink) to the flagellated pole and the *ter* region (grey) at the opposite pole with the chromosomal arms(blue) stretching between the two poles. In the second cell, the differentiation to the stalked stage begins, which coincides with initiation of replication with a visible formation of replisome (green). The third cell depicts the stage where the bud cell formation begins where PopZ is already seen localised at the distal end. The newly duplicated origin is anchored at the stalked pole of the mother cell by some unknown factors (indicated by "?"). The fourth cell shows the second step of the replication where the chromosome is translocated through the stalk to the newly formed bud compartment. The *ori* region moves through the stalk first, followed by the origin proximal region (purple). The fifth cell shows the completion of cell division after the replication of chromosomes where the stalked mother cell is ready to undergo another round of replication. The daughter cell is a swarmer cell with the chromosome arranged in a longitudinal manner.

The ParAB*S* system has been commonly found in many species across the bacterial kingdom. In the case of *H. neptunium*, the ParAB*S* system is present and is an essential component for survival. The single circular chromosome that is organised in the *ori-ter* manner is dependent on the ParAB*S* system for chromosome segregation. The longitudinal arrangement was first studied systematically in *C. crescentus* by the localisation of different chromosomal positions(Viollier et al, 2004). This technique is employed in *H.neptunium* to reveal its chromosome arrangement to be the same. Apart from *C.crescentus*, a similar arrangement has been observed in slow growing *E. coli*, *M. xanthus*, *V. cholerae*, *M. tuberculosis* etc. Interestingly, *E. coli* is devoid of a ParAB*S* system. The other species possess a ParAB*S* system and the combination of ParAB*S* dependent segregation and the anchoring of the duplicated origin at the new pole could play crucial roles in maintaining the longitudinal organisation of the chromosome. Unlike other bacteria, the chromosome segregation in *H.neptunium* takes place in a unique two-step manner, reminiscent of eukaryotic chromosome segregation. In the first step the *ori* is segregated to the stalked end of the mother cell. This step is similar to its close relative, *C.crescentus,* in a ParAB*S* dependent manner as described. The second step is the segregation of the duplicated chromosome through the stalk, finally positioning at the farthest end of the bud (away from the stalk) and further maintaining the longitudinal organisation. The second step is uniquely adapted to the stalked morphology of *H.neptunium*. There is a time gap between the first and the second step that separates the segregation event. It is possible that the new *ori* waits at the stalked junction to allow enough replication time so as to facilitate the two sister chromosomes to remain in proximity to carry out DNA repair. It is also noted that there is a minimal critical bud size after which the segregation through the stalk happens to ensure that the duplicated chromosome can be accommodated in the daughter cell. The exact signalling mechanism that initiates the second step of chromosome segregation is not known yet. It is possible to speculate that the translocation of chromosome through the stalk is likely independent of ParA and thus, could be via an unknown mechanism. It is known that ParA dependent segregation requires non-specific interaction of ParA with DNA (Hunding et al, 2003). In the case of translocation through the stalk, the first region to be translocated is the origin of the duplicated chromosome. The stalk is thus devoid of any chromosome to hold non-specifically binding ParA. It is also shown that the second step of translocation through the stalk happens faster and in a directed manner. This could suggest that the mechanism with which DNA is translocated through the stalk could be an active mechanism which remains elusive. Interestingly, some DNA associated proteins such as m-Cherry-ParBpMT1 are no longer visible in the stalk. This could mean that either the protein is stripped off in the stalk, or the change in DNA topology as it enters the narrow stalk is in some way affecting the protein folding. The DNA translocase of AAA+ FtsK is known to be actively involved in chromosome segregation (Crozat et al, 2010). *H. neptunium* also has a FtsK homologue that could potentially be involved in the segregation through the stalk.

## Implication of polar landmark proteins in chromosome segregation

Polar landmark proteins in bacteria are known to play important roles in cell cycle events such as recruiting pole specific proteins under various circumstances and chromosome anchoring during segregation. In the case of *Vibrio vulnificus*, the polar landmark protein HubP is known to localise FapA that is responsible for the flagellar assembly. In *V.cholerae*, HubP anchors the origin via its interaction with ParA. In the case of *Caulobacter crescentus*, the polar landmark protein PopZ has important implications in chromosome segregation as described later. Apart from PopZ, TipN is another important polar landmark protein in *C.crescentus* that is essential for perpetuating cell polarity (Lam et al, 2006) as well as helping out in sequestering ParA monomers to maintain the dimer gradient of ParA that is essential for chromosome segregation. In *B. subtilis,* during sporulation the DivIVA protein interacts with RacA that binds the origin proximal regions, thereby localising it to the pole (Wu et al, 2003). In *M. xanthus*, bactofilins BacNOP help localise the partition complex in the regions close to the poles (Lin et al, 2017).

The segregation of chromosomes in *H.neptunium* closely follows its relative *C.crescentus* in the first step, where the duplicated origin is stationed at the stalked end of the mother cell. The anchor point of *ori* in the case of *C.crescentus* is the polar landmark protein PopZ that interacts with ParB and can function as a velcro-like hub that attaches the newly replicated origin to the pole. Besides, PopZ also plays a role in sequestering the monomeric ParA that falls off from the DNA upon contact with the partition complex. This function is important to maintain the gradient of dimeric ParA and thus the directionality of segregation. *H.neptunium* possesses a homologue of PopZ. However, the function of PopZ seems to be not essential. While the localisation of the duplicated origin is slightly affected, the overall segregation process is not affected by the deletion of PopZ. However, we clearly see the stationing of the origin at the stalked pole. It could be that the origin waits there until the bud grows until a critical minimum size is reached, or the chromosome replication progresses to a critical point, however it is possible that *H. neptunium* has a polar factor that potentially interacts with ParB that remains unknown. It will be interesting to look at genes involved in stalk biogenesis and proteins that localise at the stalked pole during stalk formation. These proteins likely precede the newly duplicated origin and may play a role in anchoring it there or may potentially interact with or may provide a cue for the localisation of polar elements that might stall the newly duplicated origin. It is to be noted that a FtsZ ring forms at the mother cell-stalk junction as well along with the functional FtsZ ring that dictates the budding event. This other FtsZ ring dissociates at the mother cell-stalk junction. The factors that determine the dissociation of this FtsZ ring might also in some way recognize this junction as the stalk pole of the mother cell. It will be interesting to study if these factors have any connection with the anchoring of the ParB*S* complex at this pole.

It is crucial to find out the factors interacting with ParB at the stalked pole to understand the reason for initiation of the second step of segregation as well as the duration of the pause. To this end, several Co-immunoprecipitation assays were done where the ParB

protein was pulled out to find the peptides attached to it, and thus identify the potential interaction factors. Apart from the already known interaction factors of ParB, other proteins that will be identified in the assay can potentially be involved in the anchoring of origin at the stalked pole. However, this experiment did not lead to any conclusive results, as the ParB -DNA complex pulled out several proteins that could also be involved in DNA binding. However, it will be interesting in the future to figure out the other interaction partners of the partition complex.

## Implication of replication in the second step of segregation

Chromosome replication and segregation happen concomitantly in bacteria in general that has its own perks. The coordination in replication and segregation results in the re-establishment of chromosome positioning in the progeny as well as provides space for the re-establishment of intrinsic chromosome organisation. However concomitant replication and segregation is not observed in *H. neptunium* which could be a consequence of its special cell shape. Although the first step of segregation is similar to that of *C. crescentus*, the separation of the segregation process into two steps is a unique adaptation to its stalked morphology. One of the speculations as it has been already noted is that the duplicated origin stays within the mother cell until more than half chromosome is replicated presumably because for DNA repair based on homologous recombination requires the presence of sister chromosomes juxtaposed against each other. Once inside the stalk, the proximity of sister chromosomes cannot be ensured. Within the mother cell compartment this is possible. Therefore at least until the major chunk of the chromosome is replicated it is necessary for both the chromosomes to be in close proximity. It could also be that a certain landmark gene exists that needs to be replicated to trigger the second step of segregation. In the case of *C. crescentus* it is known that the presence of hemimethylated GANTC sites on the DNA inhibits the transcriptions of several cell cycle regulator genes in particular for DNA metabolism and cell division(Berdis et al, 1998), and hence the complete methylation of the DNA is coordinated with the completion of chromosome replication to restrict unwanted developmental errors. It is also tempting to speculate about the existence of cues like methylation or a similar modification of the DNA that controls the second step of segregation whereby the replication of a specific gene may initiate the transcription of genes responsible to trigger the segregation through the stalk.

In conclusion, the *H. neptunium* cells undergo a non reversible development from the replication incompetent swarmers to replication competent stalked cells, in which chromosomal positions and origin of replication were mapped and followed through the process of chromosome replication and segregation. The ParAB*S* system is indispensable for chromosome segregation. The chromosome is arranged in a longitudinal manner in the mother cell. Collectively, our data shows that chromosome segregation in *H. neptunium* is a two-step process. The first step is the ParAB*S* dependent segregation of the chromosome within the mother cell whereas the second step is the rapid segregation through the stalk. The duplicated origin waits at the stalked pole until most of the chromosome is replicated. The exact trigger of the commencement of the second step is yet to be discovered, but our

data suggests that it could be dependent on the size of the bud and/or the progress of chromosome replication.The mechanism of the rapid segregation through the stalk is yet to be discovered as well. Initial studies indicate that the localisation of FtsK in the stalk could potentially indicate its involvement in the second segregation step. This study thus sheds light on how morphologically varied bacteria could face the challenge of faithfully segregation its genetic material.

## Part 2: Characterisation of a ParA-like Protein in *Hyphomonas neptunium*

In this study we investigated the function of the ParA-like protein of *H. neptunium*, HNE-0708. *In Vitro* studies suggest that this protein has the ability to bind to DNA and hydrolyze ATP. Upon deletion, budding and stalked cells develop a defect in the stalk, by producing bulges that are clogged by DNA. The exact physiological role of this protein remains unknown. It is highly likely that this protein has an effect on chromosome replication and segregation because cells that show a morphological defect also show multiple ParB foci in the mother cells and sometimes inside the bulges.

Of all the budding cells that show a stalk bulging phenotype approximately 37% cells also have more than three ParB foci, more than 63% cells have more than two ParB foci. Sometimes, when the bud cell is just about to divide the mother cell already begins the next round of DNA replication. Hence, we cannot completely avoid the possibility of multiple foci due to replication initiation in quantifying cells with three ParB foci. However more than three ParB foci can be termed unusual, as this is possible only if the mother cell hyper-initiates the replication cycle.

Considering these observations, it is likely that the stalk develops the bulging defect prior to undergoing multiple rounds of replication. However, we cannot say this with certainty until a timelapse analysis is done to trace the defects. Since some non bulging cells also show replication defects, we don't know yet if these cells would later develop a bulging defect or not. It is also noted here that sometimes the mother cells that have a stalk-bulging phenotype divide at the bulges. In that case, the mother cells may have already initiated multiple rounds of replication and can still look like wild type. To understand these developmental defects better at least two generations of cell cycle need to be analysed by time-lapse microscopy.

TIR domain serves as a domain of protein-protein interaction in bacteria. It is conceivable that Hne-0708 is possibly interacting with other proteins to bring about its function. To find out the potential interaction partners, it is important to do a co-immunoprecipitation followed by mass spectrometry. *H.neptunium* also possesses another TIR domain containing protein, Hne-1923, that has a domain of unknown function at its C terminal. It is possible that these two proteins are interaction partners, as TIR domains can interact with other TIR domains. However, so far there is no evidence to support this hypothesis, nor do we know anything about the physiological role of Hne-1923. Hence it will be interesting to unravel the interaction partners of Hne-0708.

## Orphan ParA-like proteins

Although ParA proteins are found in association with ParB proteins that form the partition machinery in several species of bacteria, genes homologous to *parA* are also found outside of ParA/B operons. Many bacteria possess either one of the partition proteins. ParA-like proteins such as MipZ, PomZ and MinD are involved in division site placement as mentioned before. Apart from that there are *parA* genes not adjacent to any partner genes, called orphan *parA* systems. They are sometimes found in the middle of operons involved in signalling and metabolism. For example, the gene of a family of ParA-like proteins called ParC is found in chemotaxis related operons in gamma proteobacteria where they are found to be involved in polar placement of chemotaxis proteins. Some orphan ParAs have been shown to be involved in the segregation of protein clusters upon division (Ringgaard et al, 2018). An orphan ParA in *Rhodobacter sphaeroides* was found to control the segregation of protein clusters involved in its chemotactic signalling (Roberts et al, 2012). In *Synechococcus elongatus* ParA is involved in evenly distributing its multi-copy chromosomes (Watanabe et al, 2018).

In the case of *H.neptunium* several ParA homologues were found that were clustered into different families of the Mrp/MinD P-loop ATPases superfamily, out of which the orphan ParA-like protein HNE-0708 was found to not belong to any of the previously described families. It was later shown that this protein belongs to a different subfamily of its own bearing resemblances to MipZ sub-family and ParA sub-family, but different enough to form a separate sub-family of its own. Interestingly, this protein consists of the TIR(Toll/interleukin-1(IL1) Receptor) domain that is commonly found in eukaryotic proteins.

## TIR domain-containing proteins

In eukaryotes TLR(Toll-like receptor) family of proteins are involved in immunological signalling. Toll-like receptors play a major role in the downstream signalling and activation of transcription factors such as nucleation factor κB (NF-κB) and members of interferon regulatory factor family proteins that initiate the innate immunity against a pathogen that has invaded the system(Spear et al, 2009). These Toll-like receptors interact with as many as five adaptor proteins namely MyD88, MAL, TRF, TRAM and SARM that bring about these downstream activities. The interaction domain between these adaptors and Toll-like receptors that facilitate this signalling is the TIR domain on both the TLRs and the adaptors.

In microbial proteome, proteins containing TIR domains were observed in 2006 in a bioinformatic survey (Newman et al, 2006) wherein as many as 200 bacterial proteins were found to possess a TIR domain. Early studies on TIR domain containing bacterial protein involved expressing the *Salmonella enterica* TIR domain containing protein TlpA in mammalian cells. This experiment resulted in TlpA interfering with the adaptor protein MyD88 involved in the NF-κB secretion pathway. Hence it was initially assumed that

possibly the function of bacterial TIR domain containing proteins is to subvert the innate immune response of the host cell by interfering with the TLR signalling pathways. However the TlpA protein did not possess any signalling domain that could lead to its secretion outside the bacterial cell. This led to other different hypotheses that speculated on the need of TIR domains in bacterial proteins. It was observed in a study conducted in *E.coli* that its TIR domain containing protein as well as the proteins of several other non-pathogenic bacteria expressed in trans in *E. coli* cells were capable of NADPase activity. However, primarily the TIR domains on bacterial proteins are thought to be domains of protein-protein interaction.

## TIR domain containing proteins in *H.neptunium*

In order to identify the potential interaction partners of HNE-0708, a search for a TIR domain containing protein in *Hyphomonas* genome was carried out and brought to light, HNE-1923, another TIR domain containing protein (of the TIR-2 superfamily) with a second domain of unknown function. This protein is an orphan protein with no pre assigned functional domains identified yet. Most of its homologues are found in the Hyphomonadacea family along with some species of *Henriciella .spp*(BLAST analysis). Preliminary observation shows that its deletion had resulted in minor phenotypic defects in the budding cells where the stalk appeared to branch out and produce multiple buds. However without replicating this and confirming the phenotypic defect it is difficult to predict what is the implication of this protein in the physiology of *H. neptunium*. Since the TIR domains are known to interact with each other, it will be interesting to test if these proteins interact with each other. It will also be interesting to test whether the double deletion will improve the phenotype or worsen the defect or remain the same.

## Functional analysis of HNE_0708

The ParA-like protein HNE-0708 forms a separate subfamily of proteins and its homologues are predominantly found among Hyphomonodacea indicating its potential role adapted to the stalked-budding morphology. Upon deletion the cells develop a bulge at the bud end of the stalk that is sometimes clogged with DNA. The replication and segregation of chromosomes are also impaired upon deletion of HNE-0708. The stalk bulging starts to appear before the segregation begins, but the replication has already been initiated at that point. However there are multiple rounds of replication in these cells and whether the over-initiation of replication happens after the bulge is formed or before is a question that needs to be addressed. Just before the bulge formation in the cells, the morphology is wild-type-like with the process of budding just beginning and coinciding with the replication of the origin at this stage. As the development continues, the bulges start to appear. Whether the mother cell perceives this as a second bud or not is not clear. It could be possible that the mother cell might hyper initiate replication due to this reason. In that case the hyper-budding might serve as a cue for chromosome replication. On the other hand, if the deletion

of HNE-0708 directly affects the replication initiation process, then this protein presumably co-ordinates replication and the maintenance of morphology of the stalk and bud, which could be why this specific phenotypic defect arises in coordination with a replication defect. This is because hyper initiation of replication by itself cannot cause the specific stalk-bulging phenotypic defect since other strains (such as ParB-YFP instead of ParB at the native site) that show a replication initiation defect are not showing the stalk-bulging phenotype. This concludes that the HNE-0708 protein has direct connection with the stalk-bulging phenotype although it is not clear whether the replication defect precedes the appearance of the bulge or happens afterward as a consequence of the morphological aberration. In any case the segregation within the mother cell is wild type- like and the second step of segregation, that is segregation through the stalk does not happen before the formation of the bulge. Once the segregation through the stalk happens, the chromosome can be seen clogged in the bulge and the bud in most cases. This could be because at this point the identity of the bud is not clear for the mother cell and consequently the segregation is not properly done. The segregation itself does not seem to be affected but overall there is no faithful segregation of a copy of the chromosome to the bud, which is probably a consequence of the morphological and replication defects. It will be interesting to find the role of this ParA-like protein in these interesting developmental defects.

Interestingly the phenotypic defect is only observed in less than 30% of the population of the cells. It could be that the defect is visible after several rounds of budding and the population may eventually be saturated. It will be interesting to observe a population that has undergone several more rounds of replication. The buds that are separated from defective mother cells show a more elongated phenotype with tapering ends. It is also interesting to follow the growth of these newly formed bud cells to see how they develop into stalked cells.

Since HNE-0708 is a ParA-like protein, it was interesting to find out whether it could bind to DNA like other ParA-like proteins. The presence of a positively charged patch as well as the biolayer interferometry results point to the fact that nonspecific DNA binding is possible for HNE-0708. It will be interesting to know if the interaction of HNE-0708 with DNA may have anything to do with the hyper initiation of replication. More importantly it will be interesting to check if HNE-0708 can bind to ParB for the same reason. It is important to understand the interaction partners of HNE-0708 to find out its role (or absence thereof) in the morphological as well as replication defects.

## Part 3: Coordination of MipZ dependent division site placement and Chromosome segregation in *Caulobacter crescentus*

In this study we focused on the interaction between the ParA-like P-loop ATPase, MipZ and the CTP-binding partition protein ParB.

## The ParB-binding interface of MipZ

The role of ParB in binding and stimulating the ATPase activity of ParA has long been known. In the case of *Caulobacter*, ParB interacts with MipZ, another ParA-like that regulates the FtsZ ring placement. It is interesting that both dimeric and monomeric forms of MipZ interact with ParB dimers. This interaction is crucial to increase the local concentration of MipZ at the poles. This interaction is thought to be stimulating the dimer formation of MipZ. However the mechanism is not clear yet.

The HDX results point to the fact that the MipZ dimer binds to DNA and ParB by some common residues. It has been shown by a competition experiment using BLI analysis that the residues L248,L237,R221 are potentially shared between DNA and ParB. The HDX reveals that roughly the amino acids between Q240-G265 show the maximum protection during ParB binding that fall in the CT-region of MipZ. Previously it has been noted that the ParA-like protein Delta of plasmid pSM19035 of *Streptococcus pyogenes*, interacts with the ParB-like protein Omega using its C-terminal region(Dmowski et al, 2011). Besides, the ParA-like protein SopA of plasmid F of *E. coli,* interacts with the ParB-like protein SopB via its C-terminal region(Kim et al, 1999).

In the case of *Caulobacter* MipZ-ParB interaction, the engagement of helix 14 of MipZ (amino acids between H250-L260) with that of ParB might result in the weakening of the strand 9 of MipZ (amino acids between G215-D220) that might have resulted in the observed increased protection. (Figure 4.15, Figure S2) The linker region between the strand 9 and helix 14 (amino acids between 225-235) might be showing higher deuterium uptake either because it would have undergone the helix to loop transition or it is affected by the disruption of its interaction with helix14. The amino acids between R225-A235 are more rigid as a dimer and hence may not interact with ParB as dimeric MipZ. The deprotection of the beta hairpin between amino acids 140-150 might be the result of overall altered structure due to the interaction. Consistent with the HDX result, the AlphaFold results predict that predominantly residues between amino acids 240-260 are involved in MipZ binding. Among these the predicted interaction between monomeric MipZ and ParB is putatively facilitated by the residues Q249, R258, A259, L248, L251, R254, Q255 and S247 out of which R258, A259, R254, Q255 and S247 are exclusively involved in monomer interaction with ParB. As for dimeric MipZ, V246, L248, Q249 and L251 are the putative residues that interact with ParB. Out of these V246 is thought to be interacting with ParB only if MipZ is in dimeric form.

## The MipZ-binding interface of ParB

Since MipZ is a ParA-like protein it is very tempting to think that it interacts with ParB in a similar fashion. But the HDX results point to the fact that the interaction interface on ParB is not shared by MipZ and ParA. In fact, the regions of interactions for ParA and MipZ are well separated. On the one hand the interaction of ParB with ParA is mediated through the NT-region of ParB, but on the other hand the MipZ interaction interface falls in the CT region of the ParB molecule, which is the dimerisation domain. It is known that ParB is a CTP-binding molecular switch that is capable of binding and hydrolysing CTP and forming closed structures called ParB rings in a CTP dependent manner. The N-terminal region of ParB forms a closed ring (N-engagement) in the presence of CTP and par*S* sites resulting in the closing of the ring. This might bring the region that putatively interact with ParA closer together. In the case of MipZ, the CT region, that is, the interaction domain of MipZ does not undergo any change dependent on the CTP dependent switch. So it can be speculated that the interaction with MipZ will not contribute to or affect the CTPase activity or the ring formation of ParB. Neither will the open or closed state or CTP bound or CDP bound state of ParB affect the binding of MipZ. That is, the interaction between MipZ and ParB is independent of the conformational changes that ParB undergoes in the CTP-dependent cycle. As observed in the biochemical experiments, the C-terminal domain is sufficient to recruit MipZ. As long as the CTD remains dimerised, the MipZ interaction is presumed to remain intact.

The C-terminal domain of ParB is known to be involved in non-specific DNA interactions (Fisher et al, 2017) through its higher numbers of positively charged residues in the CT that are exposed outwards. This is observed in *Bacillus* in this study as the chimaera of ParB protein with the CT of *Bacillus* ParB showed high binding to the DNA. However this binding is possibly not strong enough to hold the ParB protein onto the DNA, it is the stable rings formed by ParB that results in the nucleo-protein complex formation. Predominantly, the variation in the spreading of ParB is attributed to the variation in the N-terminal domain(Tung le et al, 2020). The non-specific DNA interaction may merely aid in the spreading of ParB. The presence of several Lysine residues is thought to be the main players in the non-specific DNA interaction of the C-terminal domain. In the case of *Caulobacter* the CT-domain is considerably different, in that many of the lysine residues are not conserved. It could be that the CT of ParB has been specifically evolved to be able to bind MipZ to coordinate chromosome segregation and cell division. It has been known that ParB -like proteins can be directly involved in cell division. The Noc protein in *Bacillus* is thought to have diverged from ParB by a duplication event and is functioning as a negative regulator of cell division assembly in the vicinity of the nucleoid. Like ParB , Noc also binds DNA, but to specific Noc binding sites (NBS). It is noted that the ter region of the chromosome is devoid of NBC thus restricting the binding of Noc there. In the case of *Caulobacter*, ParB interacts with MipZ to bring about similar developmental events.

The C-terminal region of *Caulobacter* ParB is a relatively short 53 amino acid-long peptide (V252-I304) which folds into two helices ((V252-G270) and (L290-T301)) and the region

in between folds into a beta hairpin motif. The alpha fold predictions suggest that the helices are exposed outwards and consistent with this, the MipZ binding residues are located in this area. The middle region in the dimerisation region. Some residues outside of this region may also be involved in the dimerisation wherein the residues L264, L270, L296, C297, R299, L300 of one ParB monomer might be interacting with L260, L264, L270, C297, R299, L300 and T301 of the second ParB monomer. Out of these aminoacids the residues C297,T301,L260 and L264 are also residues that interact with monomeric MipZ. The L260 residue also interacts with dimeric MipZ. Overall, it could be assumed from the HDX and Alpha-fold predictions that mutating the residues N298, L293, T301, L290 will impair the interaction with monomeric MipZ alone, while mutating D263 will impair the interaction with dimeric MipZ alone. The residues D294, D256 and T257 might impair the interactions of both the monomeric and dimeric forms.

## MipZ-ParB interaction and potential mechanisms of dimerisation

The AlphaFold predictions show that the interaction interface on the surface of ParB, although not necessarily facing opposite to each other, are placed in different planes. For monomer interactions, it can be seen that if both of the MipZ-interaction interfaces on ParB are occupied by monomers, the hind side of MipZ monomers might come to closer proximity. If this proximity is enough to trigger the dimer formation, this could bring one of the monomers closer to the other and can disrupt its interaction with ParB, while the other monomer might still hold on. While this happens, the monomers may undergo dimerization resulting in the overall bonding of one dimeric MipZ to one of the interaction sites on ParB. The conformational change induced by dimerisation can be the potential reason for the slightly different regions involved in the dimer interaction. This could be one of the possible reasons for the ParB-MipZ interaction to trigger the dimer formation.

It can also be seen from the structure predictions that one ParB dimer can independently engage two separate MipZ monomers via its two interaction interfaces. It might also be possible for two separate MipZ dimers to bind to a single ParB dimer as each of the MipZ dimers approach the ParB molecule from different sides, and hence the chances of steric clashes are not particularly high. However it looks extremely difficult for the same MipZ dimer to occupy both of the binding sites on ParB because of the orientation of these interfaces of ParB surface. Similarly, the two binding sites available on the surface of MipZ dimers can possibly bind to two different ParB dimers. The interaction between the CT of ParB and dimeric MipZ are relatively high, in the range of 350-490 nM. The competition between DNA and ParB to bind to MipZ may explain the removal of dimeric MipZ from the cell poles despite the relatively strong affinity. This might provide room for more MipZ monomers to bind to ParB as MipZ monomers cannot bind DNA.

Unless the orientation of MipZ monomers is favourable for dimer formation, it need not necessarily be true that the same ParB molecule has to bring two MipZ monomers together to trigger dimerisation. Since the concentration of ParB at the poles is very high, the MipZ

molecules that will interact with the ParB proteins will also have relatively higher local concentration. It has been observed by microscopic methods that the MipZ protein has the highest concentration at the poles where it colocalizes with ParB. It could be that the interaction with ParB serves as a tool to increase the local concentration of MipZ that might have resulted in the dimer formation. It is not clear which one of these mechanisms is potentially triggering the dimerisation of MipZ. One of the ways to understand this question will be to bring MipZ monomers to very high concentrations in the absence of ParB to check the rate of dimerisation, in comparison with the rate of dimerisation in the presence of ParB. There is no direct tool to measure the rate of MipZ dimerisation. One of the methods that was tested was ATPase assay. As we know about the ATPase cycle of MipZ, one might speculate that at higher dimer concentrations, one would see highest ATPase activity. Towards this an ATPase assay was done where a fixed concentration of MipZ was subjected to ATPase test with increasing concentrations of ParB. This however did not lead to any conclusive results. Assuming that the increment in the local concentration of ParB is the cause of dimerisation, one can speculate that the presence of small amounts of ParB may not necessarily cause a high local concentration. Adding very high concentrations of ParB can lead to unwanted aggregations. One way to tackle this problem will be to repeat this experiment in the presence of a par*S* containing DNA. It will also be better to use the ParB Q58A version that does not hydrolyse CTP to avoid unwanted interference from CTPase activity of ParB. In this set up a mini partition complex can be formed where ParB concentration is very high. It will be interesting to see if this setup can increase the ATPase activity of MipZ. However if the dimerisation is independent of concentration, but dependent on the presence or absence of ParB, then ATPase assays with just the increasing concentrations on ParB should show an increment in the ATPase activity.

In the future it will be interesting to dissect the interaction between ParB and MipZ by means of point mutation to understand the molecular mechanism of this interaction. It has to be noted that the structural information we have is based on the AlphaFold predictions. In the future it will be necessary to have a crystal structure to obtain a clearer and robust understanding of this interaction. Importantly, it might be interesting to have a co-crystal structure of MipZ with the CT peptide of ParB in both dimeric and monomeric forms to better understand the dynamics of this interaction and its role in the dimer formation of MipZ. Lastly, it will also be interesting to prove this interaction by microscopy, by introducing point mutations of ParB and MipZ proteins to see if they disrupt the interaction with each other *in vivo*

## ParB interacts with two ParA-like proteins thus connecting cell division with chromosome segregation

In this study we analysed the interaction between the CTP binding molecular switch, ParB and the ParA-like P-loop ATPase, MipZ. ParB proteins are traditionally involved in binding to ParA-like proteins. However in the case of MipZ, the region of interaction is not the

same as that of canonical ParA. ParB interacts with ParA through its NT domain, which is also the domain that forms the closed ring conformation dependent on CTP binding, hydrolysis and par*S* binding. Hence the interaction of ParA with ParB is closely associated with its CTP binding property and partition complex formation. Apart from the NTD and the HTH containing DNA binding domain, ParB has a dimer forming CT domain that is linked to the rest of the protein via a flexible linker region. Of these regions, the CT domain had implications in MipZ binding. As seen from the results of this study, the linker region does not have anything to do with MipZ interaction. But the CT domain is the region MipZ interacts with. This interaction is thought to be important for the dimer formation of MipZ monomers. The mechanism still remains elusive. Whether the formation of the partition complex will have any implications in the dimerisation will depend on whether the dimerisation is a result of increased local concentration or a catalytic mechanism mediated by ParB. To understand that we will need robust structural information of this interaction. However we can conclusively say that the CTP binding property of ParB can have no effect on MipZ interaction and vice versa. It is interesting to note that the ParB of *Caulobacter* has evolved to interact with two different ParA-like proteins, through its two separate domains placed at opposite ends, to bring about seemingly opposite effects. The interaction of ParB with ParA triggers its ATPase activity thereby causing it to monomerise and fall off from the DNA whereas its interaction with MipZ brings the monomers together to dimerise and bind to DNA. Thus the interaction with ParB makes and breaks the dimers of MipZ and ParB respectively, to bring together the two important cell cycle events, cell division and chromosome segregation.

# Materials and methods

## Chemicals

Reagents used in this work were obtained from: Becton Dickinson (USA), Bio-Rad (USA), Biotium (USA), Carl-Roth (Germany), ChromoTek (Germany), Difco (Spain), GE Healthcare (UK), GenScript (USA), Invitrogen (Germany), Merck Millipore (Germany), PerkinElmer (USA), Roche (Switzerland), Sigma-Aldrich (USA) and Thermo Fisher Scientific (USA).

## Enzymes

Restriction enzymes were obtained from New England Biolabs (USA) or ThermoFisher Scientific (USA). The polymerase chain reaction (PCR) was performed either with Q5 or KOD Hot Start DNA polymerase (Merck Millipore, Germany) and colony PCR with Biomix™Red (Bioline, Germany). The ligation of two DNA molecules was catalysed by T4 DNA ligase (ThermoFisher Scientific, USA).

## PCR primers

Oligonucleotides used in this study were synthesised by Eurofins MWG-Operon (Germany) or Microsynth(Germany) and are listed in appendix.
All strains and plasmids used and generated in this study are listed in the Appendix.

## Kits

Kits used in this study are listed in table 1.

**Table 1: Commercial kits used in this study.**

| Kit | Application |
|---|---|
| GenElute™ Gel Extraction Kit (Sigma-Aldrich, USA) | Extraction of DNA fragments from agarose gel |
| GenElute™ PCR Clean-Up Kit (Sigma-Aldrich, USA) | Purification of PCR amplicons |
| GenElute™ Plasmid Miniprep Kit (Sigma-Aldrich, USA) | Isolation of plasmids |
| Illustra bacteria genomicPrep Mini Spin Kit (GE Healthcare, Germany) | Isolation of chromosomal DNA |

| | |
|---|---|
| Q5 site-directed mutagenesis kit (New England Biolabs, USA) | Introduction of point mutations |
| Western Lightening™ Chemiluminescence Reagent Plus kit (PerkinElmer, USA) | Detection of chemiluminescence |
| Roti®-Nanoquant (Carl-Roth, Germany) | Determination of protein concentrations |

## Buffers and solutions

All standard buffers and solutions were prepared according to previously published protocols. The chemical components were dissolved in deionized water (Purelab Ultra water purification systems, ELGA, Germany) and sterilised either by autoclaving (20 min at 121 ˚C, 2 bar) or by filtration (pore size 0.22 µm, Sarstedt, Germany). Specific buffers and solutions are listed in the respective method sections.

## Media and additives

All media were prepared with deionized water. Complex media were sterilised by autoclaving at 121 ˚C and 2 bar for 20 min, additives such as antibiotics and inducers were sterilised by filtration (pore size 0.22 µm, Sarstedt, Germany) and added separately. For solid media, 1.5 % (w/v) agar was added prior to autoclaving. The additives were added to pre-cooled media (below 60 ˚C) when required. The final concentration of antibiotics and other additives used in this study is listed in *Table 2*.

LB (Luria-Bertani) broth:
1% (w/v) Tryptone
0.5% (w/v) Yeast extract
1% (w/v) NaCl

Complex medium for *H. neptunium* MB (Marine Broth) medium:
5.00 g/L Bacto peptone
1.00 g/L Bacto yeast extract
0.10 g/L Fe(III) citrate
19.45 g/L NaCl
5.90 g/L $MgCl_2$ (dried)
3.24 g/L $Na_2SO_4$
1.80 g/L $CaCl_2$
0.55 g/L KCl
0.16 g/L $Na_2CO_3$
0.08 g/L KBr
34.00 mg/L $SrCl_2$
22.00 mg/L $H_3BO_3$

4.00 mg/L Na-silicate
2.40 mg/L NaF
1.60 mg/L $(NH_4)NO_3$
8.00 mg/L $Na_2HPO_4$

For preparation of MB agar plates, 2 % agar was added.

**Table 2: The final concentration of additives added into media.**

| **Additives** [stock concentration] | **Final concentration** [µg/ml] | | | |
|---|---|---|---|---|
| | ***E. coli*** **liquid** | ***E. coli*** **solid** | ***H. neptunium*** **liquid** | ***H. neptunium*** **solid** |
| Ampicillin [100 mg/ml] | 200 | 200 | - | - |
| Kanamycin [20 mg/ml] | 30 | 50 | 100 | 200 |
| Chloramphenicol [10 mg/ml] | 20 | 30 | - | - |
| Gentamycin [1 mg/ml] | 15 | 20 | 0.5 | 5 |
| IPTG [1 M] | 1 mM | 1 mM | - | - |
| DAP [60 mM] | 300 µM | 300 µM | | |
| ZnCl2 [20 mM] | | | 300 µM | 500 µM |

## Microbiological methods

## Bacterial strains and growth condition

*H. neptunium* ATCC15444 and its derivatives were grown in MB medium at 28°C under aerobic conditions (shaking at 210 rpm) in baffled flasks or on MB-agar plates. Media were supplemented with antibiotics when appropriate. Plates were grown on MB agar at 28°C. *E. coli* was cultivated in LB medium (shaking at 210 rpm) or on LB-agar plates at 37°C. Appropriate antibiotics were added to the media when working with mutant strains.

## Storage of cells

For cryo-preservation of bacterial strains, cultures of an OD of 1 or more were mixed with 20% (v/v) sterilised DMSO. The pre-sterilized cryo vials (Thermo Fisher Scientific, USA) were used as containers and stored at -80°C.

## Measurement of cell density

The optical density ($OD_{600}$) of bacterial cultures was measured photometrically using a Ultrospec™ 2100 pro UV/Visible spectrophotometer (Amersham Phamarcia Biotech, UK) at a wavelength of 600 nm. The corresponding culture media were used as blanks.

## Preparation of *E. coli* competent cells

To prepare chemically competent cells, an overnight *E. coli* culture was diluted 1:100 in 250 ml LB medium. Cells were grown to an $OD_{600}$ of ~0.6 before cooling down on ice. After 10 min of cooling, cells were pelletized by centrifugation (5000 ×g, 4 ˚C, 10 min). The pellet was resuspended in 15 ml ice-cold sterilised 0.1 M $CaCl_2$ and incubated on ice for 30 min. Afterwards, cells were centrifuged again as specified above and resuspended in 4 ml of ice-cold sterilised buffer composed of 0.1 M $CaCl_2$ and 10% (v/v) glycerol. The competent cells were split into 120 µl or 80 µl aliquots and stored at -80 ˚C.

## Transformation of *E. coli*

A 120 µl-aliquot of chemically competent *E. coli* TOP10 cells was thawed on ice and 100 ng/µl of plasmid DNA were added. The mixture was kept on ice for 30 min. The cells were then heat-shocked at 42°C for 90 sec and incubated again on ice for 1.5 min. Subsequently, 500 µl LB medium were added, and the cells were incubated for 1 h at 37°C with shaking. 250 µl of the cell suspension was then spread onto an LB agar plate containing the corresponding antibiotic. The agar plate was then incubated at 37°C overnight.
Competent *E. coli* WM3064 cells were thawed on ice and 5 µl plasmid DNA were added. The mixture was kept on ice for 30 min. The cells were then heat-shocked at 42°C for 90 sec. Afterwards, 500 µl LB medium supplemented with 300 µM DAP were added, and the cells were incubated for 1 h at 37°C without shaking. 400 µl of the cell suspension were then spread onto an LB agar plate containing the corresponding antibiotic and 300 µM DAP. The agar plates were then incubated at 37°C overnight.
Competent *E. coli* Rosetta™ (DE3)pLysS were purchased from Merck Millipore (Germany). 100 µl of cells were mixed with 5 µl plasmid DNA and incubated on ice for 30 min. The cells were then heat shocked at 42°C for 90 sec. Afterwards, 900 µl LB were added and the cells were incubated for 1 h at 37°C. 250 µl of the cell suspension was then spread onto an LB agar plate containing ampicillin and chloramphenicol, and incubated at 37°C overnight.

## Conjugation of *H. neptunium*

After transformation of *E. coli* WM3064 (donor strain) with the plasmid of interest, cells were grown to stationary phase in liquid LB medium supplemented with the amino acid diaminopimelic acid (DAP).
*H. neptunium* (recipient strain) was grown to stationary phase in MB medium. Afterwards, 1 ml of the *E. coli* WM3064 culture and 2 ml of the *H. neptunium* culture were harvested by centrifugation for 2 min at 7600 x g. Cell pellets were washed twice with MB medium (2 min, 7600 x g) and resuspended in 100 µl MB medium supplemented with 300 µM DAP. Both aliquots were mixed and spotted on an MB agar plate supplemented with 300 µM DAP. The cells were incubated overnight at 28°C, scraped from the MB agar plate with a sterile tip, washed twice in 1 ml MB medium (without DAP) (2 min, 4600 x g), and finally resuspended in 1 ml MB medium. 200 µl of the cell suspension were plated on MB agar plates supplemented with the respective antibiotic and grown for at least five days at 28°C.

## Molecular cloning

### Construction of plasmids

Plasmids used in this study were designed via SnapGene® (Version 3.3.4; Dotmatics, USA) and validated by sequencing the resulting constructs. Oligonucleotides for molecular cloning were synthesised by Eurofins Genomics (Germany) or Microsynth (Germany). The Sanger sequencing of PCR products and plasmids was performed by Microsynth (Germany) and the preparation of samples was according to the user guide. The list of plasmids and oligonucleotides used in this study is given in the appendix.

### Isolation of DNA

DNA fragments from PCR or restriction digestion were purified by using either GenElute™ PCR Clean-Up Kit (Sigma-Aldrich, USA) or GenElute™ Gel Extraction Kit (Sigma-Aldrich, USA) following the manual. Plasmids were extracted from *E. coli* cells using the GenElute™ Plasmid Miniprep Kit (Sigma-Aldrich, USA). Genomic DNA of CB15N was isolated using the NucleoSpin® Microbial DNA Kit (Macherey-Nagel, Germany).

## Polymerase chain reaction

### PCR for general purpose

To amplify DNA fragments for cloning purposes, KOD Hot Start DNA polymerase (Merck Millipore, USA) was used. The standard reaction setup and cycling conditions are listed in *Table 3*. Gradient PCRs were performed when necessary.

**Table 3: The standard setup and cycling conditions for PCR amplification using KOD Hot Start DNA polymerase.**

| **The composition of reaction** | | **Cycling conditions** | |
|---|---|---|---|
| **Components** | **Volume** | | |
| 10x KOD buffer | 5 µl | Polymerase activation | 95 ˚C for 2 min |
| DMSO | 5 µl | | |
| dNTPS (2 mM each) | 5 µl | Denaturation | 95 ˚C for 30 s |
| 25 mM $MgSO_4$ | 2.5 µl | Annealing | Lowest primer melting temperature for 30 s 35x |
| Forward primer (10 µM) | 1.5 µl | Extension | 72 ˚C for 30 s/kb |
| Reverse primer (10 µM) | 1.5 µl | | |
| Template DNA (10 ng/µl) | 1 µl | Final extension | 72 ˚C for 10 min |
| KOD polymerase (1 U/µl) | 1 µl | | |
| $ddH_2O$ | 27.5 µl | Hold | 16 ˚C for ∞ |
| **Total volume** | 50 µl | | |

## Colony PCR

To perform PCR analyses on cells, colonies were picked from the agar plate using sterilised tips and transferred into15 µl aliquots of BioMix™ Red (Bioline, Germany). The components of the reaction mixture and cycling conditions are listed in *Table 4*.

**Table 4: The standard setup and cycling conditions for colony PCR using BioMix™ Red.**

| **The reaction mixture (10 x 15 µl)** | | **Cycling conditions** | |
|---|---|---|---|
| **Components** | **Volume** | Polymerase activation | 95 ˚C for 5 min |

| | | | | |
|---|---|---|---|---|
| 2x BioMix™ Red | 75 µl | | | |
| DMSO | 7.5 µl | Denaturation | 95 ˚C for 30 s | |
| Forward primer (10 µM) | 0.75 µl | Annealing | 65 ˚C for 30 s | 35x |
| Reverse primer (10 µM) | 0.75 µl | Extension | 72 ˚C for 30 s/kb | |
| dd$H_2O$ | 66 µl | | | |
| **Total volume** | 150 µl | Final extension | 72 ˚C for 4 min | |
| | | Hold | 16 ˚C for ∞ | |

**Mutagenesis PCR**

To introduce desired mutations into the target gene, KOD Hot Start polymerase (Merck Millipore, USA) was used. For the mutagenesis with KOD polymerase, the protocol is similar to the one used for general DNA amplification, except for the number of cycles, which was reduced to 20. The master mix was separated into two fractions one each with the forward and the reverse primer. After 20 cycles, they were mixed together to continue for another round of PCR. To remove the template DNA, PCR products were treated with 1µl *Dpn*I at 37 ˚C for 2 h before transformation.

## Agarose gel electrophoresis

To determine the size of DNA fragments or purify the fragment of interest, 5µl DNA products were first mixed with 1µl 6x DNA gel loading dye (Thermo Fisher Scientific, USA) if needed and then applied to a 1 % agarose gel supplemented with GelRed® nucleic acid gel stain (Biotium, USA). GeneRuler 100 bp or 1kb DNA Ladder (Thermo Fisher Scientific, USA) were used as size standards as appropriate. Gels were immersed in a 0.5x TAE running buffer (20 mM Tris/HCl, pH 8, 0.175 % acetic acid, 0.5 mM EDTA, pH 8.0) and run at a constant voltage of 160 V for 20-25 min. The separated DNA fragments were visualised with a UV-Transilluminator (UVP-BioDoc-ITTM Imaging System; UniEquip, Germany).

## Restriction digestion

Restriction digestion was performed at 37 ˚C overnight or 4 h following the instructions provided by the manufacturers. Afterwards, the sample was cleaned either with the GenElute™ PCR Clean-Up Kit (Sigma-Aldrich, USA) or the GenElute™ Gel Extraction Kit (Sigma-Aldrich, USA).

**Table 5: The protocols for restriction digestion.**

| **Restriction enzymes from NEB** | | **FastDigest® enzymes from Thermo Fisher Scientific** | |
|---|---|---|---|
| 10x NEB buffer | 5 µl | 10x FastDigest® buffer | 2 µl |
| Enzyme A | 1 µl | Enzyme A | 1 µl |
| Enzyme B | 1 µl | Enzyme B | 1 µl |
| DNA | 1 µg | DNA | 1 µg |
| $ddH_2O$ | Up to 50 µl | $ddH_2O$ | Up to 20 µl |

## Ligation

Two DNA fragments were ligated using T4 DNA ligase (Thermo Fisher Scientific, USA) according to the manual. The molar ratio of insert and vector was 3:1. The reaction mixture (*Table 6*) was incubated at room temperature for 1 h.

**Table 6: The reaction mixture for ligation.**

| **Components** | **Volume** |
|---|---|
| 10x T4 ligase buffer | 2 µl |
| Linearized vector DNA | x µl (20 to 100 ng) |
| Insert DNA | y µl (3:1 molar ratio over the vector) |
| T4 DNA ligase | 1 µl |
| $ddH_2O$ | Up to 20 µl |

## Gibson assembly

Gibson assembly was performed as an alternative to restriction cloning. A total volume of 5 µl of linearized vector and DNA insert (molar ratio 1:1) was added to the 15 µl ready-to-use Gibson assembly master mix. The reaction mixture was incubated at 50 ˚C for 1 h. The composition of the master mix and 5x isothermal reaction buffer can be found below (*Table 7*).

**Table 7: The composition of Gibson assembly master mix and 5x isothermal reaction buffer.**

| **Master mix of Gibson assembly** | | **5x isothermal reaction buffer** | |
|---|---|---|---|
| 5x isothermal reaction buffer | 320 µl | PEG 800 | 25% (w/v) |
| T5 Exonuclease (10 U/µl) | 0.64 µl | Tris-HCl, pH 7.5 | 500 mM |
| Phusion DNA polymerase (2U/µl) | 20 µl | $MgCl_2$ | 50 mM |
| Taq DNA ligase (40 U/µl) | 160 µl | DTT | 50 mM |
| $ddH_2O$ | 699.36 µl | NAD | 5 mM |
| **Total volume** | 1200 µl | dNTPs | 1 mM |

## Nanodrop

The concentration of DNA or protein was measured with the NanoDrop® ND-1000 spectrophotometer. 1 µl of the nucleic acid solution/protein was transferred to the NanoDrop, and the absorption was measured with the elution solution or buffers as appropriate blanks.

## Generation of markerless deletions or insertion mutants of *H. neptunium*

An in-frame deletion of HNE_0708 was generated by double homologous recombination using the pNPTS138 suicide vector, leaving 30-36 bp of the 5´and 3´ends of the target gene in the genome. Towards this, 500-1000 bp long flanks up- and downstream of the target region were cloned into the pNPTS138 vector. Derivatives of the pNPTS138 plasmid were used to transform *H. neptunium* by conjugation. Cells were plated on MB agar plates supplemented with kanamycin, which serves as the selection marker for the 1$^{st}$ homologous recombination. 16 clones were tested for the successful integration of the plasmid at one of the two flanks. Positive clones were re-inoculated in plain MB medium and grown to stationary phase (2$^{nd}$ homologous recombination). Subsequently, cells were plated in a 1:200 and 1:100 dilution on MB plates supplemented with 3 % sucrose to select for the 2$^{nd}$ homologous recombination event. Single colonies from the 2$^{nd}$ homologous recombination were re-streaked in parallel on MB-kanamycin and MB-sucrose plates to analyze for kanamycin sensitive and sucrose resistant clones. These were further subjected to colony PCR to confirm the deletion. In order to replace a gene with an allele encoding a C-terminal fluorescent protein fusion such as DnaN-Venus, a construct encoding a C-terminal fluorescent protein fusion was generated first. Additionally, a 500 bp long downstream

flanking region of the target gene was amplified and cloned together with the allele encoding the C-terminal fluorescent protein fusion in the pNPTS138 vector. Derivatives of the pNPTS138 plasmid were used to transform *H. neptunium* by conjugation and generation of markerless insertion mutants was carried out as described above. Further western blotting and microscopy confirmed the presence on non-degraded fluorescent labelled target.

## Microscopy methods

## Light microscopy and fluorescence microscopy

To prepare samples for microscopy, overnight cultures of *H. neptunium* cells were diluted to an $OD_{600}$ of 0.1 and grown for another 2 h before adding appropriate inducers. After induction as indicated in figure legends, cultures were appropriately diluted as 10X dilution of $OD_{600}$ ~ 1 and 1 µl of dilutions were spotted on 1% agarose pads prepared with $ddH_2O$. For native fusions, the induction step was avoided and the rest of the protocol was followed. Images were taken with an Axio Observer. Z1 microscope (Zeiss, Germany) equipped with a Plan Apochromat 100x/1.45 Oil DIC, a Plan Apochromat 100x/1.4 Oil Ph3 phase contrast objective, and a pco.edge sCMOS camera (PCO, Germany). The X-Cite® 120PC metal halide light source (EXFO, Canada) and appropriate filter cubes (ET-CFP, ET-YFP or ET-Texas Red; Chroma, USA) were used for fluorescence detection. Images were recorded with VisiView 3.3.0.6 (Visitron Systems, Germany) and processed with ImageJ and Adobe Illustrator CS6 (Adobe Systems). For time lapse images, cultures were spotted on 1 % agarose MB pads supplied with inducers when necessary, and the cover slide was sealed with VLAP (1:1:1 vaseline, lanolin, and paraffin) to prevent dehydration. In order to keep a constant temperature of 28°C, the slides were kept in heating chambers set to the desired temperature.

In order to stain the nucleoid of *H. neptunium*, the cell suspension was incubated with 4 µg/ml DAPI (4',6- diamidino-2-phenylindole) at 28°C and 400 rpm for 20 min. Samples were then analysed by DIC and fluorescence microscopy

## Biochemical methods

## Protein overproduction

To overproduce proteins for purification, Rosetta(DE3)/pLysS cells with appropriate plasmids were grown overnight at 37 °C and diluted 100 folds on the following day. 1 mM isopropyl β–D-1-thiogalactopyranoside (IPTG) was added to the fresh culture when the $OD_{600}$ reached approximately 0.6. All proteins were produced at 37 ˚C for 4 h, except for HNE_0708, which was overproduced at 18 ˚C overnight. Afterwards, cells were harvested by centrifugation and stored at -80 ˚C.

## Protein purification

## Purification of MipZ, and its variants using affinity chromatography and SEC

His-MipZ and His-MipZR198A were purified by affinity chromatography followed by size exclusion chromatography to avoid unwanted ATPase contaminantion. For this two-step purification, cell pellets were resuspended in B1 buffer (50 mM $NaH_2PO_4$, 300 mM NaCl, 20 mM imidazole, pH 8.0 (adjusted with NaOH), 100 µg/ml PMSF, 10 U/ml DNase I) and lysed by three to four passages through a French press at 16,000 psi. The crude cell extract was centrifuged at 16,000 rpm, 4 °C for 50 min to remove the insoluble fraction. The cleared lysate was filtered and loaded onto an equilibrated 5 ml HisTrap™ HP affinity column (GE Healthcare, USA). The column was first washed with 10 column volumes (CVs) B1 buffer followed by elution of the protein with a linear gradient of 20 – 250 mM imidazole over 10 CVs. The fractions containing a high amount of the protein of interest were concentrated using Amicon® Ultra Centrifugal Filters (Merck Millipore, Germany) and then applied to HiLoad® 16/600 Superdex® 200 prep grade size exclusion column (GE Healthcare, USA) that had been equilibrated with PG buffer (50 mM HEPES/NaOH pH 7.2, 300 mM NaCl, 5 mM $MgCl_2$, 0.1 mM EDTA and 10% glycerol). The column was washed with 1.5 CVs PG buffer to separate the loaded proteins. After analysis on a 15% SDS-PAGE gel, fractions containing the protein of interest were concentrated using Amicon® Ultra Centrifugal Filters (Merck Millipore, Germany) and snap-frozen in liquid nitrogen and stored in -80°C for future use.
For the purification of HNE_0708 protein, the same method was followed using the following buffers: resuspension of pellet was done in B2(50 mM HEPES pH 8.0, 300 mM NaCl, 1 mM DTT, 100 µg/ml PMSF, 10 U/ml DNase I) and eluted through a linear gradient of 20 – 250 mM imidazole over 10 CVs. The elution fractions containing the protein peak were dialysed in 50 mM Tris pH 8.0, 250 mM NaCl, 1 mM DTT, 0.1 mM EDTA and TEV protease overnight at 4 °C. Then, it was loaded onto the size exclusion column equilibrated with 10 mM HEPES pH 7.5, 150 mM NaCl and 1 mM DTT as described above. The final eluate was snap-frozen after analysis by SDS-PAGE and concentration as described before.

## Two-step affinity chromatography for proteins with SUMO tag

The ParB variants and chimaeras were purified as N-terminal $His_6$-SUMO fusions. In the first step of purification with a 5 ml HisTrap™ HP affinity column (GE Healthcare, USA), the fusion proteins were separated from contaminants. The procedure was similar to the purifycation of MipZ, using BZ3 buffer (50 mM Tris/HCl pH 8.0, 300 mM KCl, 10% glycerol and 20 mM imidazole). The purified proteins were dialyzed overnight against imidazole-free BZ3 buffer supplemented with 30 µl Ulp1-$His_6$ protease (approximately 7 mg/ml) and 1 mM DTT to cleave off the $His_6$-SUMO tag and remove the imidazole. Subsequently, the untagged proteins, the tag and the protease were separated by passage through the affinity column one more time. The flow-through fractions were collected and the presence of the desired protein was examined by 15 % SDS-PAGE gel. The protein containing fractions were dialysed in PG buffer (as described for MipZ). After dialysis, the protein sample was concentrated and stored in small aliquots at -80 °C for later use.

## Sodium dodecyl sulphate-polyacrylamide gel electrophoresis (SDS-PAGE)

10 µl of purified protein samples were mixed with an equal volume of 2x SDS sample buffer (300 mM Tris Base, 50% (v/v) glycerol, 5% (w/v) SDS, 500 mM dithiothreitol, 0.05% bromophenol blue, pH6.8). For highly concentrated samples, they were initially diluted 10X which was further dissolved in equal volume of 2X SDS sample buffer. For cultures, cells were first pelletized by centrifugation and resuspended in 2x SDS sample buffer according to their optical density (100 µl buffer per 1 ml of culture with an $OD_{600}$ of 1). The samples were treated at 95 °C for 10 min. Subsequently, equal volumes of samples along with the PageRuler ™ Plus Prestained Protein Ladder, 10 to 250 kDa (Thermo Fisher Scientific, USA) were loaded on an SDS-PAGE gel consisting of a 5% stacking gel and an 11% or 15% resolving gel (*Table 8*). Electrophoresis was conducted in Tris/Glycine buffer (25 mM Tris Base, 192 mM glycine, 0.1 % (w/v) SDS) at 30 mA per gel using a PerfectBlue™ Twin S system (Peqlab, USA).
For the visualisation of proteins, SDS-PAGE gels were stained after electrophoresis for 1h in Coomassie solution (40 % methanol, 10 % acetic acid, 0.1 % (w/v) Brilliant Blue R 250) and excess dye was removed by incubation in destaining solution (20 % ethanol, 10 % acetic acid) for 20 min and leaving it in water for destaining overnight.

**Table 8 Composition of stacking and resolving gel.**

| **Component** | **5% stacking gel (2.5 ml)** | **11% resolving gel (5 ml)** | **15% resolving gel (5 ml)** |
|---|---|---|---|
| $ddH_2O$ | 1.43 ml | 1.874 ml | 1.2 ml |
| 4x stacking buffer (0.5 M Tris Base, 0.4% (w/v) SDS, pH6.8) | 625 µl | - | - |
| 4x resolving buffer (1.5 M Tris Base, 0.4% (w/v) SDS, pH8.8) | - | 1.25 ml | 1.25 ml |
| 30% Rotiphorese® Acrylamide/Bis (29:1) | 417 µl | 1.833 ml | 2.5 ml |
| 10% (w/v) APS (Ammoniumperoxodisulfate) | 25 µl | 40 µl | 40 µl |
| TEMED (N,N,N',N'-Terramethyletheylendiamine) | 1.9 µl | 3 µl | 3 µl |

## Immunoblot

To detect the presence and stability of fluorescently tagged proteins, proteins separated on SDS-PAGE gel were transferred onto a polyvinylidene fluoride (PVDF) membrane (Merck Millipore, Germany) using a Trans-Blot Turbo Transfer System (Bio-Rad, USA). To this end, the membrane was first activated in methanol for 15 sec, followed by washing in $H_2O$ for 2 min and equilibration in 1x Turbo transfer buffer (300 mM glycine, 300 mM Tris, 0.05% SDS) for 5 min. The transfer was performed according to the manufacturer's instruction using the pre-programmed Turbo protocol. Subsequently, the membrane was blocked with 5 % (w/v) skim milk in 1x TBST (10 mM Tris base, 150 mM NaCl, 0.1 % (w/w) Tween 20, pH 7.5) for 1 h or overnight at 4 ◦C with gentle agitation. On the following day, the membrane was first incubated with an anti-GFP (1:10,000; Sigma-Aldrich, USA) antibody diluted in blocking buffer at room temperature for 2 h. Before incubation of the membrane with a secondary antibody for 1 h, it was washed for 10 min in 1x TBST for three times. Goat anti-Rabbit IgG (H+L) secondary antibody conjugated to horseradish peroxidase (1:20,000, Invitrogen, USA) was used to visualise the protein of interest. After the incubation, the membrane was rinsed three times and incubated with Western Lightning™ Chemiluminescence Reagent Plus (PerkinElmer, USA) according to the manual for 5 min. The signal was detected with a ChemiDoc™ MP Imaging System (Bio-Rad, USA).

## Bio-layer interferometry

Bio-layer interferometry experiments were conducted using a BLItz system equipped with Octet® High Precision Streptavidin 2.0 (SAX2) Biosensors (Sartorius, Germany). First, biotinylated partners (DNA or peptides as described in the figure legends) were immobilised on the sensor appropriately supplied with additives (such as ATP, CTP etc. as mentioned in the figure legends). After the establishment of a stable baseline, association reactions were monitored. At the end of each binding step, the sensor was transferred into an analyte-free buffer to measure the dissociation kinetics. The extent of non-specific binding was assessed by monitoring the interaction of the analyte with unmodified sensors. All analyses were performed in BLItz PG buffers supplied with appropriate nucleotides.

## Hydrogen-deuterium exchange mass spectrometry

Samples were prepared using a two-arm robotic autosampler (LEAP technologies, Denmark). To analyse the surface of MipZ, 200 µl 50 µM MipZ alone or 100 µl 100 µM MipZ + 100 µl 200 µM ParB were subjected to HDX. To analyse the ParB surface, 200 µl 50 µM ParB or 100 µl 100 µM ParB + 100 µl 200 µM MipZ were subjected to HDX. The mixtures were diluted in a $D_2O$-containing buffer (220 mM HEPES-Na, pH 7.2, 50 mM KCl, 10 mM $MgCl_2$) to start the exchange reaction. After 10, 100, 1000 and 10,000 sec of incubation at 25 °C, samples were taken from the reaction and mixed with an equal volume of quench buffer (400 mM $KH_2PO_4/H_3PO_4$, 2 M guanidine-HCl, pH 2.2) kept at 1 °C. 95

µl of the resulting mixture were immediately injected into an ACQUITY UPLC M-class system with HDX technology (Waters™, USA). Non-Deuterated samples of MipZ, ParB and the mixture of them were prepared similarly by 10-fold dilution into $H_2O$-containing buffers. Proteins were digested online on an Enzyme BEH Pepsin column (300 Å, 5 µm, 2.1 mm × 30 mm; Waters™, USA) at 12 °C with a constant flow (100 µl/min) of water + 0.1 % (v/v) formic acid, and the resulting peptic peptides were collected on a trap column (2 mm × 2 cm) that was filled with POROS 20 R2 material (Thermo Fisher Scientific, USA) and kept at 0.5 °C. After 3 min, the trap column was placed in line with an ACQUITY UPLC BEH C18 1.7 µm 1.0 × 100 mm column (Waters™, USA), and the peptides were eluted at 0.5 °C using a gradient of water + 0.1 % (v/v) formic acid (A) and acetonitrile + 0.1 % (v/v) formic acid (B) at a flow rate of 30 µl/min as follows: 0-7 min/95-65 % A, 7-8 min/65-15 % A, 8-10 min/15 % A, 10-11 min/5 % A, 11-16 min/95 % A. Peptides were ionized with an electrospray ionization source operated at 250 °C capillary temperature and a spray voltage of 3.0 kV. Mass spectra were acquired over a range of 50 to 2000 *m/z* on a G2-Si HDMS mass spectrometer with ion mobility separation (Waters™, USA) in $HDMS^E$ or HDMS mode for undeuterated and deuterated samples, respectively [209, 210]. [Glu1]-Fibrinopeptide B standard (Waters™, USA) was employed for lock mass correction. After each run, the pepsin column was washed three times with 80 µl of 4 % (v/v) acetonitrile and 0.5 M guanidine hydrochloride, and blanks were performed between each sample. All measurements were carried out in triplicate.

Peptides from the non-deuterated samples (acquired with $HDMS^E$) were identified with ProteinLynx Global SERVER (PLGS, Waters™, USA), employing low energy, elevated energy and intensity thresholds of 300, 100 and 1000 counts, respectively. Peptides were matched using a database containing the amino acid sequences of the proteins of interest, pepsin and their reversed sequences. The search parameters were as follows: peptide tolerance = automatic; fragment tolerance = automatic; min fragment ion matches per peptide = 1; min fragment ion matches per protein = 7; min peptide matches per protein = 3; maximum hits to return = 20; maximum protein mass = 250,000; primary digest reagent = non-specific; missed cleavages = 0; false discovery rate = 100. Deuterium incorporation was quantified with DynamX 3.0 (Waters™, USA), using peptides that fulfilled the following criteria: minimum intensity = 10,000 counts; maximum length = 30 amino acids; minimum number of pro- ducts = 3; minimum number of products per amino acid = 0.05; maximum mass error = 25 ppm; retention time tolerance = 0.5 min. After automated data processing with DynamX, all spectra were manually inspected and, if necessary, peptides were omitted (e.g. in case of a low signal-to-noise ratio or the presence of overlapping peptides).

## Bioinformatic analyses

## Sequence analyses

*H. neptunium* ATCC15444 and *C. crescentus* CB15N nucleotide and protein sequences were obtained from NCBI (https://www.ncbi.nlm.nih.gov) or UniProt (https://www.uniprot.org). Sequences were compared and analysed with NCBI PSI-Blast

algorithm. Multiple sequence alignments were conducted by Clustal Omega (https://www.ebi.ac.uk/Tools/msa/clustalo) and the alignments were viewed and edited by Jalview. The phylogenetic tree of homologous sequences was annotated and viewed with iTOL (https://itol.embl.de). The predictions for the co-structure of MipZ and ParB C-terminal peptide were done using AlphaFold Colab (https://colab.research.google.com/github/deepmind/alphafold/blob/main/notebooks/AlphaFold.ipynb). Information about conserved protein domains and the domain organisation of proteins were obtained from the Pfam protein family database (http://pfam.xfam.org). Apart from AlphaFold, the I-TASSER server (https://zhanggroup.org/I-TASSER/) with default setting was used to predict the structure of HNE_0708, which was viewed and manipulated in PyMol (Schrödinger, USA). The ConSurf server (https://consurf.tau.ac.il/consurf-old.php) was used to predict the structural conservation of MipZ proteins. To construct the ParA protein family phylogenetic tree, sequence comparisons were done by MAFFT v6 (http://mafft.cbrc.jp/alignment/server/). The phylogenetic analysis was based on the Maximum Likelihood (ML) method using the RaxML program and a subsequent representation of the tree using iTOL [116] (http://itol.embl.de/). To verify the tree, the Neighbor Joining (NJ) method was used with the MAFFT v6 program.

## Data analysis

Data analyses of BLI data were performed by using Excel (Microsoft Office) and microscopy data quantification by open source RStudio (https://plotly.com/r/box-plots/). The visualisation of data was mainly achieved using the ggplot2 violin plots and plotly packages in R. The further modification of the generated plots was performed with Adobe Illustrator CS6 (Adobe Systems).

## References


Austin, Stuart, Marcia Ziese, and Nat Sternberg. 1981. “A Novel Role for Site-Specific Recombination in Maintenance of Bacterial Replicons.” *Cell* 25 (3): 729–36.

Ashkenazy, H., Abadi, S., Martz, E., Chay, O., Mayrose, I., Pupko, T., & Ben-Tal, N. 2016. “ConSurf 2016: an improved methodology to estimate and visualize evolutionary conservation in macromolecules.” *Nucleic acids research*, *44*(W1), W344–W350.

Badger, J. H., Hoover, T. R., Brun, Y. V., Weiner, R. M., Laub, M. T., Alexandre, G., Mrázek, J., Ren, Q., Paulsen, I. T., Nelson, K. E., Khouri, H. M., Radune, D., Sosa, J., Dodson, R. J., Sullivan, S. A., Rosovitz, M. J., Madupu, R., Brinkac, L. M., Durkin, A. S., Daugherty, S. C., … Ward, N. L. (2006). “Comparative genomic evidence for a close relationship between the dimorphic prosthecate bacteria Hyphomonas neptunium and Caulobacter crescentus.” *Journal of bacteriology*, *188*(19), 6841–6850.

Badrinarayanan, Anjana, Tung B.K. Le, and Michael T. Laub. 2015. “Bacterial Chromosome Organization and Segregation.” *Annual Review of Cell and Developmental Biology* 31 (1): 171–99.

Banigan, Edward J., Michael A. Gelbart, Zemer Gitai, Ned S. Wingreen, and Andrea J. Liu. 2011. “Filament Depolymerization Can Explain Chromosome Pulling during Bacterial Mitosis.” Edited by Dennis R. Livesay. *PLoS Computational Biology* 7 (9): e1002145.

Beattie, Thomas R., and Rodrigo Reyes-Lamothe. 2015. “A Replisomeâ€™s Journey through the Bacterial Chromosome.” *Frontiers in Microbiology* 6 (June).

Berdis, A. J., Lee, I., Coward, J. K., Stephens, C., Wright, R., Shapiro, L., & Benkovic, S. J. 1998. “A cell cycle-regulated adenine DNA methyltransferase from Caulobacter crescentus processively methylates GANTC sites on hemimethylated DNA.”*Proceedings of the National Academy of Sciences of the United States of America*, *95*(6), 2874–2879.

Bi, E. F., & Lutkenhaus, J. 1991. “FtsZ ring structure associated with division in *Escherichia coli*.” *Nature*, *354*(6349), 161–164.

Böhm, Kati, Giacomo Giacomelli, Andreas Schmidt, Axel Imhof, Romain Koszul, Martial Marbouty, and Marc Bramkamp. 2020. “Chromosome Organization by a Conserved Condensin-ParB System in the Actinobacterium Corynebacterium Glutamicum.” *Nature Communications* 11 (1): 1485.

Bürmann, Frank, and Stephan Gruber. 2015. “SMC Condensin: Promoting Cohesion of Replicon Arms.” *Nature Structural & Molecular Biology* 22 (9): 653–55.

Cserti, E., Rosskopf, S., Chang, Y. W., Eisheuer, S., Selter, L., Shi, J., Regh, C.,

Koert, U., Jensen, G. J., & Thanbichler, M. (2017). Dynamics of the peptidoglycan biosynthetic machinery in the stalked budding bacterium Hyphomonas neptunium. *Molecular microbiology*, *103*(5), 875–895

Collier, Justine. 2012. "Regulation of Chromosomal Replication in Caulobacter Crescentus." *Plasmid* 67 (2): 76–87.

Corbin, B. D., Wang, Y., Beuria, T. K., & Margolin, W. 2007. "Interaction between cell division proteins FtsE and FtsZ." *Journal of bacteriology*, *189*(8), 3026–3035.

Cordell SC, Anderson RE, Löwe J. 2001 "Crystal structure of the bacterial cell division inhibitor MinC." *EMBO J*. 20(10):2454-61

Corrales-Guerrero, Laura, Binbin He, Yacine Refes, Gaël Panis, Gert Bange, Patrick H Viollier, Wieland Steinchen, and Martin Thanbichler. 2020. "Molecular Architecture of the DNA-Binding Sites of the P-Loop ATPases MipZ and ParA from Caulobacter Crescentus." *Nucleic Acids Research* 48 (9): 4769–79.
.
Cosgriff, Sarah, Kiran Chintakayala, Ya Tsz A. Chim, Xinyong Chen, Stephanie Allen, Andrew L. Lovering, and David C. Grainger. 2010. "Dimerization and DNA-Dependent Aggregation of the Escherichia Coli Nucleoid Protein and Chaperone CbpA: Interactions of the CbpA Protein." *Molecular Microbiology* 77 (5): 1289–1300.

Crozat, E., & Grainge, I. 2010. "FtsK DNA translocase: the fast motor that knows where it's going." *Chembiochem : a European journal of chemical biology*, *11*(16), 2232–2243.

Dame, Remus T., Martijn S. Luijsterburg, Evelyne Krin, Philippe N. Bertin, Rolf Wagner, and Gijs J. L. Wuite. 2005. "DNA Bridging: A Property Shared among H-NS-Like Proteins." *Journal of Bacteriology* 187 (5): 1845–48.

Danilova O, Reyes-Lamothe R, Pinskaya M, Sherratt D, Possoz C.2007 " MukB colocalizes with the oriC region and is required for organisation of the two Escherichia coli chromosome arms into separate cell halves." Mol Microbiol. Sep;65(6):1485-92.

David, Ariane, Gaëlle Demarre, Leila Muresan, Evelyne Paly, François-Xavier Barre, and Christophe Possoz. 2014. "The Two Cis-Acting Sites, ParS1 and OriC1, Contribute to the Longitudinal Organisation of Vibrio Cholerae Chromosome I." Edited by William F. Burkholder. *PLoS Genetics* 10 (7): e1004448.

de Boer, P A et al.1989 "A division inhibitor and a topological specificity factor coded for by the minicell locus determine proper placement of the division septum in E. coli." *Cell* vol. 56,4 : 641-9.

Dmowski, M., & Jagura-Burdzy, G. 2011. "Mapping of the interactions between partition proteins Delta and Omega of plasmid pSM19035 from Streptococcus pyogenes." *Microbiology (Reading, England)*, *157*(Pt 4), 1009–1020

Dubarry, N., Willis, C. R., Ball, G., Lesterlin, C., & Armitage, J. P. (2019). *In Vivo* Imaging of the Segregation of the 2 Chromosomes and the Cell Division Proteins of *Rhodobacter sphaeroides* Reveals an Unexpected Role for MipZ. *mBio*, *10*(1), e02515-18.

Duderstadt, K. E., R. Reyes-Lamothe, A. M. van Oijen, and D. J. Sherratt. 2014. "Replication-Fork Dynamics." *Cold Spring Harbor Perspectives in Biology* 6 (1): a010157–a010157.

Ebersbach, Gitte, Ariane Briegel, Grant J Jensen, and Christine Jacobs-Wagner. n.d. "A Self-Associating Protein Critical for Chromosome Attachment, Division, and Polar Organization in Caulobacter," 13.

Ebersbach, Gitte, and Kenn Gerdes. 2005. "Plasmid Segregation Mechanisms." *Annual Review of Genetics* 39 (1): 453–79.

Ellenberger, Tom, and Arthur Landy. 1997. "A Good Turn for DNA: The Structure of Integration Host Factor Bound to DNA." *Structure* 5 (2): 153–57.

Esquilin-Lebron, K., Dubrac, S., Barras, F., & Boyd, J. M. 2021. "Bacterial Approaches for Assembling Iron-Sulfur Proteins." *mBio*, *12*(6)

Fisher, Gemma LM, Jani R Bolla, Karthik V Rajasekar, Jarno Mäkelä, Rachel Baker, Man Zhou, Josh P Prince, et al. 2021. "Competitive Binding of MatP and Topoisomerase IV to the MukB Hinge Domain." *ELife* 10 (September): e70444.

Frandi A, Collier J.2019 "Multilayered control of chromosome replication in *Caulobacter crescentus*." *Biochem Soc Trans.* 7(1):187-196.

Funnell, Barbara E, 2014 "How to build segregation complexes in bacteria: Using bridges" *Genes Dev.* 28: 1140-1142

Fung, E., Bouet, J. Y., & Funnell, B. E. 2001. "Probing the ATP-binding site of P1 ParA: partition and repression have different requirements for ATP binding and hydrolysis". *The EMBO journal*, *20*(17), 4901–4911

Gallagher, E. S., & Hudgens, J. W. (2016). Mapping Protein-Ligand Interactions with Proteolytic Fragmentation, Hydrogen/Deuterium Exchange-Mass Spectrometry. *Methods in enzymology*, *566*, 357–404

Gerdes, Kenn, Jakob Mùller-Jensen, and Rasmus Bugge Jensen. 2000. "Plasmid and Chromosome Partitioning: Surprises from Phylogeny." *Molecular Microbiology*, 12.

Gill, J., Kumar, A., & Sharma, A. 2022. "Structural comparisons reveal diverse binding modes between nucleosome assembly proteins and histones." *Epigenetics & chromatin*, *15*(1), 20.

Gorbatyuk, Boris, and Gregory T. Marczynski. 2004. "Regulated Degradation of Chromosome Replication Proteins DnaA and CtrA in Caulobacter Crescentus: C.

Crescentus DnaA Regulation by Proteolysis." *Molecular Microbiology* 55 (4): 1233–45.

Gogou, C., Japaridze, A., & Dekker, C. (2021). "Mechanisms for Chromosome Segregation in Bacteria." *Frontiers in microbiology*, *12*, 685687.

Graham TG, Wang X, Song D, Etson CM, van Oijen AM, Rudner DZ, Loparo JJ. 2014 "ParB spreading requires DNA bridging." *Genes Dev*. 28(11):1228-38.

Harms, Andrea, Anke Treuner-Lange, Dominik Schumacher, and Lotte Søgaard-Andersen. 2013. "Tracking of Chromosome and Replisome Dynamics in Myxococcus Xanthus Reveals a Novel Chromosome Arrangement." *PLOS Genetics* 9 (9): 16.

Hayes, Finbarr, Lyndsay Radnedge, Michael A. Davis, and Stuart J. Austin. 1994. "The Homologous Operons for P1 and P7 Plasmid Partition Are Autoregulated from Dissimilar Operator Sites." *Molecular Microbiology* 11 (2): 249–60.

Hirano, Tatsuya. 2005. "SMC Proteins and Chromosome Mechanics: From Bacteria to Humans," 8.

Hirano, 2006. "At the Heart of the Chromosome: SMC Proteins in Action." *Nature Reviews Molecular Cell Biology* 7 (5): 311–22.

Hu, L., Vecchiarelli, A. G., Mizuuchi, K., Neuman, K. C., & Liu, J. 2017. "Brownian Ratchet Mechanism for Faithful Segregation of Low-Copy-Number Plasmids." *Biophysical journal*, *112*(7), 1489–1502

Hunding, A., Ebersbach, G., & Gerdes, K. 2003. "A mechanism for ParB-dependent waves of ParA, a protein related to DNA segregation during cell division in prokaryotes." *Journal of molecular biology*, *329*(1), 35–43.

Iniesta, Antonio A. 2014. "ParABS System in Chromosome Partitioning in the Bacterium Myxococcus Xanthus." Edited by Adam Driks. *PLoS ONE* 9 (1): e86897.

Ishihama, Akira. n.d. "The Nucleoid: An Overview," 46.

Iyer, Radha, Priyanka Mukherjee, Kemeng Wang, Joshua Simons, Gary P. Wormser, and Ira Schwartz. 2013. "Detection of Borrelia Burgdorferi Nucleic Acids after Antibiotic Treatment Does Not Confirm Viability." *Journal of Clinical Microbiology* 51 (3): 857–62.

Jalal, Adam S. B., and Tung B. K. Le. 2020. "Bacterial Chromosome Segregation by the ParABS System." *Open Biology* 10 (6): 200097.

Jalal, Adam SB, Ngat T Tran, and Tung BK Le. 2020. "ParB Spreading on DNA Requires Cytidine Triphosphate in Vitro." *ELife* 9 (February): e53515.

Jalal, Adam SB, Ngat T Tran, Clare EM Stevenson, Afroze Chimthanawala, Anjana

Badrinarayanan, David M Lawson, and Tung BK Le. 2021. “A CTP-Dependent Gating Mechanism Enables ParB Spreading on DNA.” *ELife* 10 (August): e69676.

Jecz, Paulina, Aneta A. Bartosik, Krzysztof Glabski, and Grazyna Jagura-Burdzy. 2015. “A Single ParS Sequence from the Cluster of Four Sites Closest to OriC Is Necessary and Sufficient for Proper Chromosome Segregation in Pseudomonas Aeruginosa.” Edited by Adam Driks. *PLOS ONE* 10 (3): e0120867.

Jensen, R. B. 2001. “A Moving DNA Replication Factory in Caulobacter Crescentus.” *The EMBO Journal* 20 (17): 4952–63.

Jung, A., Raßbach, A., Pulpetta, R. L., van Teeseling, M. C. F., Heinrich, K., Sobetzko, P., Serrania, J., Becker, A., & Thanbichler, M. 2019. “Two-step chromosome segregation in the stalked budding bacterium Hyphomonas neptunium. “*Nature communications*, *10*(1), 3290.

Kamada, Katsuhiko, and Daniela Barillà. 2018. “Combing Chromosomal DNA Mediated by the SMC Complex: Structure and Mechanisms.” *BioEssays* 40 (2): 1700166.

Katayama, Tsutomu, Kazutoshi Kasho, and Hironori Kawakami. 2017. “The DnaA Cycle in Escherichia Coli: Activation, Function and Inactivation of the Initiator Protein.” *Frontiers in Microbiology* 8 (December): 2496.

Kavenoff, Ruth, and Oliver A. Ryder. 1976. “Electron Microscopy of Membrane-Associated Folded Chromosomes of Escherichia Coli.” *Chromosoma* 55 (1): 13–25.

Kawalek, A., Wawrzyniak, P., Bartosik, A. A., & Jagura-Burdzy, G. 2020. “Rules and Exceptions: The Role of Chromosomal ParB in DNA Segregation and Other Cellular Processes.” *Microorganisms*, *8*(1)

Kawalek, A., Bartosik, A. A., Glabski, K., & Jaguar-Burdzy, G. 2018. “Pseudomonas aeruginosa partitioning protein ParB acts as a nucleoid-associated protein binding to multiple copies of a parS-related motif.” *Nucleic acids research*, *46*(9), 4592–4606.

Kiekebusch, D., Michie, K. A., Essen, L. O., Löwe, J., & Thanbichler, M. (2012). “Localized dimerization and nucleoid binding drive gradient formation by the bacterial cell division inhibitor MipZ. “*Molecular cell*, *46*(3), 245–259.

Kim, S. K., & Shim, J. 1999. “Interaction between F plasmid partition proteins SopA and SopB. “*Biochemical and biophysical research communications*, *263*(1), 113–117.

Kinashi, H., Shimaji-Murayama, M., & Hanafusa, T. 1992 “Integration of SCP1, a giant linear plasmid, into the *Streptomyces coelicolor* chromosome.” *Gene*, *115*(1-2), 35–41.

Köhler, P, and M A Marahiel. 1997. “Association of the Histone-like Protein HBsu

with the Nucleoid of Bacillus Subtilis." *Journal of Bacteriology* 179 (6): 2060–64.

Krogh TJ, Møller-Jensen J, Kaleta C.2018. " Impact of Chromosomal Architecture on the Function and Evolution of Bacterial Genomes." Front Microbiol. Aug 27;9:2019. Doi

Lam, H., Schofield, W. B., & Jacobs-Wagner, C. 2006. "A landmark protein essential for establishing and perpetuating the polarity of a bacterial cell." *Cell*, *124*(5), 1011–1023

Land M, Hauser L, Jun SR, Nookaew I, Leuze MR, Ahn TH, Karpinets T, Lund O, Kora G, Wassenaar T, Poudel S, Ussery DW.2015 " Insights from 20 years of bacterial genome sequencing." Funct Integr Genomics. 15(2):141-61.

Lederberg, Joshua. n.d. "Cell Genetics and Hereditary Symbiosis," 28.

Leipe, D. D., Wolf, Y. I., Koonin, E. V., & Aravind, L. 2002. "Classification and evolution of P-loop GTPases and related ATPases." *Journal of molecular biology*, *317*(1), 41–72

Leonard, Alan C. 2019. "Changing Perspectives on the Role of DnaA-ATP in Orisome Function and Timing Regulation." *Frontiers in Microbiology* 10: 12.

Leonard, Thomas A, P Jonathan Butler, and Jan L□we. 2005. "Bacterial Chromosome Segregation: Structure and DNA Binding of the Soj Dimer ? A Conserved Biological Switch." *The EMBO Journal* 24 (2): 270–82.

Lessie, T. G., Hendrickson, W., Manning, B. D., & Devereux, R. 1996. "Genomic complexity and plasticity of Burkholderia cepacia." *FEMS microbiology letters*, *144*(2-3), 117–128.

Letek M, Ordóñez E, Vaquera J, Margolin W, Flärdh K, Mateos LM, Gil JA. 2008 "DivIVA is required for polar growth in the MreB-lacking rod-shaped actinomycete Corynebacterium glutamicum. "J Bacteriol.190(9):3283-92.

Li, Yilai, Jeremy W Schroeder, Lyle A Simmons, and Julie S Biteen. 2018. "Visualizing Bacterial DNA Replication and Repair with Molecular Resolution." *Current Opinion in Microbiology* 43 (June): 38–45.

Lim, Hoong Chuin, Ivan Vladimirovich Surovtsev, Bruno Gabriel Beltran, Fang Huang, Jörg Bewersdorf, and Christine Jacobs-Wagner. 2014. "Evidence for a DNA-Relay Mechanism in ParABS-Mediated Chromosome Segregation." *ELife* 3 (May): e02758.

Lin, Lin, Manuel Osorio Valeriano, Andrea Harms, Lotte Søgaard-Andersen, and Martin Thanbichler. 2017. "Bactofilin-Mediated Organization of the ParABS Chromosome Segregation System in Myxococcus Xanthus." *Nature Communications* 8 (1): 1817.

Lindler, L. E., Plano, G. V., Burland, V., Mayhew, G. F., & Blattner, F. R. (1998).

Complete DNA sequence and detailed analysis of the Yersinia pestis KIM5 plasmid encoding murine toxin and capsular antigen. *Infection and immunity*, *66*(12), 5731–5742

Livny, Jonathan, Yoshiharu Yamaichi, and Matthew K. Waldor. 2007. "Distribution of Centromere-Like *ParS* Sites in Bacteria: Insights from Comparative Genomics." *Journal of Bacteriology* 189 (23): 8693–8703.

López-García, Purificación, and David Moreira. 2006. "Selective Forces for the Origin of the Eukaryotic Nucleus." *BioEssays* 28 (5): 525–33.

Loose, Martin et al. 2008"Spatial regulators for bacterial cell division self-organize into surface waves in vitro." *Science* 789-92.

Lutkenhaus J. (2012). The ParA/MinD family puts things in their place. *Trends in microbiology*, *20*(9), 411–418.

Madariaga-Marcos, J., Pastrana, C. L., Fisher, G. L., Dillingham, M. S., & Moreno-Herrero, F. 2019. "ParB dynamics and the critical role of the CTD in DNA condensation unveiled by combined force-fluorescence measurements." *eLife*, *8*, e43812

Makela, Jarno. n.d. "The SMC Complex, MukBEF, Organizes the Escherichia Coli Chromosome by Forming an Axial Core," 30.

Marczynski, Gregory T., and Lucy Shapiro. 2002. "Control of Chromosome Replication in *Caulobacter Crescentus*." *Annual Review of Microbiology* 56 (1): 625–56.

Martire, Sara, and Laura A. Banaszynski. 2020. "The Roles of Histone Variants in Fine-Tuning Chromatin Organization and Function." *Nature Reviews Molecular Cell Biology* 21 (9): 522–41.

Maurya, Ganesh K, Swathi Kota, and Hari S. Misra. 2019. "Characterisation of ParB Encoded on Multipartite Genome in Deinococcus Radiodurans and Their Roles in Radioresistance." *Microbiological Research* 223–225 (June): 22–32.

Maurya, Ganesh K., Kruti Modi, and Hari S. Misra. 2016. "Divisome and Segrosome Components of Deinococcus Radiodurans Interact through Cell Division Regulatory Proteins." *Microbiology* 162 (8): 1321–34.

Méchali, Marcel. 2010. "Eukaryotic DNA Replication Origins: Many Choices for Appropriate Answers," 11.

Mercier, Romain, Marie-Agnès Petit, Sophie Schbath, Stéphane Robin, Meriem El Karoui, Frédéric Boccard, and Olivier Espéli. 2008. "The MatP/MatS Site-Specific System Organizes the Terminus Region of the E. Coli Chromosome into a Macrodomain." *Cell* 135 (3): 475–85.

Messelink, J. J. B., van Teeseling, M. C. F., Janssen, J., Thanbichler, M., &

Broedersz, C. P. 2021. “Learning the distribution of single-cell chromosome conformations in bacteria reveals emergent order across genomic scales.” *Nature communications*, *12*(1), 1963

Mori, H, Y Mori, C Ichinose, H Niki, T Ogura, A Kato, and S Hiraga. 1989. “Purification and Characterization of SopA and SopB Proteins Essential for F Plasmid Partitioning.” *Journal of Biological Chemistry* 264 (26): 15535–41.

Mott, Melissa L., and James M. Berger. 2007. “DNA Replication Initiation: Mechanisms and Regulation in Bacteria.” *Nature Reviews Microbiology* 5 (5): 343–54.

Newman, R. M., Salunkhe, P., Godzik, A., & Reed, J. C. 2006. “Identification and characterization of a novel bacterial virulence factor that shares homology with mammalian Toll/interleukin-1 receptor family proteins.” *Infection and immunity*, *74*(1), 594–601.

Nicolas, Emilien, Amy L. Upton, Stephan Uphoff, Olivia Henry, Anjana Badrinarayanan, and David Sherratt. 2014. “The SMC Complex MukBEF Recruits Topoisomerase IV to the Origin of Replication Region in Live Escherichia Coli.” Edited by Richard Gerald Brennan. *MBio* 5 (1): e01001-13.

Niki, H., R. Imamura, M. Kitaoka, K. Yamanaka, T. Ogura, and S. Hiraga. 1992. “E.Coli MukB Protein Involved in Chromosome Partition Forms a Homodimer with a Rod-and-Hinge Structure Having DNA Binding and ATP/GTP Binding Activities.” *The EMBO Journal* 11 (13): 5101–9.

Nolivos, Sophie, and David Sherratt. 2014. “The Bacterial Chromosome: Architecture and Action of Bacterial SMC and SMC-like Complexes.” *FEMS Microbiology Reviews* 38 (3): 380–92.

Nordström, KurtSøren Molin, Helle Aagaard-Hansen, 1980 “Partitioning of plasmid R1 in Escherichia coli: II. Incompatibility properties of the partitioning system”*Plasmid,*4, (3): 332-349

Osorio-Valeriano, Manuel, Florian Altegoer, Chandan K. Das, Wieland Steinchen, Gaël Panis, Lara Connolley, Giacomo Giacomelli, et al. 2021. “The CTPase Activity of ParB Determines the Size and Dynamics of Prokaryotic DNA Partition Complexes.” *Molecular Cell* 81 (19): 3992-4007.e10.

Osorio-Valeriano, Manuel, Florian Altegoer, Wieland Steinchen, Svenja Urban, Ying Liu, Gert Bange, and Martin Thanbichler. 2019. “ParB-Type DNA Segregation Proteins Are CTP-Dependent Molecular Switches.” *Cell* 179 (7): 1512-1524.e15.

Park KT, Wu W, Battaile KP, Lovell S, Holyoak T, Lutkenhaus J. 2011“The Min oscillator uses MinD-dependent conformational changes in MinE to spatially regulate cytokinesis”. *Cell*. 46(3):396-407.

Pillet, Flavien, Fanny Marie Passot, Franck Pasta, Véronique Anton Leberre, and

Jean-Yves Bouet. 2017. “Analysis of ParB-Centromere Interactions by Multiplex SPR Imaging Reveals Specific Patterns for Binding ParB in Six Centromeres of Burkholderiales Chromosomes and Plasmids.” Edited by Valentin V. Rybenkov. *PLOS ONE* 12 (5): e0177056.

Pillet, Flavien, Aurore Sanchez, David Lane, and Jean-Yves Bouet. n.d. “Centromere Binding Specificity in Assembly of the F Plasmid Partition Complex,” 10.

Pinho, Mariana G., Morten Kjos, and Jan-Willem Veening. 2013. “How to Get (a)Round: Mechanisms Controlling Growth and Division of Coccoid Bacteria.” *Nature Reviews Microbiology* 11 (9): 601–14.

Postow, Lisa, Christine D. Hardy, Javier Arsuaga, and Nicholas R. Cozzarelli. 2004. “Topological Domain Structure of the *Escherichia Coli* Chromosome.” *Genes & Development* 18 (14): 1766–79.

Quon, Kim C, Gregory T Marczynski, and Lucy Shapiro. 1996. “Cell Cycle Control by an Essential Bacterial Two-Component Signal Transduction Protein.” *Cell* 84 (1): 83–93.

Rasmussen T, Jensen RB, Skovgaard O. 2007 The two chromosomes of Vibrio cholerae are initiated at different time points in the cell cycle.” EMBO J.26(13):3124-31.

Reyes-Lamothe, Rodrigo, Emilien Nicolas, and David J. Sherratt. 2012. “Chromosome Replication and Segregation in Bacteria.” *Annual Review of Genetics* 46 (1): 121–43.

Ringgaard, Simon, Jan Löwe, and Kenn Gerdes. 2007. “Centromere Pairing by a Plasmid-Encoded Type I ParB Protein.” *Journal of Biological Chemistry* 282 (38): 28216–25.

Ringgaard, S., Yang, W., Alvarado, A., Schirner, K., & Briegel, A. 2018. “Chemotaxis arrays in *Vibrio* species and their intracellular positioning by the ParC/ParP system.” *Journal of bacteriology*, *200*(15), e00793-17.

Roberts, M. A., Wadhams, G. H., Hadfield, K. A., Tickner, S., & Armitage, J. P. 2012. “ParA-like protein uses nonspecific chromosomal DNA binding to partition protein complexes.” *Proceedings of the National Academy of Sciences of the United States of America*, *109*(17), 6698–6703

Robinett, C. C., Straight, A., Li, G., Willhelm, C., Sudlow, G., Murray, A., & Belmont, A. S. 1996. “In vivo localization of DNA sequences and visualization of large-scale chromatin organization using lac operator/repressor recognition.”*The Journal of cell biology*, *135*(6 Pt 2), 1685–1700.

Robinow, C, and E Kellenberger. n.d. “The Bacterial Nucleoid Revisited.” *MICROBIOL. REV.*, 22.

Scheffers, D. J., de Wit, J. G., den Blaauwen, T., & Driessen, A. J. 2002. “GTP hydrolysis of cell division protein FtsZ: evidence that the active site is formed by the association of monomers.” *Biochemistry*, *41*(2), 521–529.

Schofield, Whitman B, Hoong Chuin Lim, and Christine Jacobs-Wagner. 2010. “Cell Cycle Coordination and Regulation of Bacterial Chromosome Segregation Dynamics by Polarly Localized Proteins.” *The EMBO Journal* 29 (18): 3068–81.

Schumacher, Maria A. 2012. “Bacterial Plasmid Partition Machinery: A Minimalist Approach to Survival.” *Current Opinion in Structural Biology* 22 (1): 72–79.

Schumacher, D., Bergeler, S., Harms, A., Vonck, J., Huneke-Vogt, S., Frey, E., & Søgaard-Andersen, L. 2017.” The PomXYZ Proteins Self-Organize on the Bacterial Nucleoid to Stimulate Cell Division.” *Developmental cell*, *41*(3)

Shi, C., & Shi, X. 2006. “Characterization of three genes encoding the subunits of light-independent protochlorophyllide reductase in Chlorella protothecoides” CS-41. *Biotechnology progress*, *22*(4), 1050–1055

Silber, Nadine, Cruz L Matos de Opitz, Christian Mayer, and Peter Sass. 2020. “Cell Division Protein FtsZ: From Structure and Mechanism to Antibiotic Target.” *Future Microbiology* 15 (9): 801–31.

.

Sinden, R R, and D E Pettijohn. 1981. “Chromosomes in Living Escherichia Coli Cells Are Segregated into Domains of Supercoiling.” *Proceedings of the National Academy of Sciences* 78 (1): 224–28.

Soh, Young-Min, Iain Finley Davidson, Stefano Zamuner, Jérôme Basquin, Florian Patrick Bock, Michael Taschner, Jan-Willem Veening, Paolo De Los Rios, Jan-Michael Peters, and Stephan Gruber. 2019. “Self-Organization of *ParS* Centromeres by the ParB CTP Hydrolase.” *Science* 366 (6469): 1129–33.

Spear, A. M., Loman, N. J., Atkins, H. S., & Pallen, M. J. 2009. “Microbial TIR domains: not necessarily agents of subversion?.” *Trends in microbiology*, *17*(9), 393–398.

Strunnikov, Alexander V. 2006. “SMC Complexes in Bacterial Chromosome Condensation and Segregation.” *Plasmid* 55 (2): 135–44.

Sullivan, Nora L., Kathleen A. Marquis, and David Z. Rudner. 2009. “Recruitment of SMC by ParB-ParS Organizes the Origin Region and Promotes Efficient Chromosome Segregation.” *Cell* 137 (4): 697–707.

Thanbichler, M., & Shapiro, L. (2006). “MipZ, a spatial regulator coordinating chromosome segregation with cell division in Caulobacter.” *Cell*, *126*(1), 147–162.

Tišma, Miloš, Maria Panoukidou, Hammam Antar, Young-Min Soh, Roman Barth, Biswajit Pradhan, Jaco Torre, Davide Michieletto, Stephan Gruber, and Cees Dekker. 2021. *ParS -Independent Recruitment of the Bacterial Chromosome-*

*Partitioning Protein ParB*.

Toro-Nahuelpan, M., Corrales-Guerrero, L., Zwiener, T., Osorio-Valeriano, M., Müller, F. D., Plitzko, J. M., Bramkamp, M., Thanbichler, M., & Schüler, D. (2019). "A gradient-forming MipZ protein mediating the control of cell division in the magnetotactic bacterium Magnetospirillum gryphiswaldense. "*Molecular microbiology*, *112*(5), 1423–1439

Trojanowski D, Hołówka J, Zakrzewska-Czerwińska J. 2018 "Where and When Bacterial Chromosome Replication Starts: A Single Cell Perspective." *Front Microbiology* 26(9):

Trucksis, Michele, Jane Michalski, Ying Kang Deng, and James B. Kaper. 1998. "The *Vibrio Cholerae* Genome Contains Two Unique Circular Chromosomes." *Proceedings of the National Academy of Sciences* 95 (24): 14464–69.

Ucci, Amanda P., Paula M. M. Martins, Ivy F. Lau, Maurício Bacci, José Belasque, and Henrique Ferreira. 2014. "Asymmetric Chromosome Segregation in *Xanthomonas Citri* Ssp. *Citri*." *MicrobiologyOpen* 3 (1): 29–41.

Valens, M., Penaud, S., Rossignol, M., Cornet, F., & Boccard, F. 2004. "Macrodomain organization of the Escherichia coli chromosome." *The EMBO journal*, *23*(21), 4330–4341

Vecchiarelli, Anthony G., Ling Chin Hwang, and Kiyoshi Mizuuchi. 2013. "Cell-Free Study of F Plasmid Partition Provides Evidence for Cargo Transport by a Diffusion-Ratchet Mechanism." *Proceedings of the National Academy of Sciences* 110 (15).

Ventura, Barbara Di. 2013. "Chromosome Segregation by the Escherichia Coli Min System," 12.

Viollier, Patrick H., Martin Thanbichler, Patrick T. McGrath, Lisandra West, Maliwan Meewan, Harley H. McAdams, and Lucy Shapiro. 2004. "Rapid and Sequential Movement of Individual Chromosomal Loci to Specific Subcellular Locations during Bacterial DNA Replication." *Proceedings of the National Academy of Sciences* 101 (25): 9257–62.

Wang, Xindan, Tung B.K. Le, Bryan R. Lajoie, Job Dekker, Michael T. Laub, and David Z. Rudner. 2015. "Condensin Promotes the Juxtaposition of DNA Flanking Its Loading Site in *Bacillus Subtilis*." *Genes & Development* 29 (15): 1661–75.

Wang, Xindan, Xun Liu, Christophe Possoz, and David J. Sherratt. 2006. "The Two *Escherichia Coli* Chromosome Arms Locate to Separate Cell Halves." *Genes & Development* 20 (13): 1727–31.

Wang, Xindan, Paula Montero Llopis, and David Z. Rudner. 2014. "*Bacillus Subtilis* Chromosome Organization Oscillates between Two Distinct Patterns." *Proceedings of the National Academy of Sciences* 111 (35): 12877–82.

Wargachuk, Richard, and Gregory T. Marczynski. 2015. “The Caulobacter Crescentus Homolog of DnaA (HdaA) Also Regulates the Proteolysis of the Replication Initiator Protein DnaA.” Edited by P. de Boer. *Journal of Bacteriology* 197 (22): 3521–32.

Watanabe, S., Noda, A., Ohbayashi, R., Uchioke, K., Kurihara, A., Nakatake, S., Morioka, S., Kanesaki, Y., Chibazakura, T., & Yoshikawa, H. 2018. “ParA-like protein influences the distribution of multi-copy chromosomes in cyanobacterium Synechococcus elongatus PCC 7942.” *Microbiology (Reading, England)*, *164*(1), 45–56.

Whitley, K. D., Jukes, C., Tregidgo, N., Karinou, E., Almada, P., Cesbron, Y., Henriques, R., Dekker, C., & Holden, S. 2021. “FtsZ treadmilling is essential for Z-ring condensation and septal constriction initiation in Bacillus subtilis cell division.” *Nature communications*, *12*(1), 2448.

Wiggins, P. A., Cheveralls, K. C., Martin, J. S., Lintner, R., & Kondev, J. 2010. “Strong intranucleoid interactions organize the Escherichia coli chromosome into a nucleoid filament.” *Proceedings of the National Academy of Sciences of the United States of America*, *107*(11), 4991–4995.

Wilhelm, Larissa, Frank Bürmann, Anita Minnen, Ho-Chul Shin, Christopher P Toseland, Byung-Ha Oh, and Stephan Gruber. 2015. “SMC Condensin Entraps Chromosomal DNA by an ATP Hydrolysis Dependent Loading Mechanism in Bacillus Subtilis.” *ELife* 4 (May): e06659.

Wortinger M, Sackett MJ, Brun YV. 2000“CtrA mediates a DNA replication checkpoint that prevents cell division in Caulobacter crescentus.” *EMBO J.* 19(17):4503-12.

Wu, Nan, and Hongtao Yu. 2012. “The Smc Complexes in DNA Damage Response,” 11.

Wu, L. J., & Errington, J. 2003. “RacA and the Soj-Spo0J system combine to effect polar chromosome segregation in sporulating Bacillus subtilis.” *Molecular microbiology*, *49*(6), 1463–1475

Yamaichi Y, Niki H. 2000 “Active segregation by the Bacillus subtilis partitioning system in *Escherichia coli*. “*Proc Natl Acad Sci U S A*. 297(26):14656-61.

Yoshinaga, Mari, and Yuji Inagaki. 2021. “Ubiquity and Origins of Structural Maintenance of Chromosomes (SMC) Proteins in Eukaryotes.” Edited by Sandra Baldauf. *Genome Biology and Evolution* 13 (12): evab256.

Youngren, Brenda, Lyndsay Radnedge, Ping Hu, Emilio Garcia, and Stuart Austin. 2000. “A Plasmid Partition System of the P1-P7par Family from the PMT1 Virulence Plasmid of Yersinia Pestis.” *J. BACTERIOL.* 182: 5.

Zakrzewska-Czerwińska, Jolanta. 2018. “Where and When Bacterial Chromosome Replication Starts: A Single Cell Perspective.” *Frontiers in Microbiology* 9: 9.

Zhou, Huaijin, and Joe Lutkenhaus. 2005“MinC mutants deficient in MinD- and DicB-mediated cell division inhibition due to loss of interaction with MinD, DicB, or a septal component.” *Journal of bacteriology* vol. 187,8): 2846-57.

# Appendix

**Table S1 Strains used in this study**

| Strain | Genotype | Source |
|---|---|---|
| ***H.neptunium*** | | |
| RP4 | *DnaN-Venus* | Conjugation of pAJ84 and double homologous recombination |
| RP10 | *ΔHne_0708* | Conjugation of pRP03 and double homologous recombination in ATCC15444 |
| RP16 | *ΔHne_0708 ParB-YFP* | Conjugation of pRP03 and double homologous recombination in RP10 |
| RP19 | *ΔHne_0708 ParB-Cerulean* | Conjugation of pRP03 and double homologous recombination in AJ76 |
| AJ76 | *ParB-Ceulean* | A.Jung |
| SRE15 | parB-yfp parSpMT1 at 310° | Jung et al, 2019 |
| JR47 | *ParB-Ceulean DnaN-Venus* | Jung et al, 2019 |
| ***E. coli*** | | |
| TOP10 | F-*mcrA* Δ( *mrr-hsd*RMS-*mcr*BC) Φ80*Lac*ZΔM15 Δ *Lac*X74 *rec*A1 *ara*D139 Δ( *araleu*) 7697 *gal*U *gal*K *rps*L (StrR) *end*A1 *nup*G | Invitrogen |
| Rosetta(DE3) pLysS | $F^-$ *ompT hsdS*B($rB^-$ $mB^-$) *gal dcm* (DE3) pRARE ($Cam^R$) | Merck Millipore |

**Table S2 Plasmids used in this study**

| Name | Description | Mode of construction |
|---|---|---|

| | | |
|---|---|---|
| pRP001 | pMCS-2 carrying parS(pMT1) and part of Hne_1854 | pAJ36 and pAJ63 cut with Kpn1 and Nhe 1 restriction enzymes and ligated. |
| pRP002 | pNPTS138 with C terminal fusion of 3Xflag on ParB | pNPTS138 digestion with EcoRI and HindIII, amplify two Hne chromosomal regions with(1) Parb_rev and Flag_fwd and (2)HolA_fwd and Flag_rev, Gibson assembly |
| pRP003 | pNPTS138 to delete Hne_0708 | pNPTS138 cut with EcoRI and HindIII, amplify upstream and downstream regions of Hne_0708 followed by gibson asembly |
| pRP004 | pTB146 with Hne_0708 for N terminal SUMO fusion | pTB146 cut using SapI and BamHI, amplicon from chromosomal DNA using oRP011 and oRP012 cut with SapI and Bam HI, ligation |
| pRP007 | pC3FCN with C terminal 3XFLAG fusion to Hne_0708 | pRP005(pC3FCN) is cut using NdeI and KpnI, insert- amplify Hne_0708 with oRP019 and oRP020 |
| pRP009 | SUMO-Hne_0708 | pTB146 is restriction digested with SapI and BamHI. Hne_0708 is amplified from chromosomal DNA with oRP025(f) and oRP012(R) and the amplicon is RD with SapI and BamHI |
| pRP035 | Caulobacter ParB with Q58A point mutation | pLC8 site directed mutagenesis with oRP115 and 116 to introduce Q58A mutation |
| pRP036 | Chimera - ParBWT of caulobacter with CT of M.Xanthus ParB | gibson assembly of fragments of myxococcus ParB amplified withMO170 and oRP119 and caulobacter ParB amplified with oRP120 and SUMO for(common oligo) to pLC8 cut with NheI and BamHI |
| pRP037 | Chimera - ParBQ58A of caulobacter with CT of M.Xanthus ParB | point mutation using oRP115 and 116 on pRP36 |
| pRP038 | chimera - Myxo ParB with Q52A mutation and CT of caulobacter ParB | oRP134 and 135 amplifies caulobacter Parb fragment. oRP132 and SUMO ParB myxo forward amplifies ParB with Q52A from pMO104. Gibson assemble this to pTB146 cut with SapI and BamHI |
| pRP041 | StrepII/CT of caulobacter ParB | oRP135 and oRP136 used to clone the strepII tag +CT of ParB of caulobacter (ordered as geneblock) into pTB146 cut with SapI and BamHI |

**List of Oligonucleotides used in this study**

| Name | Sequence (5'to 3') |
|---|---|
| oRP001 | gtcgctgtacaagcctgcaggcg |
| oRP002 | agccggctggcgccaagcttatgttgcgagccgggtg |
| oRP006 | cggccgaagctagcgaattcgcaggcctctccaccatt |
| oRP007 | agccggctggcgccaagcttccatgccgttgatattgtcgcc |
| oRP008 | ttcgggcggactgaatgacgcgatgacg |
| oRP009 | ttcagtccgcccgaatggcttatgtatacgtg |
| oRP011 | cttgtcatcgtcatccttgtaatcgatgtcatg |
| oRP012 | ggtggtagaagagccatgtcgcacgtatacata |
| oRP013 | agccggatccccttttcaatgccgcgtcatcgcgtcatt |
| oRP014 | ttcaagctgatcagacccctgaagatttgg |
| oRP025 | atatgctcttcaggtatgtcgcacgtatacataagccat |
| oRP026 | cctggatcaggcgctcgggg |
| oRP027 | cgggcgaatacggatgatcttggct |
| oRP067 | tcccccgggctgcagctagctcaatgccgcgtcatcgcgt |
| oRP068 | atgacaagggggggggggatgtcgcacgtatacataagccatt |
| oRP103 | ttttagaaccgcatctttcacgcgtgggggggcgg |
| oRP104 | caagactgtgccgatcatggtgcgcgagctgacgacctgg |
| oRP105 | ggggccgccccccacgcgtgaaagatgcggttctaaaaga |
| oRP106 | ctttcgggctttgttagcagccggatccttatgattctcgttcagacaaaag |
| oRP107 | cgccagggttttcccagtcacgac |
| oRP108 | aggaaacagctatgaccat |
| oRP115 | cagcgcaatcccgacgctccccgtcggacctt |
| oRP116 | aaggtccgacggggagcgtcgggattgcgctg |
| oRP119 | cgccccccacgcgtgcagagcccgcaggtgaa |
| oRP120 | ttcacctgcgggctctgcacgcgtgggggggcgg |

oRP131 cagagaacagattggtgtggtgaaagcagacatgc

oRP132 cggtgtccttcaccggtgccgccttgcccg

oRP133 aaggcggcaccggtgaaggacaccgacacccaggc

oRP134 gttagcagccggatcctcagatcccgcgcgtcagt

oRP135 acagagaacagattggtggtatgtggagccacccgcag

oRP136 ggctttgttagcagccgtcagatcccgcgcgtcagt

## Supplimentary figure

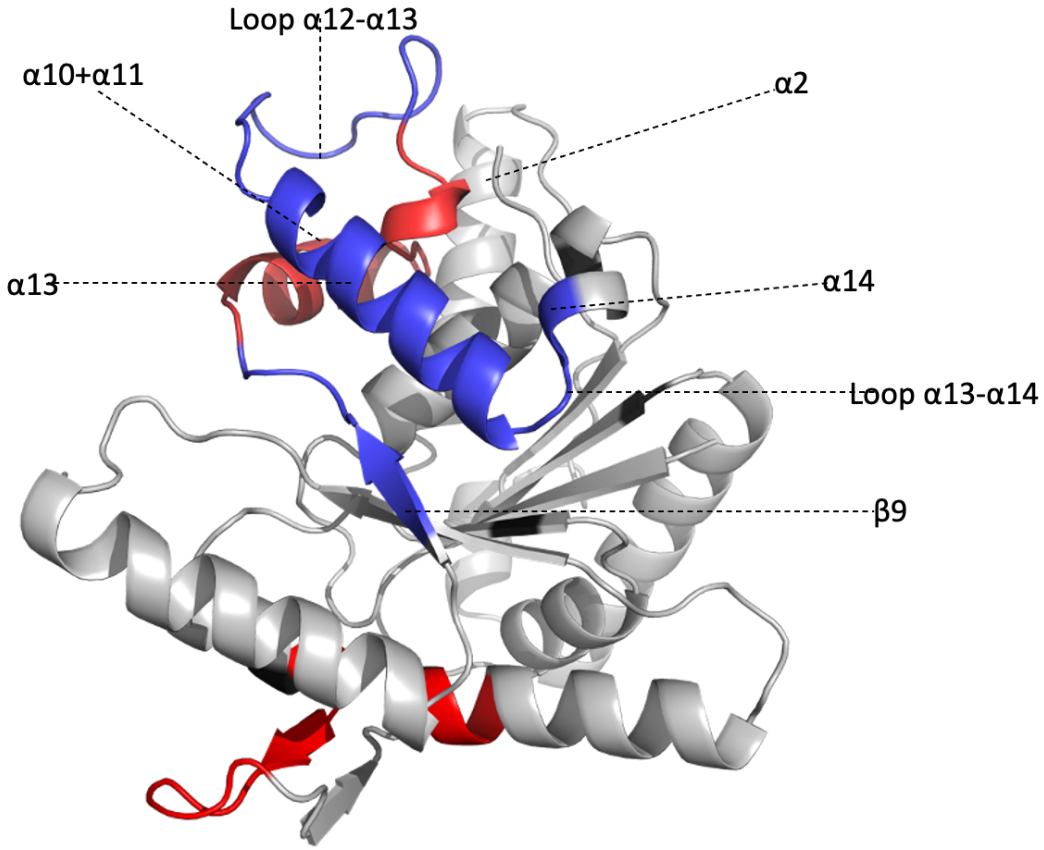


**FigureS1: Projection of the HDX-MS data on the structure of a MipZ monomer.** The blue region indicates the protected region that corresponds to the putative ParB binding interface. The red region indicates a region of higher deuterium uptake, potentially resulting from minor changes in the conformation of ParB upon MipZ binding.

## Acknowledgement

First and foremost I would like to express my sincere gratitude to Prof Dr Martin Thanbichler for being the best supervisor I can imagine and for being the kind and considerate person that he is. Thank you for giving me an opportunity to work in your lab and thank you for all the guidance, support and encouragement through all these past years.

I would also like to thank my defence committee members, Prof Dr Peter Graumann, who also kindly agreed to be my second reviewer, Prof Dr Anke Becker and Prof Dr Hans-Ulrich Mösch for agreeing to be a part of my defence committee and reviewing my thesis. Apart from that I would like to thank Dr. Chase Broedersz for being a part of the TAC committee.
I would like to thank the brilliant scientists who kindly collaborated with me for this work, Dr Wieland Steinchen for the HDX experiments, Dr. Thomas Heilmer for the TEM pictures and Dr Timo Glatter for the Co-IP experiments. I would also like to thank Joanna for being the nice student that you are.

Many thanks are also due to my wonderful labmates especially Ying, Manuel, Adrian, Maria, Laura and Yacine for being the best colleagues I could ever imagine and also for being my family away from home. Laura and Manuel, thank you for all the insightful inputs on my projects, as your works were close to what I was doing, I am very glad that you were there to guide me through many difficulties. Thank you Laura for being very understanding and patient with me. Thank you “small Manuel" for always inspiring me, and caring for me like your sister. Thank you Maria, for always motivating me and for being the kind and supportive colleague and loving friend that you are. Thank you Ying for your wonderful friendship, care and love. You are truly one of the nicest persons I know. Adrian, thank you for always calming me down during presentations, proof reading my slides and this thesis. But more importantly, thank you for being the wonderful companion that you are. Thank you Yacine for being there when I started in the lab. You made me feel very welcome and comfortable in the lab and thank you for all the fun memories that I will always cherish. Thank you Dani, Jannik, Lukas, Basti, Julia, Juri, Nidhi and all other Thanbichler lab members (the list will be too long to write down, but thank you to each and every one of you) for creating a warm lab atmosphere. Special thanks to Jannik for kindly translating my abstract and to Julia for all the help with the techniques during my initial days. There are many more people that I have not listed down here, but I would like to express my gratitude to all of you here. Lastly, I would also like to thank my friends, especially Ismath who was my family here and all my family members for all the love and support through this Journey.

# Einverständniserklärung

Ich versichere, dass ich meine Dissertation:

**“Analysis of coordination of chromosome segregation and cell division in alphaproteobacteria”**

selbstständig, ohne unerlaubte Hilfe angefertigt und mich dabei keiner anderen als der von mir ausdrücklich bezeichneten Quellen und Hilfen bedient habe. Die Dissertation wurde in der jetzigen oder einer ähnlichen Form noch bei keiner anderen Hochschule eingereicht und hat noch keinen sonstigen Prüfungszwecken gedient.

Marburg, _____ _____

Revathi